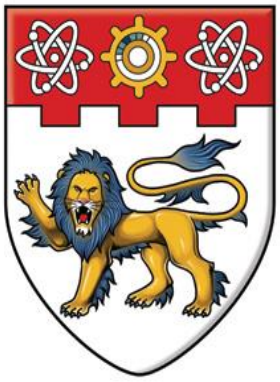

NANYANG TECHNOLOGICAL UNIVERSITY

NOVEL BIO-FUNCTIONAL ARCHITECTURES OF POLYMERSOMES

WINNA SITI

SCHOOL OF MATERIALS SCIENCE AND ENGINEERING

CENTRE FOR BIOMIMETIC SENSOR SCIENCE

2015

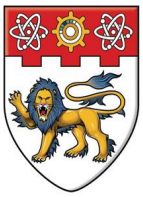

NANYANG TECHNOLOGICAL UNIVERSITY

NOVEL BIO-FUNCTIONAL ARCHITECTURES OF POLYMERSOMES

WINNA SITI

Supervisor: Asst. Prof. Madhavan Nallani

Co-supervisor: Prof. Bo Liedberg

A thesis submitted to Nanyang Technological University
in fulfillment of the requirement for the degree of
Doctor of Philosophy

2015

ABSTRACT

Cell, as a source of inspiration, is a key functional unit of living organism. Its interior consists of different structures composed of soft matter that are highly selective and functions with different roles. Compartmentalization is one of the main features of eukaryotic cells, giving organelles to achieve some essential functions, such as protein synthesis, replication and energy production within close proximity. With the purpose to mimic cellular compartments, lots of model systems based on lipids (liposomes) or polymers (polymersomes) have been developed. Polymersomes (also known as polymer vesicles) are spherical nanostructured entities with a hollow aqueous compartment enclosed by a bilayer membrane of synthetic amphiphilic block copolymers. Compared to the traditionally used liposomes, they have several properties which make them especially suited for lots of applications in biomedicine and biotechnology. Amongst others, their superior stability and excellent chemical diversity allowing their properties of its membranes to be tuned (e.g. selective permeability). Here, the thesis covers two parts of research work and the focus of the study is to use polymersomes system with specific functionality to build novel architectures for mimicking the complexity of living cells.

In the first part, the design and construction of novel multicompartmentalized (vesicle-in-vesicle) architectures from fully synthetic amphiphilic block copolymers was carried out successfully using a simple approach, known as sequential self-assembly, which results in a nanoscale range multicompartments. The inner vesicle was composed of ABA (i.e. PMOXA-PDMS-PMOXA: poly(2-methyloxazoline)–poly(dimethylsiloxane)–poly(2-methyloxazoline)) triblock copolymers, whereas the outer vesicle was composed of PS-PIAT (i.e. polystyrene–polyisocyanoalanine(2-thiophen-3-yl-ethyl)amide) diblock copolymers. Two different enzymes were encapsulated separately

and a bacterial channel protein was inserted into the inner non-permeable ABA triblock copolymer vesicle. Communication between the two compartments was then assayed by a bi-enzymatic cascade reaction catalyzed by the enzymes in the multicompartmentalized polymersomes. This work was demonstrated satisfactorily using extensive types of characterization techniques, including transmission electron microscopy (TEM), dynamic light scattering (DLS), static light scattering (SLS) and cascade reaction kinetics through bioassays, confocal microscopy and flow cytometry. Organization into multicompartments is a basic structural principle of cells, and therefore it is essential to study and understand the compartmentalization of cells.

In the second part, the design and self-assemble of novel functional compartments (termed as 'proteinionosomes') was demonstrated successfully using new building blocks from protein-polymer complexes, consisting of the milk protein β-lactoglobulin (BLG) and poly(ethylene glycol) (PEG). Using protein-polymer complexes as building blocks for preparing vesicles provides more benefits over the amphiphilic block copolymers, particularly in terms of biocompatibility, biodegradability and biofunctionality of the membranes. In this particular work, the proteinionosomes was prepared in two steps via bio-orthogonal chemistry. In the first step, positively and negatively charged PEG-BLG conjugates were synthesized by photoinduced cycloaddition reaction via click chemistry, and in the second step, both charged species were combined to self-assemble into novel nano-compartments, capable of encapsulating molecules, fluorescent and semi-permeable. The fluorescent proteinionosomes were characterized by several techniques, such as SDS-PAGE, MALDI-TOF, fluorescent measurement, TEM, DLS, and enzyme activity. This work is remarkably interesting as it also proved that amphiphilicity, coming from both PEG and BLG building blocks, was needed for the vesicles formation. In addition, the proteinionosomes will be a good model system for cellular biomimicking.

DEDICATION

This thesis is dedicated to my grandparents, Jaya Susanto and Siti for the encouragement in pursuing doctorate degree; my father, Anthony Citi for the understanding and complete support; and my mother, Lenny Ryana for the endless love, patience, and insight in my work. A special feeling of gratitude to my loving sisters, Shellvia and Lydiana, whose words of encouragements have made me come this far. My brothers, Richie and Riches, always believe in me and are very special.

I also dedicate this thesis and give special thanks to my husband, Hendrik Shen, whose sacrifice, support and unconditional love have made my life content as I complete my entire doctorate program.

ACKNOWLEDGEMENTS

First of all, I would like to thank both my supervisors, Prof. Madhavan Nallani and Prof. Bo Liedberg for the opportunity given to work on this polymersome project in the Centre for Biomimetic Sensor Science (CBSS) at Nanyang Technological University (NTU). Through their advices and guidance, I have learned a lot of knowledge and the integrity as a researcher.

I would also like to express my sincere gratitude to my mentor, Dr. Hans-Peter M. de Hoog for his patience, assistance, guidance and insightful discussions on the project. Through his help, I have learned a lot of knowledge, skills, and techniques to work independently in the future.

I would like to acknowledge Dr. Nikodem Tomczak and Mr. Zhikang Fu from Institute of Materials Research and Engineering A*STAR (Agency for Science, Technology and Research) for their help in the fluorescence spectroscopy and flow cytometry analysis, respectively. Thanks to Mr. Mahendra Yavvari, a Summer Research Intern 2011 from Indian Institute of Technology (IIT) Roorkee for his work on the TMB assay for the multicompartmentalized polymersomes project.

I would like to thank Dr. Law Jiayan from Facility for Analysis, Characterization, Testing, and Simulation (FACTS), NTU; Dr. Andrew Wong and Ms. Wee Mei Ling from Cryo-EM Laboratory, School of Biological Science (SBS), NTU for their assistance in TEM imaging.

I would also like to thank my CBSS friends. Thanks to Dr. Chia Wei Sheng for his help in FPLC. Special thanks to Mr. Liu Xiaohu, Mr. Lim Seng Koon and Mr. Chen Peng for their support, discussions and some useful insights related to my project. Thanks to Ms. Liu Yuanjun, Ms. Zhang Jinling and Ms. Tran Thi Nhung for their company, laughter and activities outside of work. Special thanks also go to Ms. Ang Wunly and Ms. Phyllis Lim, the manager and secretary of CBSS, for their help in the administrative work.

Last but not least, I would like to express my most sincere gratitude to my family and friends overseas for their continuous support, encouragements and love.

TABLE OF CONTENTS

Pages

ABSTRACT ..... **i**

DEDICATION ..... **iii**

ACKNOWLEDGEMENTS ..... **iv**

TABLE OF CONTENTS ..... **v**

LIST OF FIGURES ..... **ix**

LIST OF TABLES ..... **xvi**

LIST OF ABBREVIATIONS ..... **xvii**

CHAPTER 1: Introduction **1**

1.1. Background 1

1.2. Motivation 3

1.3. Objectives 4

1.4. Hypothesis 5

1.5. Scope 5

1.6. Synopsis of the Thesis 6

CHAPTER 2: Literature Review 8

2.1. Introduction of Polymersomes 8

2.2. Self-Assembly & Fabrication of Polymersomes from Amphiphilic Block Copolymers 8

2.3. Peptide-based Polymersomes 14

2.3.1. Peptosomes 14

2.3.2. Polyion Complex Vesicles (PICsomes) 15

2.4. Protein-based Polymersomes 19

2.5. Applications of Polymersomes 21

2.5.1. Polymersomes as Nanoreactors 22

2.5.2. Polymersomes for Medical Applications 24

2.6. Multicompartmentalized Polymersomes 28

2.6.1. Double Emulsion Method for Preparing Multicompartments 28

2.6.2. Self-Assembly Method for Preparing Multicompartments 33

2.7. Summary 35

CHAPTER 3: Development of Enzymatic Cascade Reactions in Polymersomes with Multicompartmentalized Architecture 37

3.1. Introduction 37

3.2. Experimental 40

3.2.1. Materials and Methods 40

3.2.2. Preparation of Encapsulated HRP in ABA Polymersomes with OmpF Channel Protein 41

3.2.3. Preparation of Multicompartmentalized Polymersomes 42

3.2.4. Preparation of Alexa-488 Labeled GOx 43

3.2.5. Preparation of Alexa-647 Labeled HRP 44

3.3. Results and Discussion 45

3.4. Conclusion 55

3.5. Output 55

CHAPTER 4: Synthesis & Assembly of Novel Functional Compartments from New Building Blocks of Protein-Polymer Complexes 56

4.1. Introduction 56

4.2. Experimental 60

4.2.1. Materials and Methods 60

4.2.2. Preparation of 4-(2-phenyl-2*H*-tetrazol-5-yl) benzoic acid 61

4.2.3. Preparation of Tetrazole-functionalized Poly(ethylene glycol) 61

4.2.4. Preparation of Allyl-functionalized β-Lactoglobulin 62

4.2.5. Preparation of Positively Charged Allyl-functionalized β-Lactoglobulin 62

4.2.6. Preparation of Negatively Charged Allyl-functionalized β-Lactoglobulin … 63

4.2.7. Preparation of Positively Charged Protein-Polymer Conjugates using Photoinduced Cycloaddition Chemistry 63

4.2.8. Preparation of Negatively Charged Protein-Polymer Conjugates using Photoinduced Cycloaddition Chemistry 64

4.2.9. Self-Assembly of Proteinionosomes 64

4.3. Results and Discussion 65

4.4. Conclusion 71

4.5. Output 72

CHAPTER 5: Photoinduced Cycloaddition Reaction of Tetrazoles to Proteins in a Conjugation System 73

5.1. Introduction 73

5.2. Experimental 75

5.2.1. Materials and Methods 75

5.2.2. Photoinduced Cycloaddition Reaction of PEG-tetrazoles to Native Proteins 75

5.2.3. Preparation of Allyl-functionalized JR2EC Polypeptides 76

5.3. Results and Discussion 77

5.4. Conclusion 88

5.5. Output 88

CHAPTER 6: Conclusion & Future Perspectives 89

LIST OF PUBLICATIONS & CONFERENCES 91

BIBLIOGRAPHY 92

APPENDIX A: Transmission Electron Microscope (TEM) Imaging 106

APPENDIX B: Cryo-TEM Imaging 107

APPENDIX C: Static Light Scattering (SLS) Measurements 108

APPENDIX D: Labeling of GOx with Alexa-488 109

APPENDIX E: Flow Cytometry Analysis 111

APPENDIX F: 1H-NMR Spectra 113

APPENDIX G: Ellman's Test 115

APPENDIX H: Fast Protein Liquid Chromatography (FPLC) 116

APPENDIX I: SDS-PAGE 117

APPENDIX J: Protein Database Structures 119

LIST OF FIGURES

Figure 2.1. Schematic representation of block copolymer geometries with the respective cryogenic transmission electron microscopy images. Vesicles, wormlike micelles and spherical micelles are observed (**A**). Scaling of polymersome membrane thickness with copolymer molecular weight (MW) (**B**). Reprinted with permission from ref.[34] Copyright © 2006 Annual Reviews. 10

Figure 2.2. Particle size distribution obtained by dynamic light scattering for PB-PEO polymersomes prepared by rehydration + extrusion/sonication and by image analysis for polymersomes prepared by simple rehydration or electroformation, together with their respective TEM images (**A**). Reprinted with permission from ref.[35] Copyright © 2009 Royal Society of Chemistry. Schematic diagram of the microcapillary geometry for generating double emulsions for use in polymersome formation, together with the bright-field microscope and fluorescence microscope images of PEG-PLA polymersomes encapsulating the green FITC-Dextran (**B**). Reprinted with permission from ref.[39] Copyright © 2008 American Chemical Society. 13

Figure 2.3. Schematic representation of the proposed self-assembly of poly(L-lysine)60-b-poly(L-leucine)20 into polymersomes. Reprinted with permission from ref.[49] Copyright © 2005 American Chemical Society. 15

Figure 2.4. Schematic representation of PICsomes composed by mixing a pair of oppositely charged block copolymers in aqueous medium (**A**). Synthesis of a pair of oppositely charged block copolymers from poly(ethylene glycol)-b-poly(β-benzyl-L-aspartate) (PEG-PBLA) (**B**). Reprinted with permission from ref.[48] Copyright © 2006 American Chemical Society. 16

Figure 2.5. Time development of the morphological transformation of a PIC droplet upon laser irradiation (**A-J**) and after irradiation (**K-N**) (75 mM NaCl, laser power 0.25 W). The time of image is set as 0 s (**A**), and the elapsed times are 2.5 s (**B**), 3.5 s (**C**), 9.0 s (**D**), 12 s (**E**), 26 s (**F**), 65 s (**G**), 96 s (**H**), 140 s (**I**), and 165 s (**J**). The images **K-N** show the time course of the morphological transformation after laser irradiation was stopped. The intersections of the two white dashed lines indicate the position of the laser spot (**A, F-J**). The red arrow indicates a dark spot (**B**) and the black arrows indicate individual vesicular compartments (**D-G**). Reprinted with permission from ref.[57] Copyright © 2009 WILEY-VCH Verlag GmbH & Co. KGaA, Weinheim 17

Figure 2.6. Schematic representation of a vesicle with a corona of segregated polymer chains, as formed in a mixture of oppositely charged block ionomers (**A**). TEM image of the PIC vesicles (negatively stained with CsI), prepared from 0.01 wt % THF solution (**B**). Magnification of the framed area in (**B**), showing an individual vesicular aggregate (**C**). Reprinted with permission from ref.[59] Copyright © 2003 American Chemical Society. 18

Figure 2.7. Schematic representation of the preparation of proteinosomes. Mercaptothiazoline-activated PNIPAAm polymer chains were coupled with primary amine groups of cationized BSA-NH2 to generate protein-polymer nano-conjugates (BSA-NH2/PNIPAAm) (**A**). The spontaneous assembly of proteinosomes in oil, and their transfer into a bulk water phase (**B**). Reprinted with permission from ref.[60] Copyright © 2013 Macmillan Publishers Ltd.: Nature. 19

Figure 2.8. Schematic representation of a proteinosome membrane-mediated three-stage cascade reaction in water (**A**). Confocal fluorescence microscopy images of the same multi-enzyme proteinosome in water, showing red **(B)**, green (**C**), and blue (**D**) fluorescence associated with GA, GO and HRP, respectively, in the cross-linked membrane; scale bar = 10 μm. Reprinted with permission from ref.[62] Copyright © 2014 Royal Society Chemistry. 20

Figure 2.9. Schematic representation of various methods of polymersomes designed for therapeutic and diagnostic applications, for instance the antioxidant nanoreactor (**A**),[69] reconstitution of channel proteins in protein membrane (**B**),[68] polymersome nanoreactor (**C**),[30] polymersome encapsulated siRNA or antisense oligonucleotides (**D**),[70] image of a tumor-bearing mouse (**E**),[71] and third-party ATP sensor in polymersome (**F**).[64] Copyright © 2008 American Chemical Society, © 2001 Springer-Verlag Wien, © 2007 WILEY-VCH Verlag GmbH & Co. KGaA, Weinheim, © 2009 Elsevier Ltd., © 2008 Elsevier Ltd., and © 2014 WILEY-VCH Verlag GmbH & Co. KGaA, Weinheim. Reproduced with permission. 21

Figure 2.10. Schematic representation of the multistep reaction taking place in the three-enzyme PS-PIAT polymersome system (**A**). The generation of ABTS ·+ in the three-enzyme system at pH 7.2, followed by UV/Vis spectroscopy (**B**). GAc4 = 1,2,3,4-tetra-O-acetyl-b-glucopyranose. Reprinted with permission from ref.[30] Copyright © 2007 WILEY-VCH Verlag GmbH & Co. KGaA, Weinheim. 23

Figure 2.11. Single injection of (DOX + TAX)-loaded polymersomes shows rapid shrinkage of the tumor, compared to the free drug (administered at maximum tolerated doses) (**A**). Fluorescent microscopy images of TUNEL labeled MDA-MB231 tumor tissue, with large increases in TUNEL positive cells observed 48 hours after polymersome-drug treatments. Scale bar: 20 μm (**B**). Quantitation of apoptosis in tumors day 1 and 2 post-injection (**C**). Reprinted with permission from ref.[75] Copyright © 2006 Elsevier Ltd. 25

Figure 2.12. Tumor imaging of NIR-emissive polymersomes. Fluorescence images of the same mouse (prone position) taken prior to administration of NIR-emissive polymersomes, and at 4, 8, and 12 hours after tail-vein injection (λex = 785 nm, λem = 830-900 nm). Reprinted with permission from ref.[71] Copyright © 2008 Elsevier Ltd. 26

Figure 2.13. Schematic representation of the proposed method for the detection of ATP conversion inside the porous vesicular compartment. Reprinted with permission from ref.[64] Copyright © 2014 WILEY-VCH Verlag GmbH & Co. KGaA, Weinheim. 27

Figure 2.14. The synthesis of non-spherical multicompartmentalized polymersomes through water-oil-water (W/O/W) double emulsion technique with the block copolymers in the oil phase (**A**). As the organic solvent evaporates, the block copolymers attract each other at the interface to form the membrane bilayers (**B**). Upon complete evaporation of the organic solvent, multicompartmentalized polymersomes result (**C**). Fluorescence microscopy image of PEG_{5000}-b-PLA_{5000} polymersomes encapsulating fluorescent FITC-Dextran solution and a non-fluorescent PEG solution in the separate compartments (scale bar is 200 μm) (**D**). Reprinted with permission from ref.[92] Copyright © 2011 Macmillan Publishers Ltd.: Nature 29

Figure 2.15. Confocal microscope image of polymersomes containing several inner polymersomes encapsulating sulforhodamine B (red), 8-hydroxyl-1,3,6-pyrenetrisulfonic acid (green), and a mixture of both dyes (yellow) (**A**). Schematic representation of a triple polymersome showing bilayers with no internal

homopolymer on top and two of the bilayers containing homopolymer on the bottom (**B**). Series of confocal images showing sequential dissociation of membranes from the outermost to the innermost polymersomes (**C**) and from the innermost to the outermost polymersomes (**D**). Reprinted with permission from ref.[93] Copyright © 2011 American Chemical Society. 30

Figure 2.16. Schematic representation of the multicompartmentalized polymersomes assemblies equipped with pH-responsive transmembrane channels from two-stage double emulsion of poly(AAc-co-DSA) (**A**). The pH-responsive process is reversible in the range of pH 5-8. Confocal microscope images of Nile Red stained polymersomes (**B**) with the addition of calcein at pH 5.0 (polymersomes are impermeable to calcein) (i.), after pH adjustment to 8.0 (calcein diffuses into polymersomes) (ii.), and after replacement with fresh buffer of pH 5.0 (calcein is confined within polymersomes) (iii.) Reprinted with permission from ref.[94] Copyright © 2008 WILEY-VCH Verlag GmbH & Co. KGaA, Weinheim. 31

Figure 2.17. Schematic representation of the emulsion centrifugation technique generating polymersome-in-polymersome model system (the smaller red vesicles represent the inner nanosize polymersomes of PTMC-b-PGA in an aqueous solution at 380 mOsm sucrose) (**A**). Spinning disk confocal microscopy images of red nanosize polymersomes (Alexa Fluor 568) in a green giant polymersome (Alexa Fluor 488) (**B**). From left to right: green channel, red channel, overlay and 3D reconstruction (red channel). Scale bar: 20 μm. Reprinted with permission from ref.[87] Copyright © 2008 WILEY-VCH Verlag GmbH & Co. KGaA, Weinheim. 32

Figure 2.18. Schematic representation of the preparation of functional cell mimic, showing encapsulation of different enzymes in PS-PIAT vesicles, followed by mixing of the artificial organelles, cytosolic enzymes and reagents, prior to encapsulation into PB-PEO vesicles to create multicompartmentalized structure (**A**). Detailed cascade reaction scheme, in which phenyl acetone monooxygenase (PAMO) catalyzes profluorescent substrate **1** in the presence of cofactor nicotinamide adenine dinucleotide phosphate (NADPH) under a Baeyer-Villiger reaction to form ester **2**, which is then being hydrolyzed by the enzyme Candida Antarctica lipase B (CalB) or Alcalase to give primary alcohol **3**. Using the cofactor nicotinamide adenine dinucleotide (NAD+), the alcohol is later oxidized by alcohol dehydrogenase (ADH) to generate aldehyde **4**, which subsequently undergoes spontaneous beta-elimination to produce fluorescent resorufin **5** (**B**). Reprinted with permission from ref.[95] Copyright © 2014 WILEY-VCH Verlag GmbH & Co. KGaA, Weinheim. 33

Figure 2.19. Schematic representation of the multicompartmentalized polymersomes (**A**). Scanning confocal fluorescence image of multicompartmentalized polymersomes (**B**). Red spots correspond to Cy5-IgG encapsulated in individual PS-PIAT polymersomes (**C**), whereas green spots correspond to GFP encapsulated in individual ABA polymersomes (**D**). Yellow spots result from the overlap of the ABA and PS-PIAT signals, which correspond to the multicompartmentalized polymersomes (**E**). Reproduced with permission from ref.[89] Copyright © 2011 Royal Society of Chemistry. 34

Figure 3.1. The absorbance at 295 nm and the peroxidase activity for each fraction of ABA polymer vesicles with OmpF channel proteins (**A**) and without OmpF channel proteins (**B**) collected from the Sepharose 4B column. The activity was measured as change in fluorescence emission at 590 nm min (FI min^{-1}). The schematic representation of the architecture of polymersome is shown on the top left corner. HRP enzyme activity in ABA vesicles with OmpF channel proteins (*red line*)

compared to a blank without OmpF channel proteins (*blue line*) using either TMB substrate (**C**) or amplex red substrate (**D**). ……46

Figure 3.2. TEM images of individual ABA polymersomes (**A**) and multicompartmentalized polymersomes (**B**). The samples were stained with 1% phosphotungstic acid. Scale bars are 100 nm. The average size of ABA polymersomes (*red line*) and MC polymersomes (*green line*) measured with DLS (**C**)..... 47

Figure 3.3. Activity of GOx enzyme (measured by addition of HRP) of the flow-throughs (ft 1-ft 6) from the centrifuge filtration compared to the MC polymersomes (i.e. the supernatant/sn). Activities were measured at 590 nm. 48

Figure 3.4. Activity of the cascade reactions in MC polymersomes (*green line*) compared to a blank where no OmpF channel proteins were embedded in the ABA vesicles (*blue line*) using TMB assay (**A**) or Amplex red assay (**B**). 49

Figure 3.5. Cascade activity of the MC polymersomes as compared to the controls using Amplex red assay, showing an increased conversion of amplex red..... 50

Figure 3.6. Bulk cascade measurements. Conversion of amplex red versus time by the GOx/HRP cascade, as measured by the increase of fluorescence at 590 nm (**A**). For comparison, the time trace of the reaction in the presence of MC polymersomes (orange dots), as well as that of ABA nanoreactors in the presence of free GOx (0.3 mg mL^{-1}) is also shown. Plot of initial velocities of the bulk reactions measured in A versus HRP concentration (**B**). 51

Figure 3.7. Confocal microscope images of MC polymersomes (**A**) and the blank MC polymersomes where no OmpF porins were embedded in the inner compartment (**E**). MC polymersomes and the blank MC polymersomes were prepared as described before. GOx was labeled with Alexa Fluor 488 and imaged in the blue channel (**B**; and **F** for the blank). After preparation of MC polymersomes, HRP was stained by its reaction with Alexa Fluor 647 tyramide and imaged in the red channel. (**C**). Fluorescence in the red channel was only observed when the OmpF porin was present in the inner compartment (compare **C** and **G**). The composite image of the blue and red channel which show the *colocalization* of the images (**D**). (**B, C, D** are the magnification of **A**, as specified by the white square; whereas **F, G** are magnification of **E**). The scale bars are 20 μm. 53

Figure 3.8. Flow cytometry analysis of the multicompartmentalized polymersomes. MC polymersomes containing unlabeled HRP and GOx enzymes, in which no fluorescence is detected in the sample (**A**). MC polymersomes containing alexa-674 labeled HRP and alexa-488 labeled GOx (**B**). Here, HRP is labeled with tyramide staining, in which only active HRP is observed. Regions P4 and P5 denote alexa-647 labeled HRP (i.e. ABA polymersomes, *red dots*) and alexa-488 labeled GOx (i.e. PS-PIAT polymersomes, *dark green dots*), respectively, whereas region P6 denote the double-labeled enzymes (i.e. MC polymersomes, *blue dots*). For a detailed discussion of the flow cytometry results, see **Appendix: Figure E1**..... 54

Figure 4.1. Self-assembly of fluorescent proteinionosomes from new building blocks of oppositely charged PEG-BLG complexes that are fluorescent. ....……57

Figure 4.2. Schematic representation for the chemical modification of BLG at the free cysteine residue at Cys-121 to the formation of positive (A) and negative (B) charged of PEG-BLG conjugates under photoinduced cycloaddition chemistry. The positive and negative groups of BLG-allyl were introduced by reacting the glutamate and lysine residues with suitable reagents, respectively. 66

Figure 4.3. SDS-PAGE gel for each different purified products (A). MALDI-TOF spectra for the positively charged PEG-BLG conjugates (B) and negatively charged PEG-BLG

conjugates (C) showing the presence of singly, doubly and triply conjugated BLG, apart from the unreacted modified BLG. 67

Figure 4.4. MALDI-TOF spectra for the positively charged PEG-BLG conjugates (**A**) and negatively charged PEG-BLG conjugates (**B**) after purification by FPLC via ionic-exchange column chromatography. Inset is the DLS data showing that the size of the charged conjugates is about 8 nm. 68

Figure 4.5. Fluorescence measurement shows that the proteinionosomes are fluorescent with strong fluorescence emission at 490 nm (**A**). DLS data shows the hydrodynamic diameter (D_H) of the proteinionosomes is about 80 nm (**B**). TEM images of the proteinionosomes (**C**), stained with 2% uranyl acetate. Scale bars are 100 nm. 69

Figure 4.6. Enzyme activity inside the proteinionosomes was compared with the free HRP enzymes (roughly having similar concentration, i.e. 0.1 mg/mL) and the blank (without HRP). The enzyme encapsulated proteinionosomes shows an increased conversion of amplex red, indicating that the enzyme is active 71

Figure 5.1. Characterization of the products formed by photoinduced cycloaddition of PEG-tetrazole (5.0 equiv.) with BLG-allyl and native BLG by fluorescence spectroscopy (**A**) and SDS-PAGE gel (**B**), showing the formation of PEG-BLG conjugate. Fluorescence spectra after photoirradiation of increasing equivalents of PEG-tetrazole (0.5 – 5.0 eqs) with BLG-allyl (**C**) and native BLG (**D**) show formation of chemically distinct conjugates. Chart representation of the fluorescence intensity at 510 nm versus increasing equivalents of PEG-tetrazole used with BLG-allyl (*red line*) and native BLG (*blue line*) (**E**). ..……..78

Figure 5.2. MALDI-TOF spectra for the photoinduced cycloaddition reactions of PEG-tetrazole to native BLG (A) and PEG-tetrazole to BLG-allyl (B), showing the presence of multiple site conjugates of BLG, apart from the externally introduced dipolaraphile. 80

Figure 5.3. Fluorescence spectra for the photoinduced cycloaddition reaction of PEG-tetrazole to native HRP, CalB and lysozyme before (**A**) and after (**B**)UV irradiation. 81

Figure 5.4. Fluorescence spectra, MALDI-TOF and SDS-PAGE gel for the photoirradiation of increasing equivalents of PEG-tetrazole to unmodified lysozyme (**A**), CalB (**B**), and HRP (**C**), respectively. For SDS-PAGE, bands indicated by i represents the conjugated product, while ii represents the free enzyme. 82

Figure 5.5. Amino acid sequence of JR2EC (**A**). A cysteine is present at position 22. Reproduced with permission from ref.[122] Copyright © 2008 WILEY-VCH Verlag GmbH & Co. KGaA, Weinheim. Fluorescence spectra of the photoirradiation of increasing equivalents of PEG-tetrazole (0.5–3.0 eqs) with unmodified polypeptide JR2EC (*blue line*) and JR2EC-allyl (*red line*), showing absence of fluorescent product for unmodified polypeptide JR2EC (**B-C**). 84

Figure 5.6. Fluorescence spectra (**A**) and MALDI-TOF analysis (**B**) for the reaction of PEG-tetrazole with excess tryptophan before irradiation (*red line*) and after irradiation (*blue line*), indicating addition of amino acid to the PEG polymer. 85

Figure A1. TEM images of individual ABA polymersomes encapsulating HRP and OmpF incorporated in the membrane before (**A**) and after addition of THF (**B**), individual PS-PIAT polymersomes (**C**), and the multicompartmentalized polymersomes (**D**). The samples were stained with 1% phosphotungstic acid. Scale bars are 100 nm.……...……..106

Figure B1. Cryo-TEM images of individual ABA polymersomes (**A**) and multicompartmentalized polymersomes (**B**). Arrows indicate the presence of inner compartments. Scale bars are 100 nm and 200 nm respectively…… 107

Figure C1. Berry plot of the MC polymersomes at various concentrations. A concentration range of 62.5–500 μg mL^{-1} was employed in the static light scattering measurements. Static light scattering measurements provided a radius of gyration of 163 nm (± 28), as determined from slope and intercept of the linear fit at different measurement angles, resulting in a R_G/R_H (ρ-value) of 1.10, indicative of the vesicular structure.[96]…….. 108

Figure D1. Absorption spectra of alexa-488 labeled Gox encapsulated in the multicompartmentalized polymersomes (MCPs). Spectra were acquired before and after filtration, with (black line), and without OmpF (dotted line) present in the ABA membrane. Although the absorption spectra are obscured by scattering from the polymersomes, a clear signal from the dye is observed……..……..109

Figure E1. Flow cytometry analysis of the multicompartmentalized polymersomes. FSC/SSC dot plots of PBS (**A**) and MC polymersomes (**B**) respectively. Gating was applied (region P7) to capture the majority of the polymersomes and to exclude background from PBS. Dot plot of FITC (530 ± 15 nm for detection of alexa-488) against APC (660 ± 10 nm for detection of alexa-647) for PS-PIAT polymersomes with alexa-488 labeled GOx (**C**), ABA polymersomes with alexa-647 labeled HRP (**D**), and MC polymersomes containing unlabeled enzymes (**E**) after applying gate P7. Regions P4, P5, and P6 were selected to reflect polymersomes containing alexa-647 only (*red dots*), polymersomes containing alexa-488 only (*dark green dots*), and polymersomes containing both alexa-647 and alexa-488 (*blue dots*), respectively. Dot plot of FITC/APC for MC polymersomes containing labeled enzymes (**F**) after applying gate P7. Note that region P5 was narrowed to exlcude intrinsic fluorescence of individual PS-PIAT polymersomes (as observed in **C**). MC polymersomes containing alexa-647 and alexa-488 make up 28% of the total polymersome population, while individual ABA polymersomes containing alexa-647 and individual PS-PIAT polymersomes containing alexa-488 make up 5.7% and 16.2% of the total polymersome population respectively. The remainder of the polymersome population does not contain labeled enzymes.……..111

Figure G1. The reaction of DTNB with thiol group. Reprinted with permission from ref.[115] Copyright © 1983 Elsevier Ltd……115

Figure H1. FPLC chromatograms following the purification of positively charged PEG-BLG conjugates (**A**) and negatively charged PEG-BLG conjugates (**B**) via ionic-exchange column chromatography…….……..116

Figure I1. SDS-PAGE of the product of PEG-tz and native BLG, after photoirradiation at increasing equivalents of PEG-tz (0.5, 1.0, 2.0, 3.0 and 5.0 eqs). Bands indicated by **i** represent the conjugated product, while **ii** represents native BLG……..117

Figure I2. SDS-PAGE of the product of PEG-tz and native HRP, after photoirradiation at increasing equivalents of PEG-tz (0.5 – 10.0 eqs). Bands indicated by **i** represent the conjugated product, while **ii** represents native HRP. 117

Figure I3. SDS-PAGE of the product of PEG-tz and native CalB, after photoirradiation at increasing equivalents of PEG-tz (0.5 – 10.0 eqs). Bands indicated by **i** represent the conjugated product, while **ii** represents native CalB. 117

Figure I4. SDS-PAGE of the product of PEG-tz and native lysozyme, after photoirradiation at increasing equivalents of PEG-tz (0.5 – 10.0 eqs). Bands indicated by **i** represent the conjugated product, while **ii** represents native lysozyme. 118

Figure J1. Graphic representations of HRP, CalB, Lysozyme and BLG, with tryptophan residues shown in red. The picture was rendered using PyMOL (PDB ID for HRP, CalB, lysozyme, and BLG: 1ATJ, 3ICV, 6LYZ and 1QG5, respectively). HRP,

CalB, BLG and lysozyme contain one (Trp-117), five (Trp-86, Trp-99, Trp-138, Trp-147, and Trp-189), two (Trp-19 and Trp-61), and six tryptophan residues (Trp-28, Trp-62, Trp-63, Trp-108, Trp-111, and Trp-123), respectively…….119

Scheme 3.1. Flow diagram for the preparation of vesicle-in-vesicle structure (**A**). Schematic representation of location of the enzymes in multicompartmentalized (MC) polymersome and the reaction scheme of the bi-enzymatic cascade reactions forming the basis for the assay of glucose, using either substrate TMB or amplex red (**B**)…….……..38

Scheme 3.2. Schematic representation of tyramide signal amplification (TSA). HRP-catalyzed reaction of tyramide-functional fluorescent dyes with tyrosine moieties, giving rise to self-staining. The dye depicted is alexa-488. The structure of tyramide-alexa-647 has not been reported at this time. 44

Scheme 4.1. Photoinduced cycloaddition reaction involves tetrazole and alkene to generate pyrazoline cycloadduct, which is fluorescent. Reproduced with permission from ref.[100] Copyright © 2008 WILEY-VCH Verlag GmbH & Co. KGaA, Weinheim……..58

Scheme 4.2. Schematic representation for the chemical modification of BLG at the free cysteine residue at Cys-121 to the formation of positive and negative charged of PEG-BLG conjugates under photoinduced cycloaddition chemistry. The positive and negative groups of BLG-allyl were introduced by reacting the glutamate and lysine residues with suitable reagents, respectively. 59

Scheme 5.1. Preparation of PEG-BLG conjugates by the photoinduced cycloaddition reaction of PEG-tetrazole. Apart from the procedure outlined (**A**), which involves reaction of BLG with allyl chloride, a significant side reaction occurs when performing the photoinduced cycloaddition reaction in the presence of native protein (**B**).……74

Scheme 5.2. Proposed structure (**1**) of the possible conjugate formed by photoinduced cycloaddition reaction of PEG-tetrazole to tryptophan residues in proteins. Structure (**2**) shows a possible bisadduct of the PEG-tetrazole. The amide back bone of the protein is shown as a single residue. 87

LIST OF TABLES

Table 2.1. The chemical structures of common examples of amphiphilic block copolymers that assemble into polymersomes. 11

Table D1. Calculation of encapsulation efficiency. Area of the alexa-488 absorption peak in the UV-Vis spectra of MCPs, before and after filtration, and estimation of the GOx concentration. The scattering has been substracted by fitting to an exponential decay function. 110

Table E1. Encapsulation efficiencies as calculated from Figure E1.D. 112

Table E2. Encapsulation efficiencies as calculated from Table E1. 112

Table G1. Ratio of free thiols to BLG molecule before and after reaction. 115

LIST OF ABBREVIATIONS

ABTS:	2,2'-azinobis(3-ethylbenzothiazoline-6-sulfonic acid)
ALP:	alkaline phosphatase
ATP:	adenosine triphosphate
BLG:	β-lactoglobulin
BSA:	bovine serum albumin
CalB:	*Candida Antarctica* lipase B
DMAP:	4-dimethylaminopyridine
DLS:	dynamic light scattering
DMF:	dimethylformamide
DMSO:	dimethyl sulfoxide
DNA:	deoxyribonucleic acid
DOX:	doxorubicin
DTNB:	5,5'-dithio-bis-(2-nitrobenzoic acid)
EDC:	1-Ethyl-3-(3-dimethylaminopropyl)carbodiimide hydrochloride
FPLC:	fast protein liquid chromatography
GA:	glucose amylase
GAc4:	1,2,3,4-tetra-O-acetyl-b-glucopyranose
GO/GOx:	glucose oxidase
HRP:	horseradish peroxidase
OmpF:	outer membrane protein F
MALDI:	matrix-assisted laser desorption/ionization
MC:	multicompartmentalized
M_n:	number average molecular weight
M_w:	weight average molecular weight
NIRF:	near infrared fluorescence
PAA:	polyacrylic acid
PAGE:	polyacrylamide gel electrophoresis
PB:	polybutadiene
PBLA:	poly(β-benzyl-L-aspartate)
PBS:	phosphate buffer saline

PDI:	polydispersity index (M_w/M_n)
PDMS:	polydimethylsiloxane
PEE:	polyethyl ethylene
PEG/PEO:	polyethylene glycol/ polyethylene oxide
PGA:	poly(L-glutamic acid)
PIAA:	polyisocyano dialanine
PIAT:	polyisocyanoalanine(2-thiophene-3-yl-ethyl)amide
PIC:	polyion complex
PLA:	polylactic acid
P(Leu):	poly(L-leucine)
PLG:	poly(L-glutamate)
PLL:	poly(L-lysine)
PMOXA:	poly-(2-methyloxazoline)
PNIPAAm:	poly(*N*-isopropylacrylamide)
PS:	polystyrene
PTFE:	polytetrafluoroethylene
PTQ:	poly(1-(3-((4-methylthiophen-3-yl)oxy) propyl) quinuclidin-1-um)
PTMC:	poly(trimethylene carbonate)
PVDF:	polyvinylidene fluoride
R_G:	radius of gyration
R_H:	hydrodynamic radius
RNA:	ribonucleic acid
SCFM:	scanning confocal fluorescence microscope
SDS:	sodium dodecyl sulfate
SLS:	static light scattering
TAX:	paclitaxel (taxol)
TEM:	transmission electron microscope
THF:	tetrahydrofuran
TMB:	3,3',5,5'-tetramethylbenzidine
TOF:	time-of-flight
W/O/W:	water-oil-water

CHAPTER 1
Introduction

1.1. Background

All living organisms are built from cells, the building blocks of life, of which a fundamental feature is that they are enveloped by a membrane or plasma membrane, made from a double layer of amphiphilic molecules termed lipids. Cell membrane has diverse roles in nature: they separate and protect the cell from the outside environment, facilitate the selective transport of substance, such as essential molecules or ions into the cell by virtue of its 'semi-permeable' characteristics, as well as recognize and transduce biological signals.[1-4] Besides plasma membrane, cells contain many features and soft cellular organelles; each with different functions and unique chemistry. For instance, the cell nucleus – known as a cell's information center – consists of chromosomes in which the inheritable genetic materials (i.e. DNA) are located; cytoplasm, which comprises of cytosol (a fluid segment), organelles and other particulates suspended within the plasma membrane; and ribosomes, are organelles that involve in the protein synthesis.[1,2] Indeed, the complexity of the cell has fascinated scientists and engineers to develop novel architecture to mimic cellular compartments.

In order to achieve this, researchers have designed a model system based on lipids to mimic and study the basic design principles of biological membranes. Since the first discovery by A. D. Bangham and R. W. Horne in 1961,[5-7] lipid vesicles, commonly known as liposomes, have attracted ample of scientific attention. Liposomes are spherical vesicles composed of phospholipids which spontaneously self-assemble into a bilayer membrane architecture, typically about 3-5 nm thick, with hydrophobic chains of the lipids outlining the bilayer, and polar groups of the lipids facing towards the inner compartment and the extra-vesicular solvent. Since their inception, liposomes have been

implicated for use in various applications, including medicine, diagnostics, and cosmetics.[8-15] However, only in cosmetics have they found widespread practical applications. In the area where such vesicles have been envisioned to really make an impact, i.e. drug delivery and targetting, only one commercial product has been approved by the FDA: Doxil, which is a liposome-encapsulated anticancer drug. This lack in commercial applications is mainly the results of the inherently labile structure of the liposomal membrane and the tendency of liposomes to fuse and aggregate, limiting both shelf life and their applicability in demanding (i.e.) practical applications. Furthermore, to mimic liposomes as functional compartments, the lipid bilayer has to be made permeable for transport of molecules and this can be achieved only by incorporating small porin channel to the membrane to overcome this limitation.[16-17] Scientists, inspired by progress in polymer sciences and biotechnology, have therefore come up with alternative approaches to construct vesicular, cell-mimicking architectures, such as layer-by-layer particles, modified viruses and other protein capsules and polymersomes.

Polymer vesicles or polymersomes are formed by the self-assembly of amphiphilic block copolymers in dilute aqueous medium, resulting in physically more resilient membranes that can vary in thickness from 4 to 30 nm, as compared to natural or synthetic lipid membranes.[18-25] Compared to liposomes, this polymer-based architecture has shown to be superior in mechanical stability and chemical versatility which allows one to tune their properties in terms of permeability and stimuli-responsiveness, as was most convincingly shown by two seminal Science publications by the groups of Discher and Eisenberg.[21-22] The superior mechanical stability is attributed to the lower critical aggregation concentration of the constituting amphiphilic block copolymers because of the increased molecular weight of the amphiphiles and the entagled nature of the membranes formed (as opposed to the fluid-like organization of lipid membranes).[19,24] Practically this means that the consituting polymers allow a much higher degree of

chemical modification and fuctionalization without having a negative effect on their self-assembly properties. It furthermore results in dispersions that are stable and not prone to fusion and aggregation that limit the shelf-life of liposomes.[22] As a result, with respect to practical applications, polymersomes may prove to be advantageous over liposomes. In fact, their potential has been demonstrated in numerous applications, ranging from drug delivery, gene therapy, protein delivery, medical imaging, nanoreactors, and artificial organelles.[19-20,25,27] In addition, polymersomes are promising platforms as carriers of pharmaceutically active molecules, such as drugs, enzymes, antibodies and peptides, and DNA and RNA fragments.[19,26-31]

1.2. Motivation

Although much progress has been made in constructing singular compartments, we are still far in away in mimicking the basic functions of cells such as self-replication, energy homeostasis and the synthesis of essential building blocks. Mimicking these processes and even constructing a basic synthetic cell is not only exciting from an academic perspective, giving insight into the origin of life on earth, but also from an application perspective, as it would progress the field of targeted delivery of genes and drugs, which is currently still mainly an academic undertaking.

One principle of cellular life is the concept of compartmentalization, where simultaneous chemical processes occuring are separated in space so as not to obstruct each other. For instance, chemical pathways to synthesis and degradation of molecules (both small molecules and macromolecules) need to be separated. Energy homeostasis depends on gradients that are maintained and protected from lethal interference by the complex membraneous organization of the mitochondrium.

Since it is now possible to create stable and addressable (single-compartment) cell-mimicking architectures, which in addition can be tweaked to a large extent for specific functions, *this thesis' main focus is to take these single-compartments and assemble higher-order (i.e. multicompartment) functional architectures.* Direct applications for such architectures are in the field of drug delivery, where multicompartmentalization could be of use to better control the release of drugs (or even cocktails of drugs) by multiple stages of stimuli-responsive release (i.e. combination of temperature and redox sensitive) particles. One could envision the localized synthesis of drugs from so-called prodrugs or simple bulding blocks by the action of intricate enzymatic cascades.

For in-vitro application to be succesful, it has been shown that the optimal particle size should be between 200-500 nm to prevent direct absorption by globular membranes. Hence, this thesis especially focuses on the construction of multicompartment architectures in this size range.

1.3. Objectives

My PhD study is to create novel bio-functional architectures of polymersomes as an attempt to mimic the complexity of the living cells in particularly organelles; these are compartments within cells with unique functions and chemistries. In order to mimic this cell function, I self-assemble novel higher-order architectures of polymersomes using amphiphilic block copolymers. The focus is then on the *functionality* of these compartments and how they affect the perfomance of the entire structure. To do so, multicompartment nanoreactors are constructed from permeable polymersomes that separately contain enzyme and hence are able to carry out a simple chemical reaction. These are then combined into one multicompartment structure and their integration is

shown by a cascade reaction between enzymes in the separate compartments. Finally, in the search for novel biocompatible compartments that could serve as building blocks for multicompartment architectures, I present the synthesis of a new type of polymer-protein conjugate that assembles into proteinaceous capsules.

1.4. Hypothesis

Eukaryotic cells consist of many features with different functions and chemistries. In order to study them, a model system using synthetic amphiphilic polymers as key building blocks are built to mimic the features of cells, particularly compartmentalization. In order to mimic simple-like organelle complexity, polymersomes with multi-compartment structures are developed. In addition, protein-polymer complexes are synthesized as new building blocks to self-assemble as unique compartments.

1.5. Scope

In the first part, to develop higher-order architectures that mimic cellular compartmentalization, synthetic amphiphilic ABA (i.e. PMOXA-PDMS-PMOXA: poly(2-methyloxazoline)–poly(dimethylsiloxane)–poly(2-methyloxazoline)) and PS-PIAT (polystyrene–polyisocyanoalanine(2-thiophen-3-yl-ethyl)amide) block copolymers are employed since they have been thoroughly studied in literature, albeit separately, and they are (or can be made) permeable to small organic molecules. The ABA triblock copolymer has been shown to have a hydrophilic and a biocompatible low protein-binding surface, as well as high mechanical and thermal stability. Importantly, it has been shown that membrane protein channels can be integrated to allow exchange of solutes, and nanoreactors have been reported where an encapsulated enzyme performs a chemical

reaction on externally added substrate. Similarly, PS-PIAT polymersomes are intrinsically permeable to small molecules and their use as nanoreactors have been demonstrated. In this work, we use a sequential self-assembly method to prepare multicompartments polymersomes from ABA and PS-PIAT, since this method results in nanoscale vesicles that are applicable for in-vivo application. In addition to the dimensions, the novelty of this architecture is its close resemblance with natural membranes where an inner compartment exchanges molecules with the outside compartment via a channel protein. Hence, our system could make use of the high selectivity of channel proteins and transporters found in nature, a selectivity that greatly surpasses what would be available by simple polymer membranes.

In the second part, in order to develop unique compartments that are biocompatible and biodegradable, protein-polymer complexes are designed and synthesized. The major bovine milk protein β-lactoglobulin (BLG) has been chosen in this work because of a) its documented self-assembly behavior, b) its availability in pure form, and c) its low price, which bodes well for actual application. The novelty of this work is further the use of a photoinduced cycloaddition reaction (a type of click chemistry) to conjugate the chemically-tuned protein to polymer, which results in fluorescent nanocompartments upon self-assembly.

1.6. Synopsis of the thesis

This thesis will focus on the development of novel bio-functional higher-order architectures of polymersomes using synthetic amphiphilic block copolymers to mimic cell compartments, and on the development of novel self-assembled vesicles using new building blocks of protein-polymer complexes. It is divided into 6 chapters as summarized below:

Chapter 2 describes the current literature on polymersomes focusing on their physical properties, their fabrication, and applications in biomedicine and biotechnology. This chapter will include the latest development of self-assembled vesicles using building blocks of peptide-based and protein-based block copolymers. Their recent applications in the formation of multicompartmentalized systems with several aqueous compartments will also be covered.

Chapter 3 covers the preparation of multicompartmentalized architectures from diblock and triblock copolymers as model systems to mimic cells. Two different enzymes are encapsulated at separate compartments and a bi-enzymatic cascade reaction is carried out to demonstrate the functionality and complexity of cells.

Apart from using amphiphilic block copolymers, peptide-based and protein-based block copolymers can be used as building blocks for the construction of vesicles, as they are known to be more biodegradable and biocompatible. Chapter 4 presents the design and development of new supramolecules using a facile route of bio-orthogonal chemistry. PEG and BLG will be used for the construction of protein-polymer conjugates, in which they will be self-assembled into novel functional compartments. This chapter will also cover the study on the structural and functional characterization of the compartments to be used as cell mimics.

Chapter 5 will describe the further investigations of a side-reaction observed from the conjugation of polymer to protein of interest using bio-orthogonal chemistry reported in Chapter 4, where side reaction refers to an unwanted or unexpected chemical reaction taking place. Here, different proteins or enzymes commonly used in nanobiotechnology, along with a small polypeptide will be used and compared. Lastly, Chapter 6 will present a conclusion and future perspectives on the use of novel biofunctional architectures of polymersomes.

CHAPTER 2

Literature Review

2.1. Introduction of Polymersomes

In the past decade, polymersomes (also known as polymeric vesicles) have attracted ample interest as a result of their analogy to cellular compartments, and they have seen extensive application in medicine and biotechnology, such as drug or gene delivery and nanoreactors. To demonstrate the diversity of polymersome designs already reported, this chapter first presents a review on (single-compartment) polymersomes made of amphiphilic block copolymers and their formation, where we focus on polymersomes that display some type of biological functionality (e.g., containing a peptide or protein block). Applications of polymersomes as nanoreactors, drug delivery devices and nanomedicine, as well as biosensors are highlighted. Finally, advances in the construction of multicompartment polymersomes are presented.

2.2. Self-Assembly & Fabrication of Polymersomes from Amphiphilic Block Copolymers

Polymersomes are nanoscale objects with a bilayer membrane enclosing an aqueous compartment. They self-assemble in dilute aqueous solution from various synthetic amphiphilic block copolymers; such as diblock copolymers,[20-21] triblock copolymers,[20,28] grafted polymers[32] and dendritic polymers.[33] This chapter will focus on the vesicular self-assembly from amphiphilic block copolymers of the AB and ABA types. For the AB-type block copolymers, two blocks of opposing polarity (hydrophilic and hydrophobic) are placed tail-to-tail to self-assemble into bilayers, whereas for ABA-type triblock

copolymers, the central B-block is isolated from the environment by its adjoining A-blocks.[20-22,28]

Polymersomes range in diameter from 10 nm to ~100 μm, depending on their chemical constitution and the size of their polymer blocks, as well as their preparation method.[19] Similar to lipids, the resulting aggregate morphology of amphiphilic block copolymers is dictated by the time-average molecular shape or geometry of the molecule which is reflected by the weight fraction of the hydrophilic block (denoted as *f*).[18] In practice, it has been observed that for self-assembly of block copolymers of polybutadiene-*b*-poly(ethylene glycol) (PB-PEG), in order to generate vesicles in an aqueous solution, the amphiphile geometry should approach a cylindrical shape, which correlates to *f* of 25-40%. Apparently, the cylindrically shaped molecule suggests the ability of hydration to balance an excessively large hydrophobic fraction.[21,34] Molecular shape in the form of wedge or cone will give rise to wormlike micelles (if f = 40-50%) or spherical micelles (if f > 50%) (See **Figure 2.1A**), or inverted microstructures (if f < 25%).[20,34-36]

It was found that increasing the *f* values (or the hydrophilic block length) of amphiphilic block copolymers results in the formation of smaller vesicles. For instance, an increase in the polyacrylic acid (PAA) block length of polystyrene-polyacrylic acid (PS-PAA) diblock copolymers would enhance the steric repulsion among the chains. The higher repulsion favors a decrease in the radius of curvature and contributes to the formation of smaller vesicles from copolymers with longer hydrophilic block length.[37] Moreover, in the case of biocompatible block copolymers, such as poly(ethylene glycol)-*b*-poly(lactic acid) (PEG-*b*-PLA), increasing the hydrophilic fraction leads to micellar structures as a result of the hydrolytic degradation of hydrophobic block.[25,34,36]

In most cases, the membrane thickness of polymersomes depends on the molecular weight or size of the hydrophobic block (**Figure 2.1B**).[34-35] Polymers of high molecular weight thus yield thicker, less permeable and mechanically more stable membranes.[20-22,28,34] In addition, because of the chemical versatility of polymers, polymersomes can be engineered easily to improve their mechanical stability, to endow stimuli responsiveness, or to introduce target functionality.[19,38] Several common examples of amphiphilic block copolymers that assemble into polymer vesicles are shown in Table 2.1.

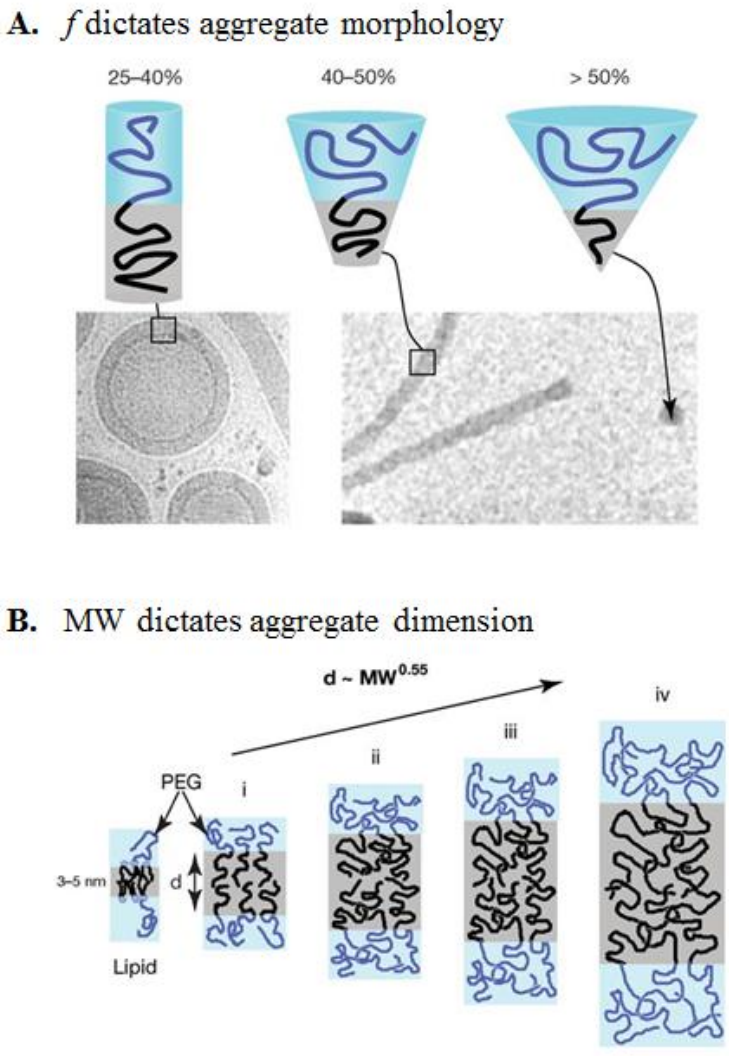

Figure 2.1. Schematic representation of block copolymer geometries with the respective cryogenic transmission electron microscopy images. Vesicles, wormlike micelles and spherical micelles are observed (**A**). Scaling of polymersome membrane thickness with copolymer molecular weight (MW) (**B**). Reprinted with permission from ref.[34] Copyright © 2006 Annual Reviews.

Table 2.1. The chemical structures of common examples of amphiphilic block copolymers that assemble into polymersomes.

Chemical Structure	Abbreviation
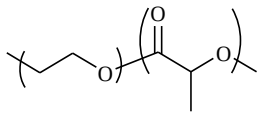	PEG-PLA
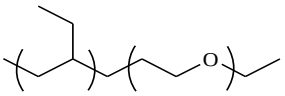	PEE-PEO
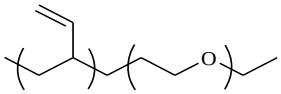	PB-PEO
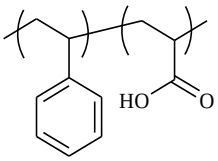	PS-PAA
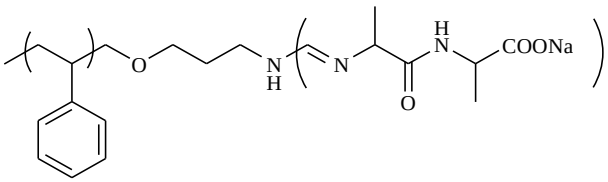	PS-PIAA
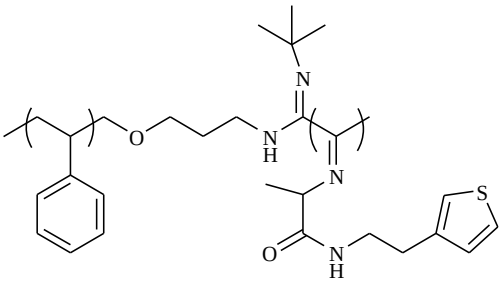	PS-PIAT
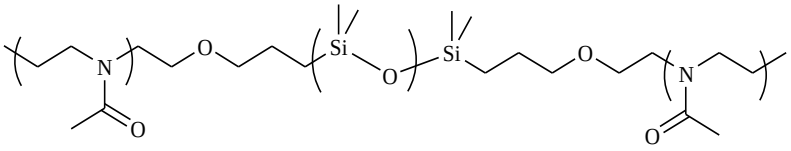	PMOXA-PDMS-PMOXA
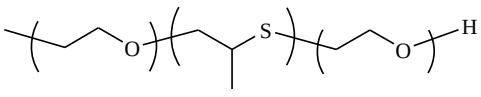	PEO-PPS-PEO

PEG = polyethylene glycol, PLA = polylactic acid, PEE = polyethyl ethylene, PEO = polyethylene oxide, PB = polybutadiene, PS = polystyrene, PAA = polyacrylic acid, PIAA = polyisocyano dialanine, PIAT = polyisocyanoalanine(2-thiophene-3-yl-ethyl)amide, PMOXA = poly-(2-methyloxazoline), PDMS = polydimethylsiloxane, PPS = polypropylene sulfide.

There are several techniques available to prepare polymersomes, i.e. direct dissolution of the polymers, hydration of a copolymer film, or the addition of water to a copolymer that is molecularly dissolved in an organic solvent, also known as direct injection method.[19,21-22] Usually, these methods result in a polydisperse size distribution of polymersomes and the aggregates of some polymersomes need to be extruded to reduce their polydispersity.[35,39-41] In general, these techniques will produce nano-polymersomes (in the 10-100 nm range). However, in order to form giant polymersomes (in the 10-100 μm range), alternative preparation protocols such as electroformation and spontaneous swelling in aqueous solution are utilized (See **Figure 2.2A**).[21-22,35,42-43] A novel approach was recently reported to prepare monodisperse polymersomes (in the μm range) by the use of water-oil-water (W/O/W) double emulsions generated by a glass capillary microfluidic technique (**Figure 2.2B**).[39] The amphiphilic block copolymer which was dissolved in the oil phase, assembled into polymersomes upon removal of the organic solvent by evaporation to yield high uniform polymer vesicles with excellent encapsulation efficiency.[39-41] In addition, the size of the vesicles could be adjusted by changing the polymer structure in the organic phase or by changing the organic solvent composition.[40]

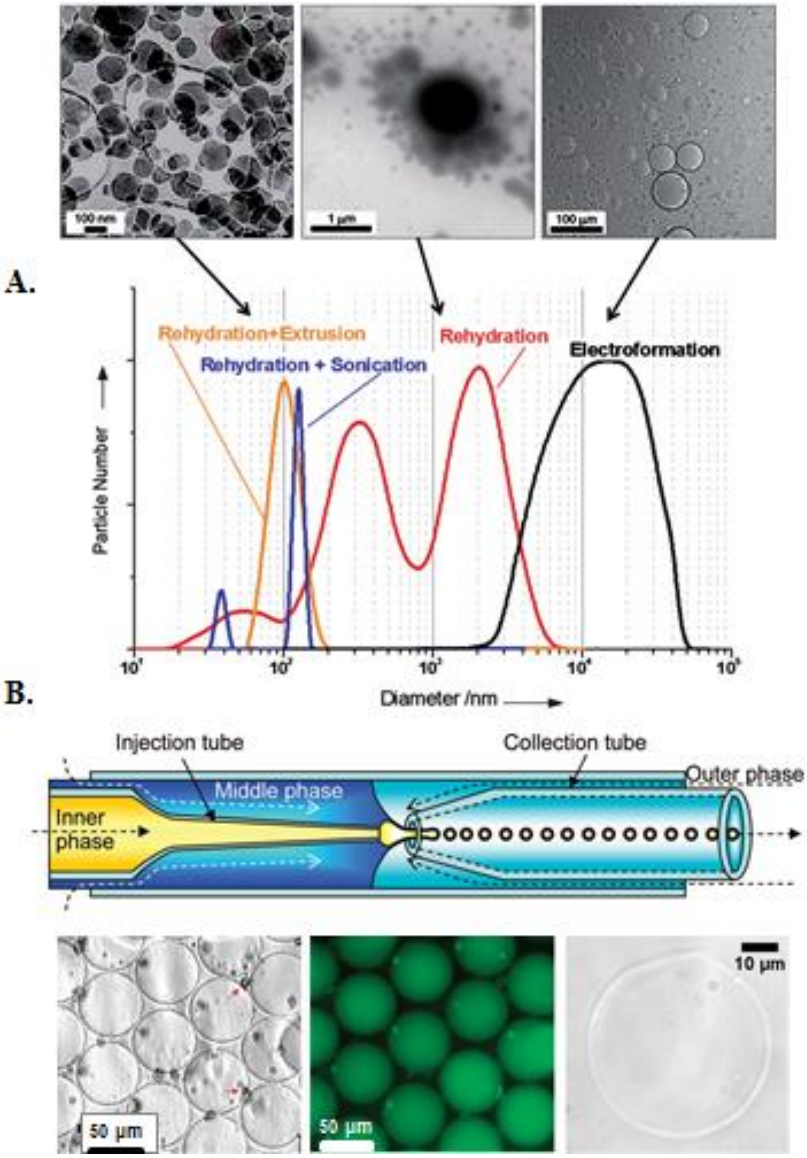

Figure 2.2. Particle size distribution obtained by dynamic light scattering for PB-PEO polymersomes prepared by rehydration + extrusion/sonication and by image analysis for polymersomes prepared by simple rehydration or electroformation, together with their respective TEM images (**A**). Reprinted with permission from ref.[36] Copyright © 2009 Royal Society of Chemistry. Schematic diagram of the microcapillary geometry for generating double emulsions for use in polymersome formation, together with the bright-field microscope and fluorescence microscope images of PEG-PLA polymersomes encapsulating the green FITC-Dextran (**B**). Reprinted with permission from ref.[39] Copyright © 2008 American Chemical Society.

2.3. Peptide-based Polymersomes

Apart from the amphiphilic synthetic block copolymers mentioned in **Table 2.1**, polymersomes can also be prepared using polypeptides as the hydrophilic and/or the hydrophobic block.[44-46] This is particularly interesting approach because of the possibility of introduce biofunctional features, and furthermore, they are biocompatible and biodegradable.

2.3.1. Peptosomes

Vesicular assemblies from amphiphilic α-helical polypeptides in the sizes of about 100 nm in the aqueous medium were first reported by Imanishi group.[45-46] Using a helical peptide antibiotics, Gramicidin A conjugated with PEG, and injecting the peptide solution into buffer, vesicular structures were formed in which the α-helices were regularly packed to form a unilamellar membrane. Those vesicles assembled from amphiphilic polypeptides as building blocks were named as 'peptosomes'.[46] They have an inner aqueous phase capable of encapsulating water-soluble compounds, and they retained their vesicular morphology even at higher concentration of Triton-X, a nonionic surfactants used for solubilizing membrane proteins.[45-47]

Another peptide-based polymersomes with diameters ranging from 50-1000 nm were fabricated by Deming *et al.* using either poly(L-lysine)-*b*-poly(L-leucine) (PLL-P(Leu)) or poly(L-glutamate)-*b*-poly(L-leucine) (PLG-P(Leu)).[49] The formation of the vesicles was explained by disruption of the sheet forming P(Leu) block by charge-charge repulsion from the PLL blocks, directing the formation of the vesicular architecture (**Figure 2.3**).[44,49]

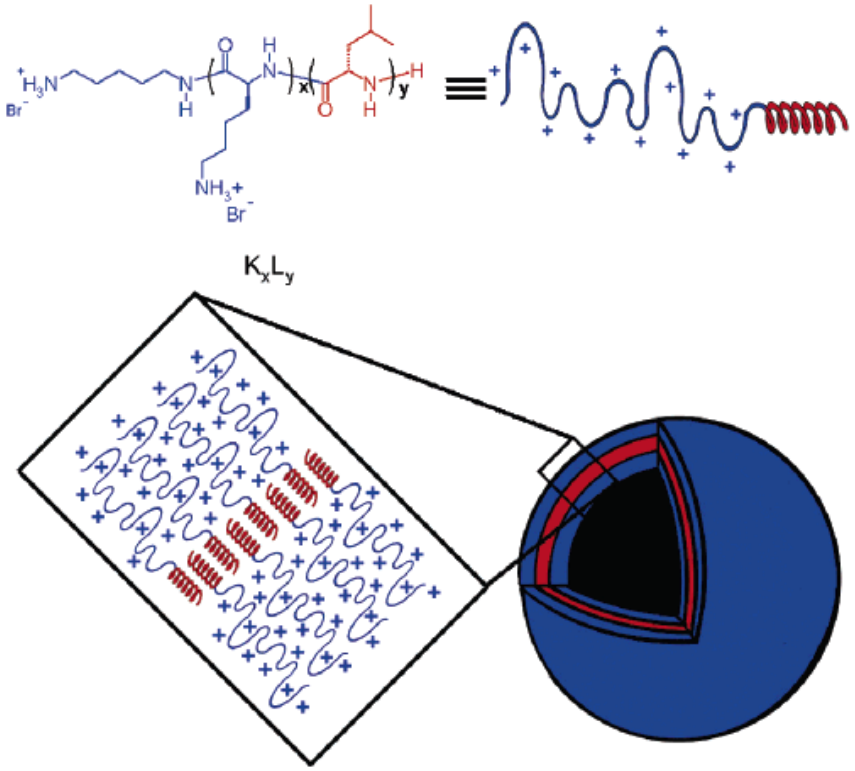

Figure 2.3. Schematic representation of the proposed self-assembly of poly(L-lysine)$_{60}$-*b*-poly(L-leucine)$_{20}$ into polymersomes. Reprinted with permission from ref.[49] Copyright © 2005 American Chemical Society.

2.3.2. Polyion Complex Vesicles (PICsomes)

Development of polyion complex vesicles from polypeptide-based polymersomes using a pair of oppositely charged polypeptide block copolymers were reported extensively by Kataoka *et al*.[50-56] Their design consisted of the anionic poly(ethylene glycol)-*b*-poly(α,β-aspartate) and cationic poly(ethylene glycol)-*b*-poly([2-aminoalkyl]-α,β-aspartamide), which were accessed from poly(ethylene glycol)-*b*-poly(β-benzyl-L-aspartate) (PEG-PBLA). The simple mixing of these polymers in aqueous buffer formed polyion complex (PIC) membranes with a unique three-layered structure. The polymersomes constructed in this way were termed 'PICsomes', and later were called 'Nano-PICsomes' due to their sizes of ~100 nm in diameter (**Figure 2.4**).[50-53] Besides the semi-permeability of the vesicle wall, PICsomes possess several characteristics that have proven to be advantageous over other vesicles, including the facile encapsulation of water-soluble

macromolecules, the absence of the use of organic solvents in their preparation,[50] pH sensitivity,[51] and protease resistance.[52] As a result, PICsomes may be promising as carriers for therapeutic compounds and as compartments for diagnostic enzymes.

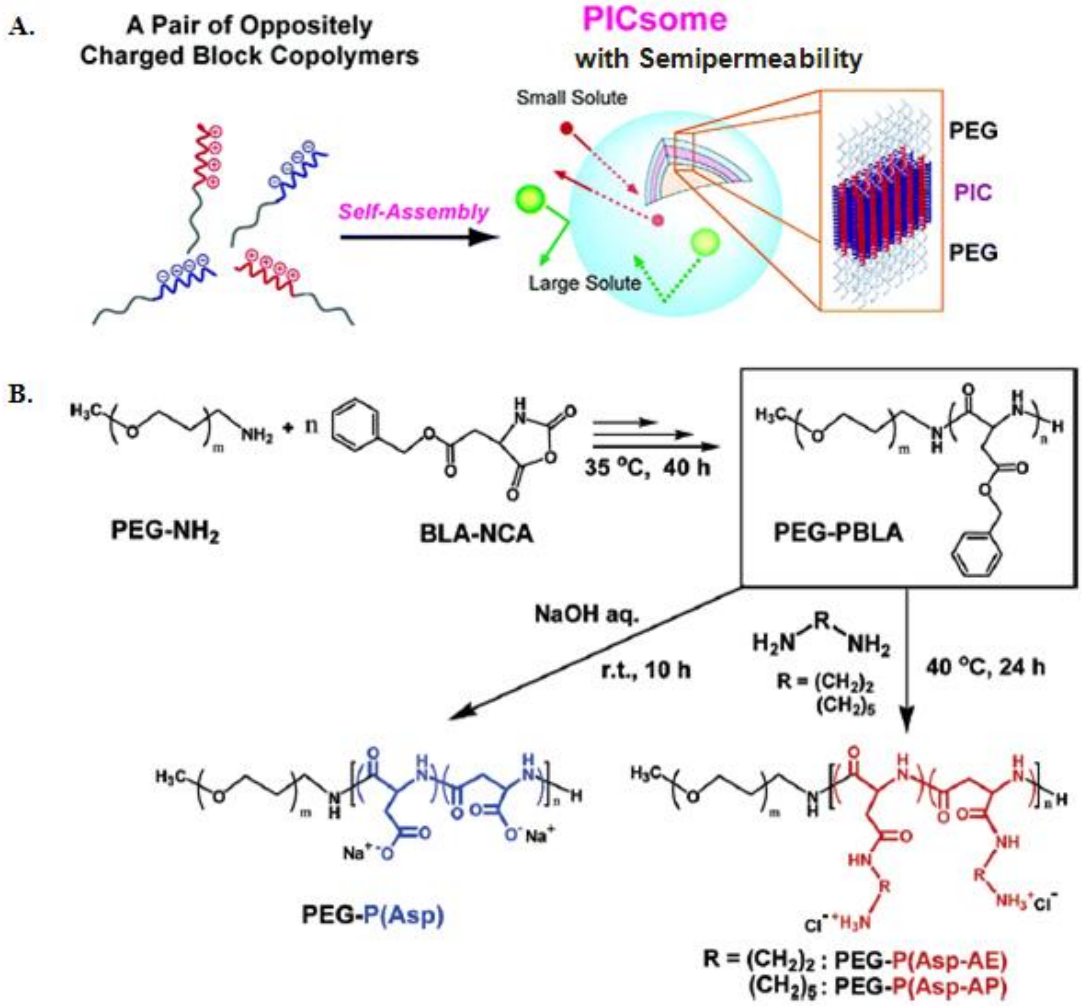

Figure 2.4. Schematic representation of PICsomes composed by mixing a pair of oppositely charged block copolymers in aqueous medium (**A**). Synthesis of a pair of oppositely charged block copolymers from poly(ethylene glycol)-*b*-poly(β-benzyl-L-aspartate) (PEG-PBLA) (**B**). Reprinted with permission from ref.[50] Copyright © 2006 American Chemical Society.

Furthermore, giant micrometer-sized unilamellar spherical PICsomes were generated spontaneously from microdroplets by thermal perturbation using a focused infrared laser beam (optical tweezers).[55,57] Upon irradiation with the infrared beam, a PIC particle slowly transformed into a vesicular structure, and the resulting vesicle returned to the initial PIC droplet after laser irradiation was stopped (**Figure 2.5**).[57] The size of the

resulting vesicles was dependent on the initial size of the PIC droplet. In addition, further studies on formation of giant PICsomes from microparticles using a microfluidic chamber showed that decreasing the additive salt concentration of the PIC system induced the formation of the PEG-PIC-PEG lamellar domains and simultaneously resulting in unilamellar giant PIC vesicles.[58] The development of these giant PICsomes shows great promising applications for encapsulating cosmetic, therapeutic and nutritional compounds in the future.

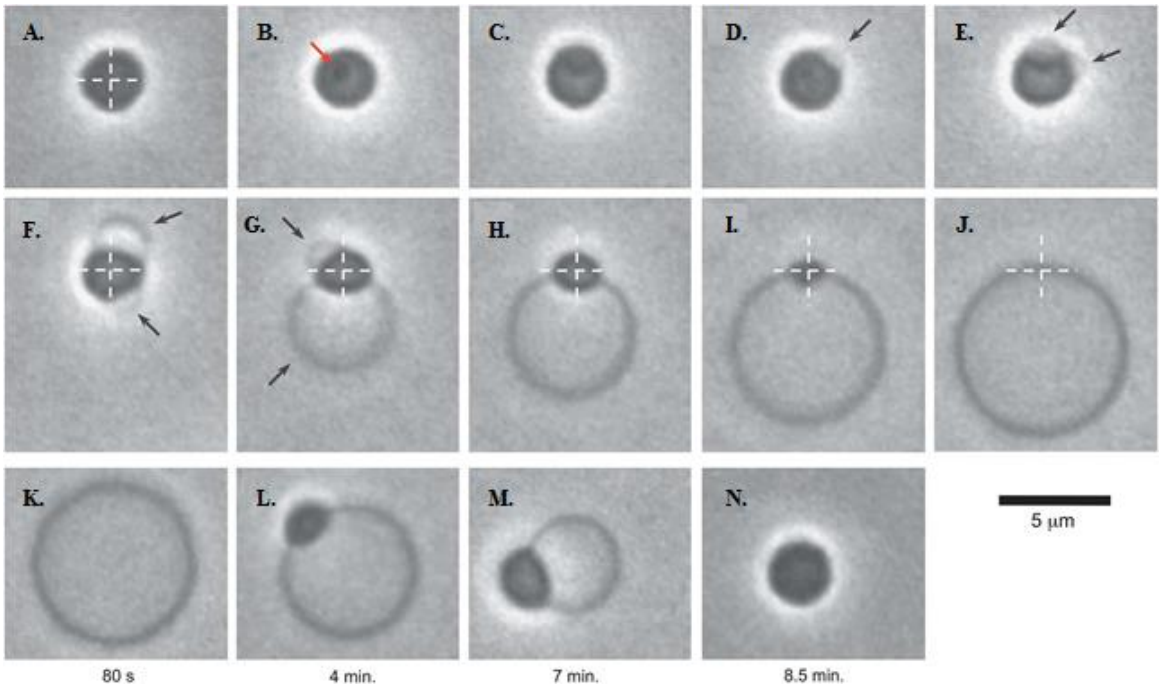

Figure 2.5. Time development of the morphological transformation of a PIC droplet upon laser irradiation (**A**-**J**) and after irradiation (**K**-**N**) (75 mM NaCl, laser power 0.25 W). The time of image is set as 0 s (**A**), and the elapsed times are 2.5 s (**B**), 3.5 s (**C**), 9.0 s (**D**), 12 s (**E**), 26 s (**F**), 65 s (**G**), 96 s (**H**), 140 s (**I**), and 165 s (**J**). The images **K**-**N** show the time course of the morphological transformation after laser irradiation was stopped. The intersections of the two white dashed lines indicate the position of the laser spot (**A**, **F**-**J**). The red arrow indicates a dark spot (**B**) and the black arrows indicate individual vesicular compartments (**D**-**G**). Reprinted with permission from ref.[57] Copyright © 2009 WILEY-VCH Verlag GmbH & Co. KGaA, Weinheim

Another type of amphiphilic polyion complex vesicles formed from mixtures of oppositely charged block ionomers (i.e. copolymers with an ionic content of less than ~15 mol %) was reported by Schlaad and coworkers.[59] Upon mixing the solutions of oppositely charged biocompatible block ionomers of poly(1,2-butadiene)$_{216}$-*block*-

poly(cesium methacrylate)$_{29}$ and polystyrene$_{211}$-*block*-poly(1-methyl-4-vinylpyridium iodide)$_{33}$ in tetrahydrofuran (THF), vesicles (about 100-200 nm in diameter) with a corona of segregated polymer chains were formed (**Figure 2.6**). The generation of these amphiphilic PIC vesicles was controlled mainly by the electrostatic interactions, as well as other interactions, such as hydrogen bonding or donor-acceptor interactions.[59]

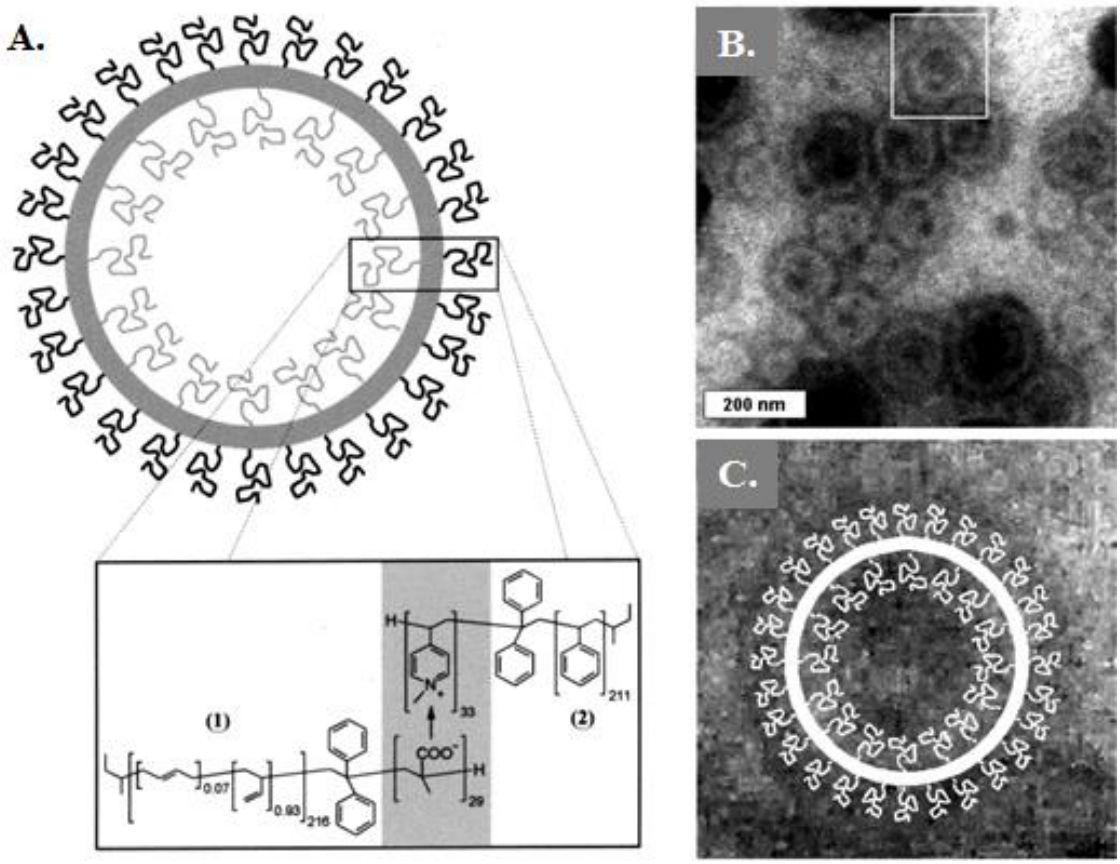

Figure 2.6. Schematic representation of a vesicle with a corona of segregated polymer chains, as formed in a mixture of oppositely charged block ionomers (**A**). TEM image of the PIC vesicles (negatively stained with CsI), prepared from 0.01 wt % THF solution (**B**). Magnification of the framed area in (**B**), showing an individual vesicular aggregate (**C**). Reprinted with permission from ref.[59] Copyright © 2003 American Chemical Society.

2.4. Protein-based Polymersomes

The construction of compartmentalized structures for modelling complex biological systems using protein-based building blocks offers more benefits in term of biocompatibility, biodegradability and biofunctionality of the protein membranes. Mann *et al.* pioneered for the work to assemble protein-based polymersomes, which they referred as 'proteinosomes'.[60-61] The amphiphilic protein-polymer nano-conjugates of bovine serum albumin (BSA) and poly(*N*-isopropylacrylamide) (PNIPAAm) were designed and self-assembled at water droplet/oil interfaces to generate micro-compartments (typically 20-50 μm in diameter) which are semi-permeable, stimulus responsive, and enzymatically active (**Figure 2.7**).[60]

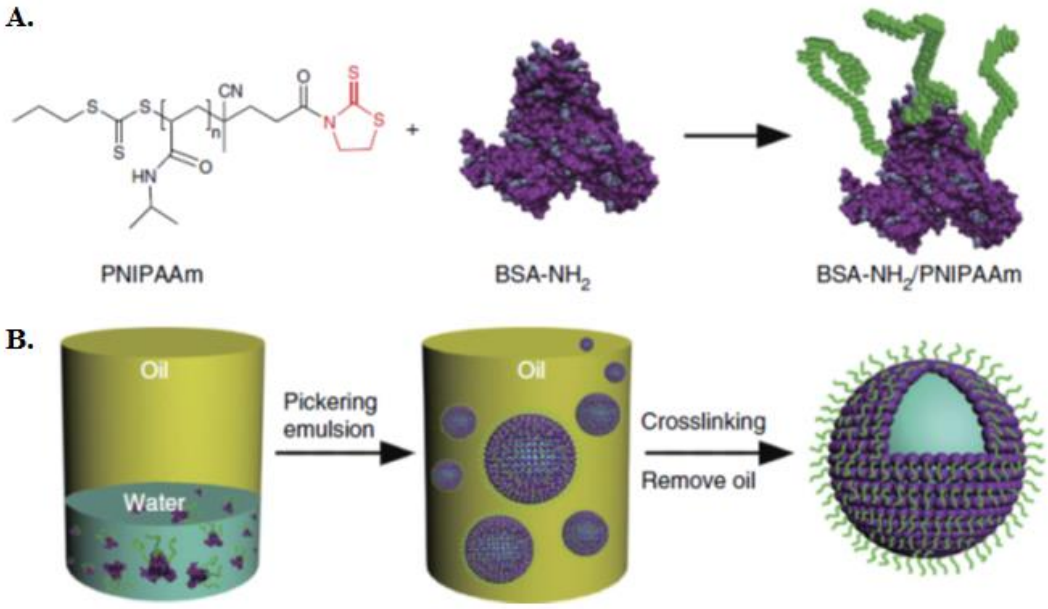

Figure 2.7. Schematic representation of the preparation of proteinosomes. Mercaptothiazoline-activated PNIPAAm polymer chains were coupled with primary amine groups of cationized BSA-NH_2 to generate protein-polymer nano-conjugates (BSA-NH_2/PNIPAAm) (**A**). The spontaneous assembly of proteinosomes in oil, and their transfer into a bulk water phase (**B**). Reprinted with permission from ref.[60] Copyright © 2013 Macmillan Publishers Ltd.: Nature.

Following that, Mann group has also designed and constructed higher-order functionality in proteinosome microcompartments made of amphiphilic BSA-NH_2/PNIPAAm nanoconjugates by encapsulating DNA in the water-filled proteinosomes

and use protease-mediated hydrolysis of BSA to activate the rapid disassembly of the compartments, which simultaneously release the genetic polymer.[61] Their investigations show the potential of combining aspects of supramolecular and polymer chemistry into the development of novel proteinosome-based protocells.

Further development of proteinosomes involving a triad of amphiphilic enzyme-polymer building blocks which was able to function simultaneously as a multi-step membrane-mediated cascade system was reported by the same group recently.[62] Glucose amylase (GA), glucose oxidase (GO) and horseradish peroxidase (HRP) were used to form amphiphilic enzyme-PNIPAAm nano-conjugates, followed by combining them equimolarly to prepare a multi-enzyme proteinosomes (15-30 μm in size) (**Figure 2.8**).[62] The colocalization of the triad of enzymes within the membrane, as well as temperature-dependent changes in the conformation of the covalently attached PNIPAAm polymers were used to control the membrane-mediated cascade reactions.

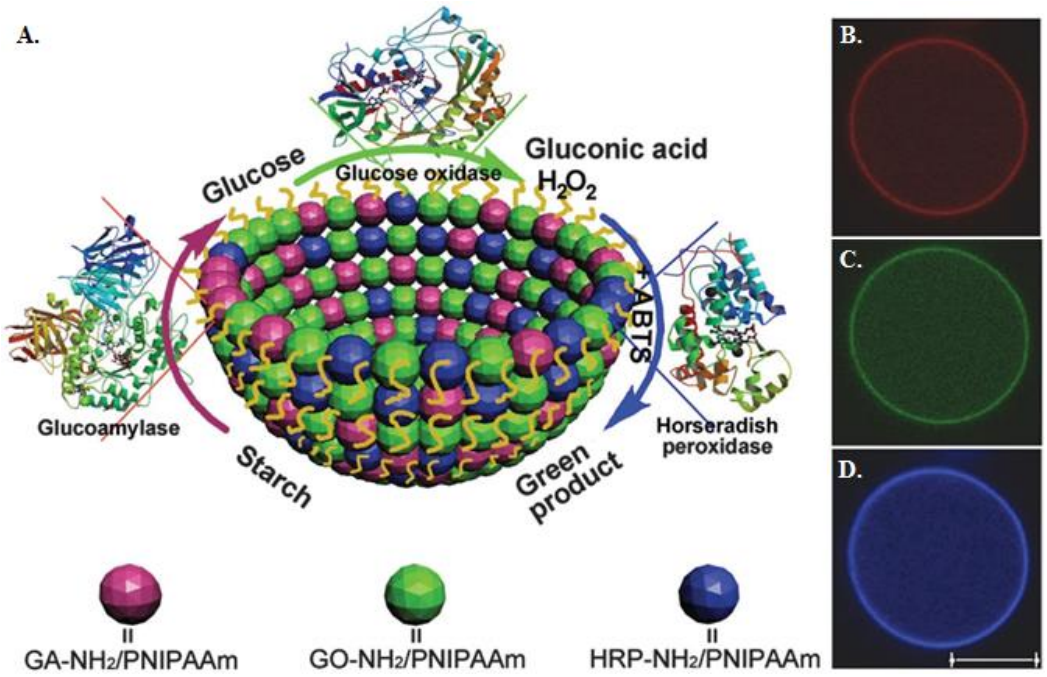

Figure 2.8. Schematic representation of a proteinosome membrane-mediated three-stage cascade reaction in water (**A**). Confocal fluorescence microscopy images of the same multi-enzyme proteinosome in water, showing red (**B**), green (**C**), and blue (**D**) fluorescence associated with GA, GO and HRP, respectively, in the cross-linked membrane; scale bar = 10 μm. Reprinted with permission from ref.[62] Copyright © 2014 Royal Society Chemistry.

2.5. Applications of Polymersomes

Since polymersomes can function as carriers of hydrophilic and hydrophobic loads, they are promising entities for many applications, such as drug delivery, gene therapy, protein delivery, medical imaging, nanoreactors, artificial organelles and biosensors.[19-20,25,27,43,63-64] In addition, many studies have focused on studying and modifying their permeability by incorporating channel proteins, such as OmpF, effectively turning them into simple cell models (**Figure 2.9**).[65-68] Below are just a brief review and some examples of the applications of polymersomes found in literature.

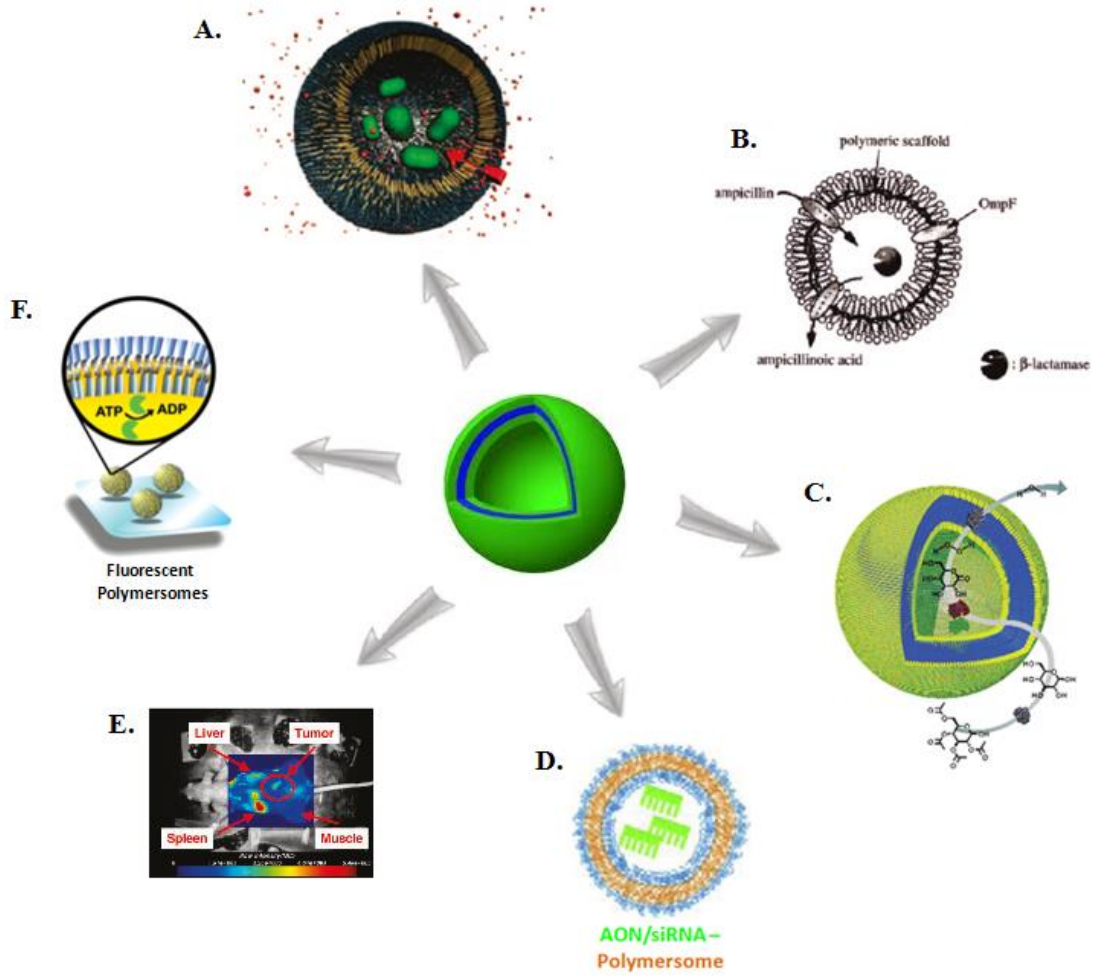

Figure 2.9. Schematic representation of various methods of polymersomes designed for therapeutic and diagnostic applications, for instance the antioxidant nanoreactor (**A**),[69] reconstitution of channel proteins in protein membrane (**B**),[68] polymersome nanoreactor (**C**),[30] polymersome encapsulated siRNA or antisense oligonucleotides (**D**),[70] image of a tumor-bearing mouse (**E**),[71] and third-party ATP sensor in polymersome (**F**).[64] Copyright © 2008 American Chemical Society, © 2001 Springer-Verlag Wien, © 2007 WILEY-VCH Verlag GmbH & Co. KGaA, Weinheim, © 2009 Elsevier Ltd., © 2008 Elsevier Ltd., and © 2014 WILEY-VCH Verlag GmbH & Co. KGaA, Weinheim. Reproduced with permission.

2.5.1. Polymersomes as Nanoreactors

Polymersomes with encapsulated enzymes are known as nanoreactors. In order for polymer vesicles to serve as nanoreactors, their polymer membranes should be selectively permeable. Typically, this can be achieved by using the appropriate block copolymers that form nanoporous membranes, such as using PS-PIAT,[29,72-74] or by inserting various bacterial channel proteins into the vesicle walls, such as LamB, OmpF, maltoporin, and aquaporin.[19,65-68]

In this way, substrate that penetrates through the membrane will be converted by the encapsulated enzyme. For instance, antioxidant nanoreactors composed of PMOXA-PDMS-PMOXA block copolymers, which are oxygen-permeable, were formed by encapsulating the antioxidant enzyme superoxide dismutase (**Figure 2.9A**).[69] Superoxide radicals present in the surrounding environment will be 'detoxified' to hydrogen peroxide and oxygen by the activity of the enzyme molecules inside the compartment.

By inserting the bacterial channel protein OmpF into the PMOXA-PDMS-PMOXA polymersomes (**Figure 2.9B**), transport of low molecular weight organic molecules over the membrane can be achieved. The substrate ampicillin was converted to ampicillinoic acid when the enzyme β-lactamase was encapsulated inside the nanoreactors.[68]

Another example of polymersomes as nanoreactors can be seen from the cascade reaction that was performed by incorporating different enzymes in the inner compartment and within the membranes of PS-PIAT polymer vesicles (**Figure 2.9C**). Interestingly, the membrane of PS-PIAT polymersomes proved to be semi-permeable to low molecular weight substances, and hence, a multistep cascade reactions could be accomplished. In this work, monoacetylated glucose was deprotected by the enzyme *Candida Antarctica* lipase B (CalB), which was embedded in the polymersome membrane. Glucose oxidase (GOx) was encapsulated in the aqueous compartment of the polymersome, oxidized

glucose to gluconolactone, providing a molecule of hydrogen peroxide (H_2O_2). In addition, H_2O_2 was used by horseradish peroxidase (HRP), which was tethered to the polymersome surface, to convert ABTS to the chromogenic ABTS $^{\cdot+}$ (**Figure 2.10**).[30]

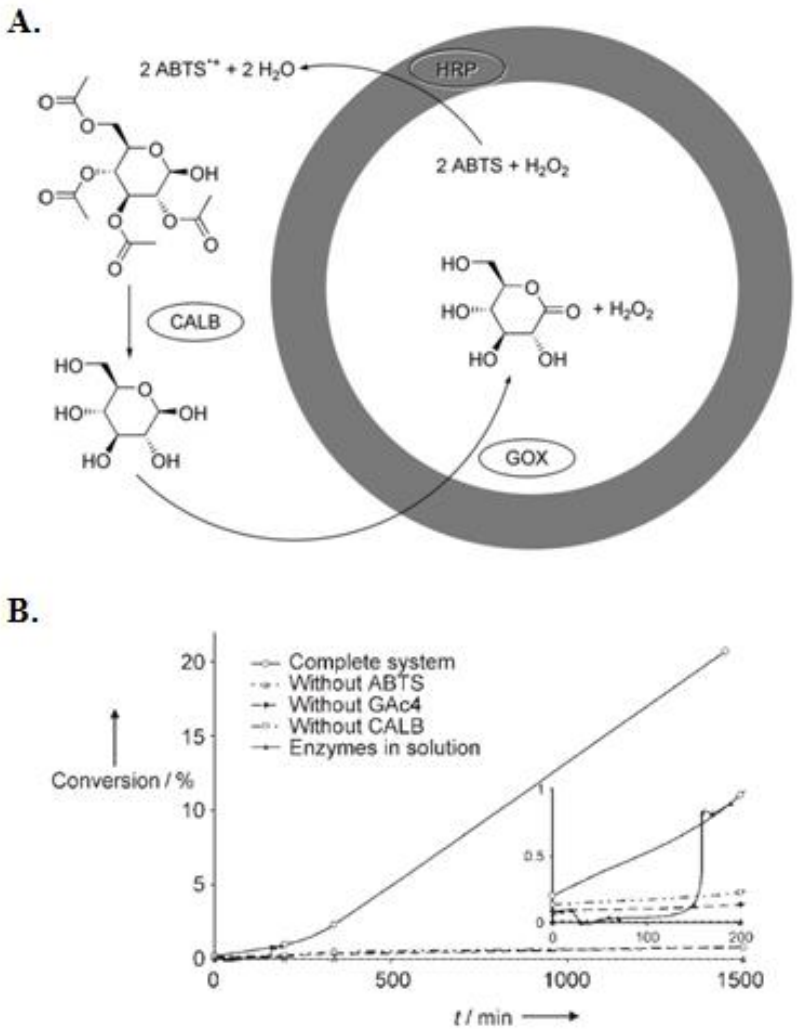

Figure 2.10. Schematic representation of the multistep reaction taking place in the three-enzyme PS-PIAT polymersome system (**A**). The generation of ABTS $^{\cdot+}$ in the three-enzyme system at pH 7.2, followed by UV/Vis spectroscopy (**B**). GAc4 = 1,2,3,4-tetra-O-acetyl-b-glucopyranose. Reprinted with permission from ref.[30] Copyright © 2007 WILEY-VCH Verlag GmbH & Co. KGaA, Weinheim.

2.5.2. Polymersomes for Medical Applications

The potential use of polymer vesicles for medical applications, such as drug delivery, gene therapy and protein delivery has also been demonstrated in various studies. For instance, Discher *et al.* developed polymersomes which are able to load and deliver functional small interfering RNAs (siRNA) and antisense oligonucleotides (AON) into cells (**Figure 2.9D**).[70] In general, these degradable carriers were taken up non-specifically by the cultured cancer cells, which later transformed them into micelles that allowed endolysosomal escape and the delivery of either siRNA into cytosol for mRNA knockdown or AON into the nucleus for exon skipping within the mRNA.[70]

In drug delivery, biodegradable polymersomes composed of PEG-PLA loaded with two anticancer drugs, paclitaxel (TAX) in the membrane and doxorubicin (DOX) in the lumen of polymersomes showed rapid shrinkage in tumor while being injected into tumor-bearing mice (**Figure 2.11**).[75-77] Both TAX and DOX are two common anticancer drugs used to target different cellular points, i.e. microtubules for TAX and DNA for DOX. Here, the dual-drug polymersomes displayed effective drug delivery systems in vivo as they permeate and shrink tumor cells. Combination therapy with dual-drug polymersomes triggers massive cell death or 'apoptosis' in tumors.[75]

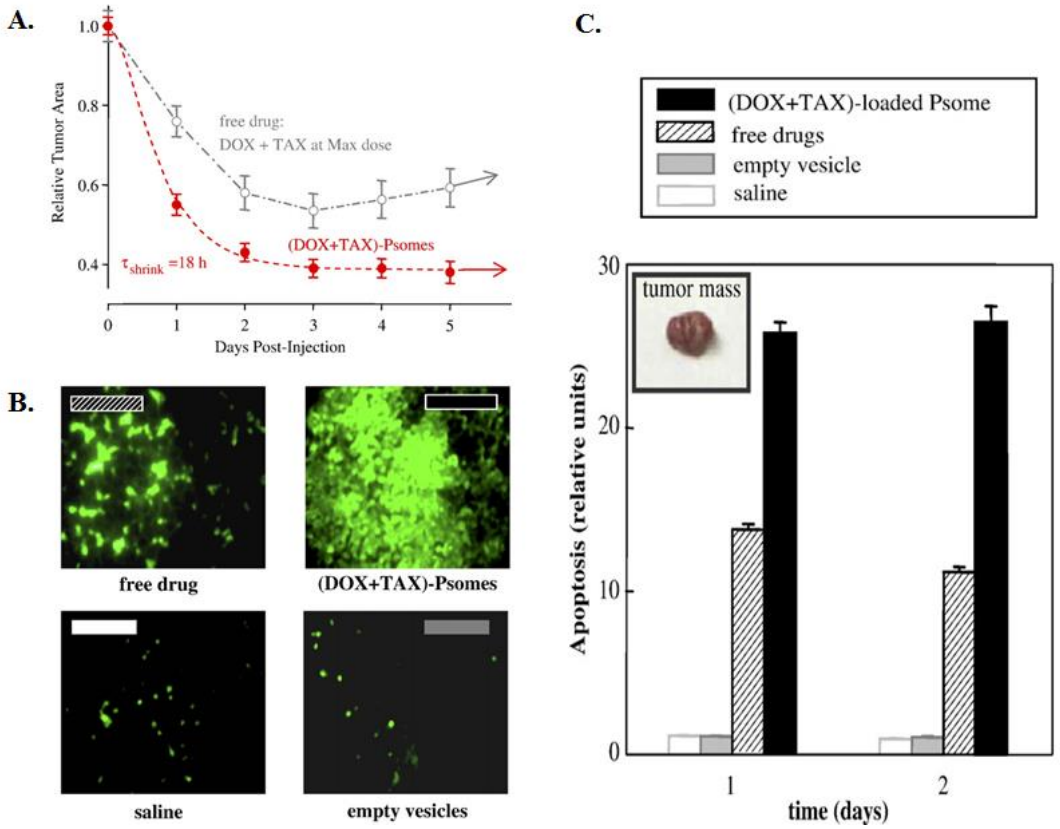

Figure 2.11. Single injection of (DOX + TAX)-loaded polymersomes shows rapid shrinkage of the tumor, compared to the free drug (administered at maximum tolerated doses) (**A**). Fluorescent microscopy images of TUNEL labeled MDA-MB231 tumor tissue, with large increases in TUNEL positive cells observed 48 hours after polymersome-drug treatments. Scale bar: 20 μm (**B**). Quantitation of apoptosis in tumors day 1 and 2 post-injection (**C**). Reprinted with permission from ref.[75] Copyright © 2006 Elsevier Ltd.

In addition, functionalization of polymersomes with specific ligands could target them to certain cell types and locations inside the body, which is useful for drug delivery applications.[19] Peptide vesicles or peptosomes labeled with a near-infrared fluorescence (NIRF) probe showed long circulation in rat blood, which proved that peptosome is an excellent nanocarrier for molecular imaging due to its enhanced permeability and retention effect.[47] On the other hand, cross-linked PICsomes showed a size-dependent residence time in the blood circulation, and could be particularly promising carriers in drug delivery because of their biocompatibility.[78]

For use in diagnostics, polymersomes encapsulating fluorescent agents were developed and studied for optical imaging (**Figure 2.9E**). The group of Hammer developed porphyrin-based near infrared fluorophores which are able to generate a signal

with enough intensity to penetrate through 1 cm of a solid tumor when encapsulated inside PBD-PEO polymersomes.[71] When being injected into the tail-vein of mice, the near infrared (NIR)-emissive polymersome could be tracked *in vivo* via non-invasive optical imaging (**Figure 2.12**).[71,79]

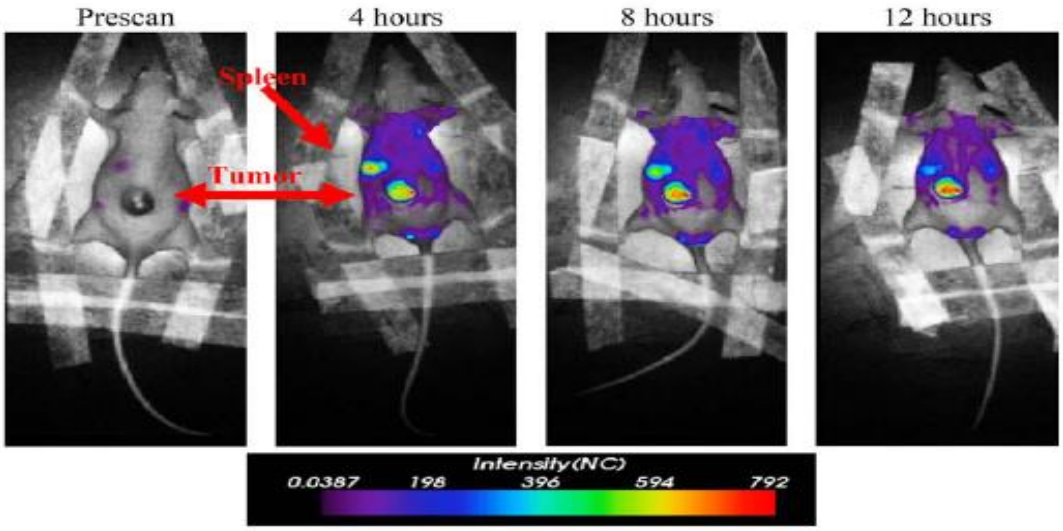

Figure 2.12. Tumor imaging of NIR-emissive polymersomes. Fluorescence images of the same mouse (prone position) taken prior to administration of NIR-emissive polymersomes, and at 4, 8, and 12 hours after tail-vein injection (λ_{ex} = 785 nm, λ_{em} = 830-900 nm). Reprinted with permission from ref.[71] Copyright © 2008 Elsevier Ltd.

Besides optical imaging, an alternative approach was reported by Zhou and coworkers who prepared polymersome bubbles by lyophilization and rehydration procedures for targeted ultrasound imaging.[80] The air-encapsulated polymer vesicles were imaged using medical scanner and were visible as bright spots, verifying that the polymersomes were acoustically active.[80-81]

Recently, our group reported on using the permeability advantage of polymersomes to create a "third-party" ATP sensor (**Figure 2.9F**).[64] In this work, the fluorescent conjugated polymers reporter, i.e. poly(1-(3-((4-methylthiophen-3-yl)oxy) propyl) quinuclidin-1-um) (PTQ) and ATP-hydrolyzing enzyme, alkaline phosphatase (ALP) were first co-encapsulated inside the porous polymersomes of PS-PIAT. Passive

diffusion of externally added ATP into the polymersome would quench PTQ rapidly, resulting in non-fluorescent polymersomes. ATP-dependent reaction was then observed by using the real-time consumption of ATP by ALP within the vesicular compartments, followed by the recovery of the PTQ fluorescence (**Figure 2.13**).[64]

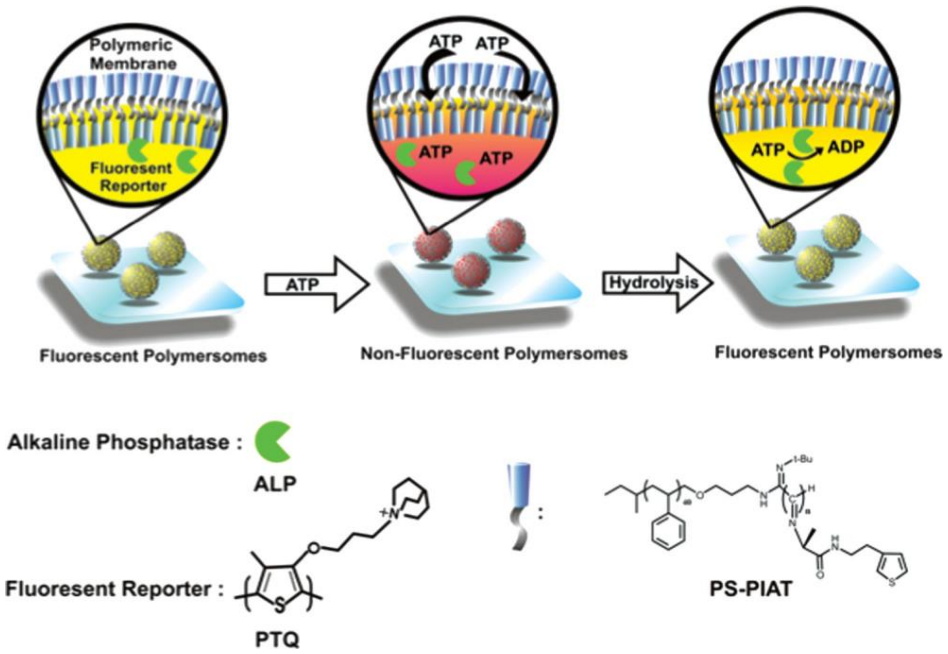

Figure 2.13. Schematic representation of the proposed method for the detection of ATP conversion inside the porous vesicular compartment. Reprinted with permission from ref.[64] Copyright © 2014 WILEY-VCH Verlag GmbH & Co. KGaA, Weinheim.

2.6. Multicompartmentalized Polymersomes

Polymersomes have been explored for mimicking cell function because of their inner aqueous space that can be used for encapsulation of biofunctional compounds, and which resembles the cell in a very basic way. An important design principle of the complexity of cells is that of compartmentalization and, likewise, synthetic systems have been developed with a similar architecture, such as vesosomes (liposomes–in–liposome),[82-83] capsosomes (liposomes–in–polymersome),[84-86] polymersomes–in–polymersome,[87-89] double emulsions, and their combinations.[90-91] Here, a summary of recent development of multicompartmentalized polymersomes (polymersomes–in–polymersome) from amphiphilic block copolymers is given.

Two different methods of constructing multicompartmentalized polymersomes have been reported: double emulsion method and self-assembly method, leading to non-spherically and spherically organized multicompartments.[90] Below are some examples of preparing multicompartments using amphiphilic block copolymers and their applications.

2.6.1. Double Emulsion Method for Preparing Multicompartments

Firstly, the preparation of non-spherical multicompartmentalized polymersomes made of biocompatible block copolymers of poly(ethylene glycol)-*b*-poly(lactic acid) (PEG-*b*-PLA) through the double emulsion technique, was reported by Weitz *et al.*[40-41] The W/O/W double emulsions were prepared with two solvents and block copolymers as the oil phase. During evaporation of the organic solvent, the block copolymers attracted each other at the interface to form the membrane bilayers, which subsequently generated the multicompartmentalized polymersomes. These multicompartmentalized polymersomes were then used for the encapsulation of separate cargoes (**Figure 2.14**).[41,90-92]

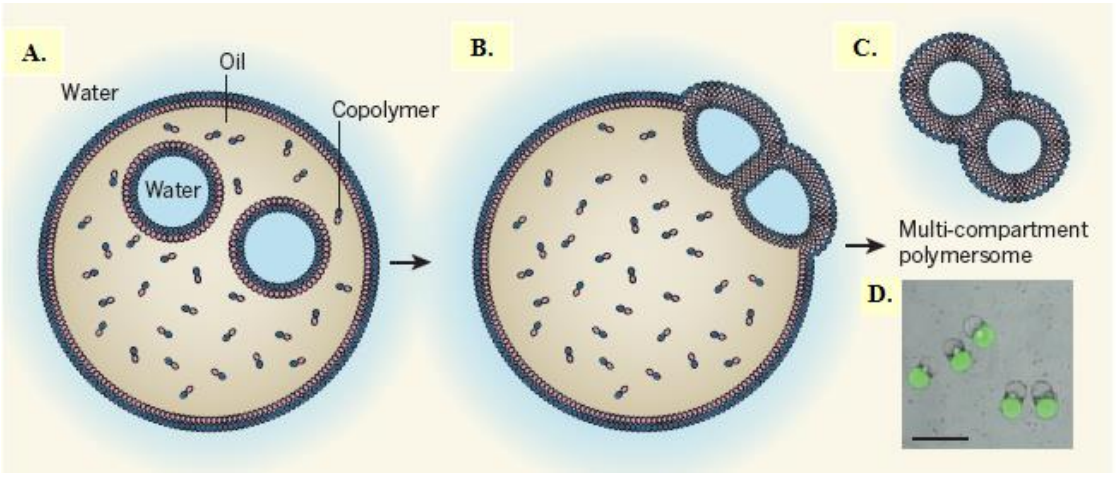

Figure 2.14. The synthesis of non-spherical multicompartmentalized polymersomes through water-oil-water (W/O/W) double emulsion technique with the block copolymers in the oil phase (**A**). As the organic solvent evaporates, the block copolymers attract each other at the interface to form the membrane bilayers (**B**). Upon complete evaporation of the organic solvent, multicompartmentalized polymersomes result (**C**). Fluorescence microscopy image of PEG_{5000}-*b*-PLA_{5000} polymersomes encapsulating fluorescent FITC-Dextran solution and a non-fluorescent PEG solution in the separate compartments (scale bar is 200 μm) (**D**). Reprinted with permission from ref.[92] Copyright © 2011 Macmillan Publishers Ltd.: Nature.

Secondly, spherically organized multicompartmentalized polymersomes were also prepared by Weitz and coworkers via double emulsion technique using the same biodegradable PEG-*b*-PLA diblock copolymers.[93] The size of multicompartment polymersomes prepared in this way ranges from 50-200 μm in diameter, and contains 2-8 inner compartments (**Figure 2.15**). By introducing mechanical strain or the selective dissociation of the polymersome membranes through hydrolysis, the programmed release of the encapsulated cargo was accomplished.[90,93] .

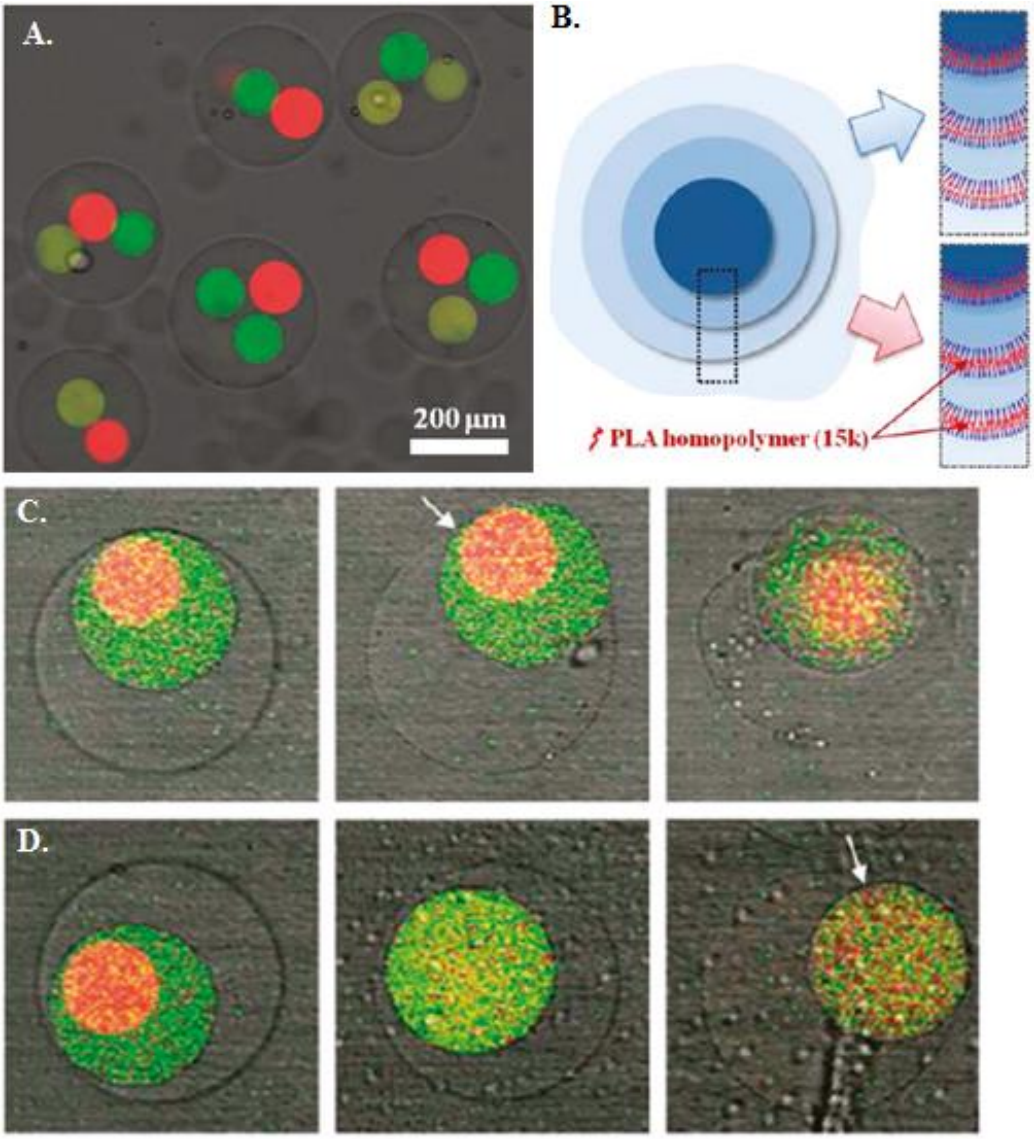

Figure 2.15. Confocal microscope image of polymersomes containing several inner polymersomes encapsulating sulforhodamine B (red), 8-hydroxyl-1,3,6-pyrenetrisulfonic acid (green), and a mixture of both dyes (yellow) (**A**). Schematic representation of a triple polymersome showing bilayers with no internal homopolymer on top and two of the bilayers containing homopolymer on the bottom (**B**). Series of confocal images showing sequential dissociation of membranes from the outermost to the innermost polymersomes (**C**) and from the innermost to the outermost polymersomes (**D**). Reprinted with permission from ref.[93] Copyright © 2011 American Chemical Society.

In another example, multicompartmentalized polymersomes having pH-responsive channels in both compartments were prepared via the W/O/W double emulsion technique was reported by Chiu and coworkers.[94] The polymersomes were composed of random copolymers of acrylic acid and distearin acrylate, with size ranging from 1-15 µm. Here, the transmembrane channels were thought to be formed from acrylic acid-rich regions of the membrane and were permeable to hydrophilic solutes depending

on the pH. At pH 5.0, calcein added could not enter the vesicle membrane, whereas at pH 8.0, the calcein freely diffused into the polymersomes' aqueous compartments. By adjusting the pH value back to 5.0, the calcein was entrapped inside the polymersomes (**Figure 2.16**).[90,94]

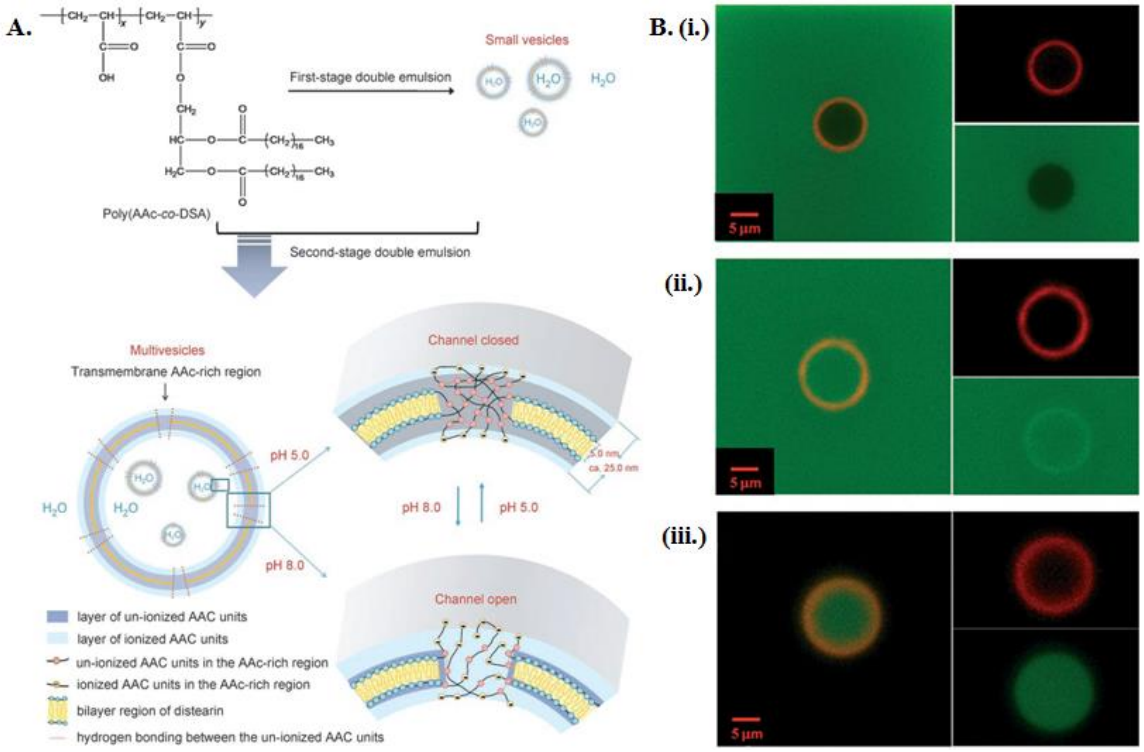

Figure 2.16. Schematic representation of the multicompartmentalized polymersomes assemblies equipped with pH-responsive transmembrane channels from two-stage double emulsion of poly(AAc-*co*-DSA) (**A**). The pH-responsive process is reversible in the range of pH 5-8. Confocal microscope images of Nile Red stained polymersomes (**B**) with the addition of calcein at pH 5.0 (polymersomes are impermeable to calcein) (i.), after pH adjustment to 8.0 (calcein diffuses into polymersomes) (ii.), and after replacement with fresh buffer of pH 5.0 (calcein is confined within polymersomes) (iii.) Reprinted with permission from ref.[94] Copyright © 2008 WILEY-VCH Verlag GmbH & Co. KGaA, Weinheim.

The next example of polymersome-in-polymersome model systems which closely resembled biological cells using emulsion method was reported by Lecommandoux *et al.*[87-88] Biocompatible poly(trimethylene carbonate)-*b*-poly(L-glutamic acid) (PTMC-*b*-PGA) polymersomes formed by nanoprecipitation were encapsulated into poly(butadiene)-*b*-poly(ethylene oxide) (PB-*b*-PEO) polymersomes by emulsion centrifugation, resulting in ~20 μm in diameter of multicompartments (**Figure 2.17**).[87,91] Anticancer drug doxorubin was encapsulated into the inner polymersomes of

multicompartments, and the release rate of doxorubin was compared to the single-compartment, which showed about half time slower than those from the single-compartment due to the additional diffusion barrier.[87] This study further brings new opportunity for the applications of multicompartmentalized polymersomes in biomedical and cosmetic fields.

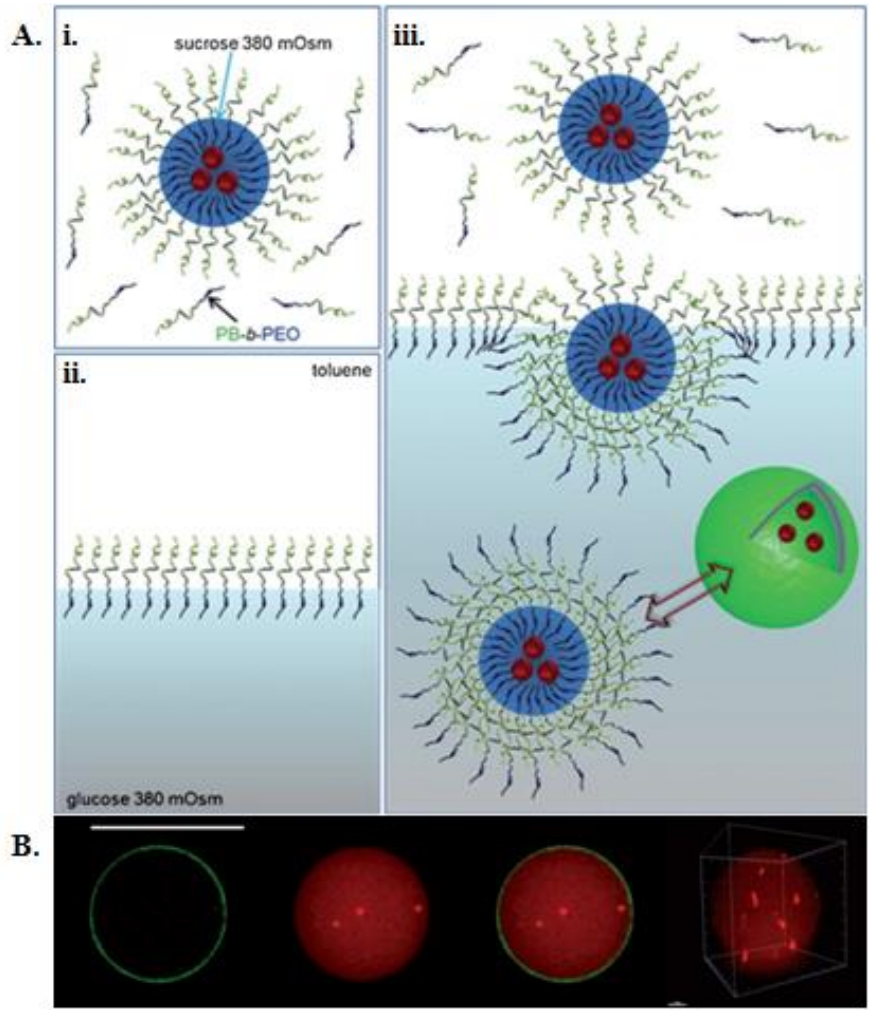

Figure 2.17. Schematic representation of the emulsion centrifugation technique generating polymersome-in-polymersome model system (the smaller red vesicles represent the inner nanosize polymersomes of PTMC-*b*-PGA in an aqueous solution at 380 mOsm sucrose) (**A**). Spinning disk confocal microscopy images of red nanosize polymersomes (Alexa Fluor 568) in a green giant polymersome (Alexa Fluor 488) (**B**). From left to right: green channel, red channel, overlay and 3D reconstruction (red channel). Scale bar: 20 μm. Reprinted with permission from ref.[87] Copyright © 2008 WILEY-VCH Verlag GmbH & Co. KGaA, Weinheim.

Another development of functional multicompartmentalized structure using polymersomes which mimics cell function was reported recently by van Hest group.[95]

Enzyme-filled sub-micrometer sized polystyrene-polyisocyanoalanine(2-thiophene-3-yl-ethyl)amide (PS-PIAT) vesicles were encapsulated concurrently with reagents and free enzymes in a larger micrometer-sized PB-PEO vesicle by an emulsion centrifugation method. A three-enzyme cofactor-dependent cascade reaction is carried out across multiple compartments to yield resorufin as final fluorescent product (See **Figure 2.18**).[95]

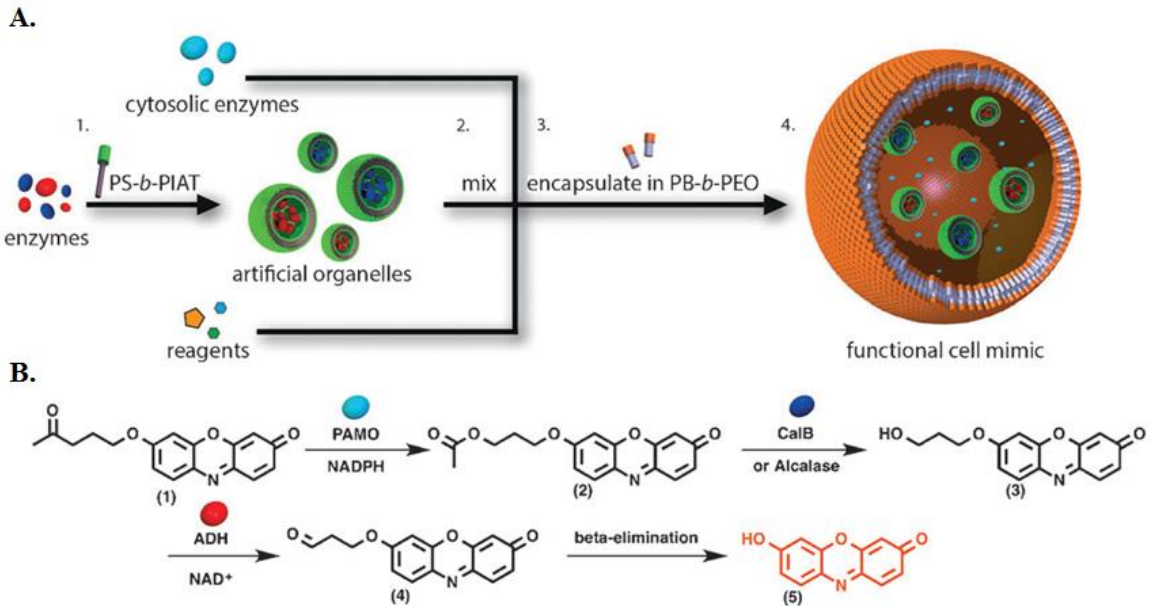

Figure 2.18. Schematic representation of the preparation of functional cell mimic, showing encapsulation of different enzymes in PS-PIAT vesicles, followed by mixing of the artificial organelles, cytosolic enzymes and reagents, prior to encapsulation into PB-PEO vesicles to create multicompartmentalized structure (**A**). Detailed cascade reaction scheme, in which phenyl acetone monooxygenase (PAMO) catalyzes profluorescent substrate **1** in the presence of cofactor nicotinamide adenine dinucleotide phosphate (NADPH) under a Baeyer-Villiger reaction to form ester **2**, which is then being hydrolyzed by the enzyme *Candida Antarctica* lipase B (CalB) or Alcalase to give primary alcohol **3**. Using the cofactor nicotinamide adenine dinucleotide (NAD^+), the alcohol is later oxidized by alcohol dehydrogenase (ADH) to generate aldehyde **4**, which subsequently undergoes spontaneous beta-elimination to produce fluorescent resorufin **5** (**B**). Reprinted with permission from ref.[95] Copyright © 2014 WILEY-VCH Verlag GmbH & Co. KGaA, Weinheim.

2.6.2. Self-Assembly Method for Preparing Multicompartments

Further development in preparing multicompartmentalized polymersomes using multistep self-assembly approach, consisted of diblock and triblock copolymers was recently reported by our group.[89] In contrast to the W/O/W double emulsion method reported

above, the dimensions of these multicompartments are truly nanoscale, i.e. in 150-200 nm range. The ABA (i.e. PMOXA-PDMS-PMOXA: poly(2-methyloxazoline)–poly(dimethyl siloxane)–poly(2-methyloxazoline) triblock copolymers acted as inner vesicle, encapsulating green fluorescent proteins (GFPs), while PS-PIAT diblock copolymers acted as outer vesicle, encapsulating the inner vesicle and cyanine-5 conjugated immunoglobulin G proteins (Cy5-IgG). The selective encapsulation of biomacromolecules in separate compartments could be clearly demonstrated (**Figure 2.19**).[89-90] In fact, these multicompartmentalized polymersomes show a promising architecture in the therapeutic applications and cell mimicry due to their nanoscale size.

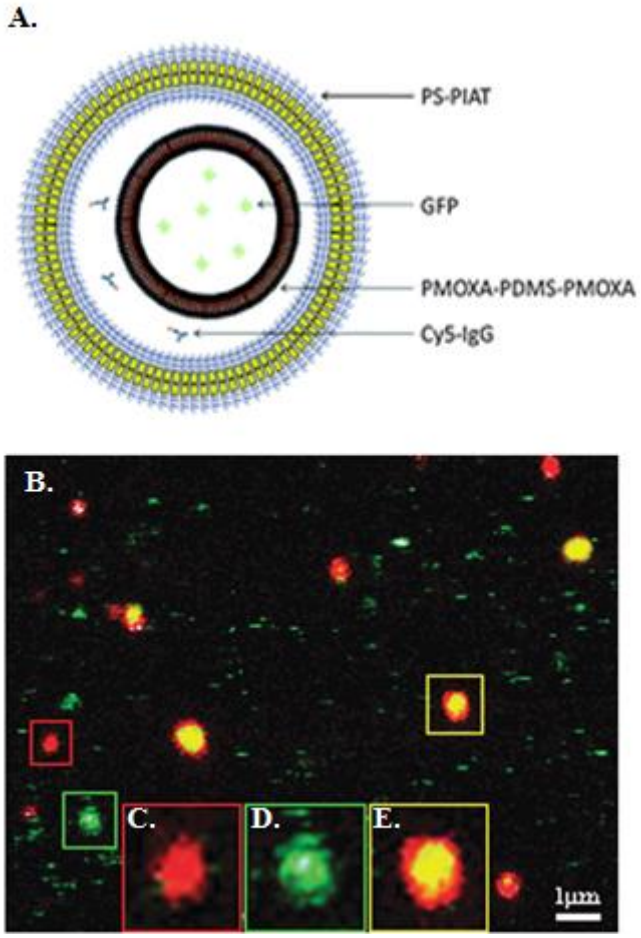

Figure 2.19. Schematic representation of the multicompartmentalized polymersomes (**A**). Scanning confocal fluorescence image of multicompartmentalized polymersomes (**B**). Red spots correspond to Cy5-IgG encapsulated in individual PS-PIAT polymersomes (**C**), whereas green spots correspond to GFP encapsulated in individual ABA polymersomes (**D**). Yellow spots result from the overlap of the ABA and PS-PIAT signals, which correspond to the multicompartmentalized polymersomes (**E**). Reproduced with permission from ref.[89] Copyright © 2011 Royal Society of Chemistry.

In brief, both double emulsion and self-assembly methods had been reported to prepare multicompartments of polymersomes, in which each method had its own advantages and disadvantages. The W/O/W double emulsion method using microcapillary device gives more reliable, reproducible and uniform monodisperse polymer vesicles with great encapsulation efficiency than the self-assembly method. Nevertheless, it yields giant polymersomes of micrometer-sized. In contrast, self-assembly method using film dehydration and direct dissolution methods results in smaller nanoscale vesicles, which can be used in medical applications as containers for therapeutic compounds and as nanoreactors. One of the disadvantages from this method is the polymersomes formed usually have polydisperse size distribution; however, the polydispersity of the vesicles can be reduced by extrusion through specific nanometer-sized syringe filters to obtain the monodispersed vesicles.

2.7. Summary

Following the literature review, the next few chapters will cover my research work on developing novel bio-functional architectures of polymersomes. As becomes clear from the overview, several interesting functional multicompartment architectures have recently been described. One shortcoming of these structures is evidently their size. Even though many authors present these structures as applicable for in-vivo use, their dimensions of several tens of micrometers, would cause there almost instantaneous removal from the blood stream. In this thesis, we, therefore, research the construction of multicompartments with dimensions that are compatible for in-vivo applications. Secondly, since we focus on multicompartmentalization and the mimicry of cellular compartments, we are especially interested in how exchange of molecules between compartments can be engineered. Since polymer membranes are evidently limited in their

selectivity, we instead use membrane protein to regulate permeability of the polymer membrane. Although in our case, we use a simple channel protein that is permeable to organic solutes, this nevertheless demonstrates that the unrivaled selectivity found in nature can be transferred to semi-synthetic capsules.

Next, in order to develop biocompatible and biodegradable novel compartments, protein-polymer bioconjugated complexes from PEG and major milk protein β-lactoglobulin (BLG) was synthesized via bio-orthogonal chemistry (Chapter 4). Upon introducing positive and negative charged to the protein-polymer complexes, both charged species were combined and self-assembled to form unique nanocompartments, (termed as 'proteinionosomes'), which were fluorescent.

CHAPTER 3

Development of Enzymatic Cascade Reactions in Polymersomes with Multicompartmentalized Architecture

3.1. Introduction

As it has been described in **Section 2.6**, compartmentalization as a feature of cell is essential for cellular functions, and therefore, many different multicompartmentalized architectures, particularly polymersomes-in-polymersome have been developed to mimic cellular compartments. Our group has also recently reported the construction of multicompartmentalized (MC) polymersomes where an ABA polymersome consisting of $PMOXA_{12}$-$PDMS_{55}$-$PMOXA_{12}$ was enclosed into the aqueous volume of a PS_{40}-$PIAT_{50}$ polymersome (See **Section 2.6.2**).[89] These MC polymersomes with a vesicle-in-vesicle structure were prepared by a simple method known as sequential self-assembly and the dimension of the multicompartments was in nm-sized. At the same time, two different biomacromolecules were encapsulated into separate compartments to mimic cellular compartmentalization (See **Figure 2.19**).[89]

In addition to this concept and in order to increase the complexity of the system for mimicking cellular compartments, here, in this chapter, we demonstrate a multicompartment architecture where we show control over the exchange of molecules between the compartments. The design features an inner compartment equipped with a channel protein and a semi-permeable outer compartment that allows the passive diffusion of small molecules. By encapsulating two different enzymes separately at different compartments and performing the cascade reaction, the complexity of cells is mimicked.

First of all, we demonstrate the incorporation of OmpF (a porin or passive diffusion channel) into the membrane of the inner ABA compartment to allow the

exchange of small molecules and ions between the compartments, which leads to a catalytically active nanocontainers.[51-52,65-66] This process is facilitated by the outer PS-PIAT membrane, which is known to be semi-permeable membrane and allows the diffusion of small molecules.[19,26,27-29,31,72-74] As the cascade reaction, a commonly used bi-enzymatic reaction used for colorimetric determination of glucose has been chosen, which is catalyzed by horseradish peroxidase (HRP), encapsulated in the inner ABA compartment and glucose oxidase (GOx) which was located in the outer compartment (**Scheme 3.1**).

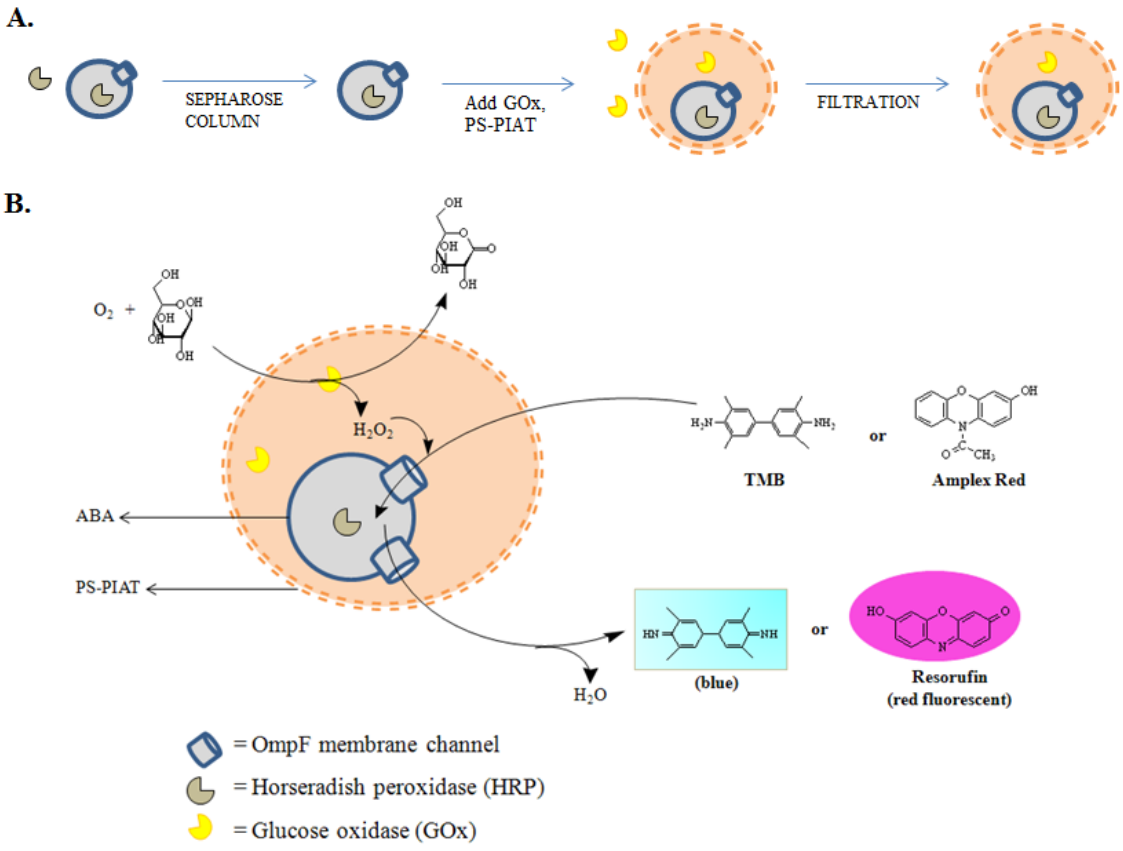

Scheme 3.1. Flow diagram for the preparation of vesicle-in-vesicle structure (**A**). Schematic representation of location of the enzymes in multicompartmentalized (MC) polymersome and the reaction scheme of the bi-enzymatic cascade reactions forming the basis for the assay of glucose, using either substrate TMB or amplex red (**B**).

More specifically, the encapsulated GOx enzyme catalyzes the oxidation of β-D-glucose to produce D-glucono-δ-lactone and hydrogen peroxide (H_2O_2), which together with the

substrate either 3,3',5,5'-tetramethylbenzidine (TMB) or 10-acetyl-3,7-dihydroxyphenoxazine (amplex red) diffuses through the OmpF channel into the inner vesicle where HRP resides, and which subsequently catalyzes the one-electron oxidation of either TMB or amplex red into a detectable reaction product.

Several characterization techniques are used to prove the existence of individual ABA and MC polymersomes, including transmission electron microscopy (TEM), dynamic light scattering (DLS) and static light scattering (SLS). DLS showed that the ABA polymersomes had an average hydrodynamic diameter (D_H) of 106 nm, whereas the MC polymersomes had an average D_H of 295 nm suggesting encapsulation of ABA vesicles into the PS-PIAT polymersomes. The functionality of the MC polymersomes was demonstrated by a cascade reaction kinetics using the separately encapsulated enzymes. Fluorescence microscopy and flow cytometry were performed to differentiate multiple species of polymersomes that could be present in the MC polymersomes samples (i.e. single ABA and PS-PIAT polymersomes, apart from MC polymersomes), eventually showing the segregation of the separately encapsulated enzymes.

3.2. Experimental

3.2.1. Materials and Method

The ABA ($PMOXA_{12}$-$PDMS_{55}$-$PMOXA_{12}$) (M_n = 6,325 Da, PDI = 1.01) triblock copolymer was purchased from Polymer Source. The OmpF protein channel was provided by the group of Prof. Wolfgang Meier, University of Basel, Switzerland. PS_{40}-$PIAT_{50}$ (M_n = 11,750 Da, PDI = 1.10) diblock copolymer was synthesized as described previously.[84-85] HRP, GOx, TMB, amplex red reagent, β-D-glucose, and H_2O_2 were purchased from Sigma-Aldrich. Phosphate buffer saline (PBS, 1X, pH 7.4) was from Invitrogen. Absolute ethanol and THF were obtained from Merck. Alexa Fluor 488 protein labeling kit and Alexa Fluor 647 tyramide were purchased from Life technologies. All reagents, buffer and solvents were used as received, without further purification.

TEM was performed with a Carl Zeiss Libra 120 Plus TEM, operated at 120 kV at the Facility for Analysis, Characterization, Testing, and Simulation (FACTS) in Nanyang Technological University, Singapore (Appendix A). Cryo-TEM was performed with Titan Krios microscope (80-300 kV, FEG, LN2-cooled stage for 12 grids, Ultrascan 4000 (4k CCD), Tridiem GIF (Ultrascan 1000, 2k CCD)) (FEI company, Netherlands) (See Appendix B for method and images).

DLS measurements were performed on a Malvern Nano Sizer. SLS measurements were conducted using a Brookhaven Instruments BI-200 SM (See Appendix C). Enzyme activities (UV-Vis and fluorescence spectroscopy) were measured with a Tecan Infinite M200 microplate reader using 96-well plates (Corning).

Fluorescence imaging of polymersomes was carried out using a MicroTime 200 scanning confocal microscope (Pico Quant, Germany). The samples were excited by picosecond pulsed lasers emitting at 467 nm (LDH-D-C-470, PicoQuant, Germany) and 640 nm (LDH-D-C-640, PicoQuant, Berlin) controlled by a PDL 828 Sepia II laser driver (Pico Quant, Germany). Excitation light was focused on the sample to a diffraction-

limited spot using a high NA objective (Olympus, Plan-Apo, NA = 1.4, 100 ×, oil immersion) mounted in a Olympus IX 71 microscope frame, and the emission was collected from the sample using the same objective and directed through a pinhole onto a Single Photon Avalanche Diode (SPAD, PDM series, Micro Photon Devices, Italy). To separate the fluorescence emission from the excitation, suitable dichroic mirrors, emission, and excitation filters were used. The samples for microscopy were prepared by drop-casting diluted vesicle solutions onto a glass cover slip (circularly shaped glass cover slides, Ø = 20 mm) for few seconds to allow for adhesion of the polymersomes to the glass surface. Excess solution was removed by a pipette. All experiments were performed in air under ambient conditions.

For flow cytometry, polymersomes (prepared in similar way as the fluorescence microscopy experiments) were analyzed using a BD FACS Canto II flow cytometer.

3.2.2. Preparation of Encapsulated HRP in ABA Polymersomes with OmpF Channel Protein

The ABA polymersomes were prepared by the film rehydration method. Approximately 7.5 mg (0.83 μmol) of ABA triblock copolymer was dissolved in 1.5 mL of ethanol and dried slowly under a stream of nitrogen in a test tube to form a thin film of polymer. Subsequently, 40 μL of 0.75 mg/mL OmpF solution (19.5 μM) was added on the polymer film and vortexed shortly to solubilize the majority of the polymer. The film was further dried under a high vacuum for at least 4 hours in a desiccator. Next, 300 μL of 0.20 mg/mL HRP (4.5 μM) in PBS was added to the tube, followed by 1.2 mL of PBS. The mixture was stirred gently at room temperature overnight to rehydrate the film and allow the formation of polymer vesicles, yielding a uniformly turbid suspension. The suspension was extruded through 0.45 μM PVDF and 0.20 μM PTFE syringe filters (Millipore) to obtain the monodisperse and unilamellar vesicles. The HRP containing

ABA polymer vesicles were purified from the non-encapsulated HRP by a Sepharose 4B size exclusion column, eluting with PBS. The vesicles were characterized by TEM and DLS.

Activity Assays for HRP in ABA Polymersomes

TMB Assay

A stock solution of 5.0 mg/mL TMB (20.8 mM) in 10% DMSO was freshly prepared. In a single well of a 96-well plate (Corning), 50 μL of the ABA polymer vesicles was placed. To this, a mixture of 50 μL of PBS, 50 μL of TMB solution and 10 μL of freshly prepared 0.3% H_2O_2 was added. The absorbance at 370 nm was measured immediately after mixing using a microplate reader (Infinite M200, Tecan, Austria) for 2000 seconds.

Amplex red Assay

A stock solution of 2.5 mg/mL amplex red (9.7 mM) in DMSO was prepared and stored at -20 °C. For assay measurement, the amplex red stock solution was diluted ten times in milliQ. In a single well of a 96-well plate (Corning), 20 μL of the ABA polymer vesicles was placed. To this, a mixture of 100 μL of PBS, 5 μL of amplex red solution (1.0 mM) and 5 μL of freshly prepared 0.03% H_2O_2 was added. The fluorescent emission at 590 nm of the resorufin product was measured immediately after mixing using a microplate reader for 2000 seconds.

3.2.3. Preparation of Multicompartmentalized Polymersomes

The multicompartmentalized polymersomes were prepared by the sequential self-assembly method. Purified encapsulated HRP in ABA polymer vesicle solution (100 μL) was added to 400 μL of 1.0 mg/mL GOx (6.25 μM) in PBS in a glass vial. Then, 50 μL of 1.0 mg/mL PS-PIAT block copolymer in THF was added drop-wise to the solution and

incubated at room temperature for 1 hour. The suspension was filtered six times through Nanosep 100K omega centrifuge filters at 3500 rpm for 15 minutes (Legend Micro 21 Centrifuge, Thermo Scientific, Sorvall) to remove the non-encapsulated molecules. The resulting MC vesicles were re-dispersed in 1.0 mL PBS. These vesicles were characterized by TEM imaging and DLS.

Activity Assay for Multicompartmentalized Polymersomes

TMB Assay

In a single well of a 96-well plate (Corning), 50 µL of the MC vesicles was placed. To this, a mixture of 50 µL of PBS, 50 µL of stock TMB and 10 µL of *β*-D-glucose (2% w/v in PBS) was added. The activity of the cascade reaction in the MC vesicles was measured at wavelength of 370 nm immediately after mixing using a microplate reader for 2000 seconds.

Amplex red Assay

In a single well of a 96-well plate (Corning), 50 µL of the MC vesicles was placed. To this, a mixture of 50 µL of PBS, 5 µL of amplex red solution (1.0 mM) and 10 µL of *β*-D-glucose (2% w/v in PBS) was added. The activity of the cascade reaction in MC vesicles was measured at a fluorescent emission of 590 nm immediately after mixing using a microplate reader for 2000 seconds.

3.2.4. Preparation of Alexa-488 Labeled GOx

For confocal microscopy, flow cytometry, and estimation of the encapsulation efficiency, GOx was labeled with alexa-488 using an alexa fluor 488 protein labeling kit (Life technologies), following the protocol supplied. The labeling efficiency was calculated from the ratio of the absorbance at 280 nm ($\varepsilon_{protein}$ = 267,200 M^{-1} cm^{-1}) and 495 nm (ε_{dye} =

71,000 M^{-1} cm^{-1}) yielding a labeling efficiency of 3.77. For (crude) estimation of the encapsulation efficiency, the absorbance of alexa-488 labeled GOx before and after encapsulation at 488 nm was measured. The scattering of the polymersomes was corrected by fitting the spectra to a first-order exponential decay function using GraphPad Prism 6.01 for Windows (See Appendix D: Figure D1). After correction, the relative areas before and after filtration were determined, allowing calculation of the concentration (See Appendix D: Table D1).

3.2.5. Preparation of Alexa-647 Labeled HRP

For flow cytometry and confocal microscopy, the MC polymersomes were prepared as described above and stained with alexa-647 tyramide (**Scheme 3.2**) using a TSA signal amplification kit (Life technologies), essentially following the procedure supplied, except for the source of the HRP which in this case were the MC polymersomes. After 1 hour incubation, the polymersomes were dialyzed against Milli-Q overnight. To completely remove buffer salts, which otherwise would interfere with the measurement, the samples were spun down twice at 12,000 rpm for 15 minutes, followed by resuspension in Milli-Q water.

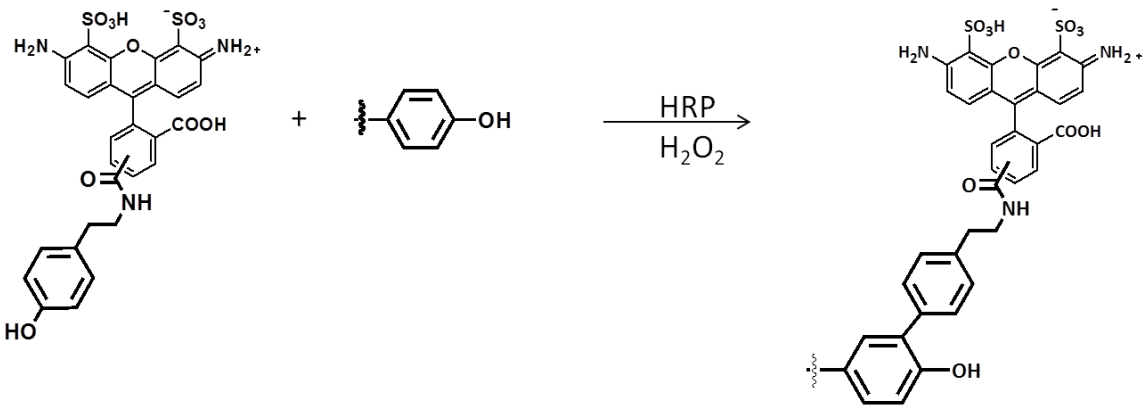

Scheme 3.2. Schematic representation of tyramide signal amplification (TSA). HRP-catalyzed reaction of tyramide-functional fluorescent dyes with tyrosine moieties, giving rise to self-staining. The dye depicted is alexa-488. The structure of tyramide-alexa-647 has not been reported at this time.

3.3. Results and Discussion

The encapsulated HRP in ABA polymer vesicles carrying channel protein were prepared by the film rehydration method and were purified by Sepharose 4B size-exclusion column (**Scheme 3.1)**. The OmpF channel protein acts as a gate for the diffusion of the substrate and H_2O_2 into the vesicle, where HRP catalyzes the oxidation of either TMB into the blue dienimine product or amplex red into the fluorescent resorufin. Sepharose 4B column was used to purify the polymersomes from the non-encapsulated HRP and free OmpF (sample volume applied: 200 µL, fractionation range: 60 kDa–20 MDa) and fractions of 200 µL were collected. As a control, the encapsulated HRP in ABA polymer vesicles without OmpF porin was prepared with the same procedure. To identify the fractions that contain catalytically active polymersomes, the fractions were examined by measuring the absorbance at 295 nm and assaying the HRP enzyme activity by amplex red. The absorbance values and the enzymatic activity (as measured by the change in fluorescence emission at 590 nm minute (FI min^{-1})) are plotted against the fraction number in **Figure 3.1A** and **B**, which show overlapping peaks as the polymersomes eluted. For the blank polymersomes, a similar curve was seen for the absorbance, indicating the presence of polymersomes, while for the enzymatic activity a slight peak was observed, probably due to the presence of a small quantity of free/absorbed HRP in the fractions. **Figure 3.1C** shows the catalytic activity of the ABA and blank polymersomes measured by the absorbance at 370 nm using TMB substrate, whereas **Figure 3.1D** shows the activity measured by the fluorescence emission at 590 nm using amplex red substrate. Both substrates show virtually no activity for the blank polymersomes, i.e. the ABA polymer vesicles without OmpF porins. This outcome was comparable with the results from the previous literature.[65,67] Fractions which showed both increased absorbance and activity were pooled, and used subsequently for the preparation of the MC polymersomes.

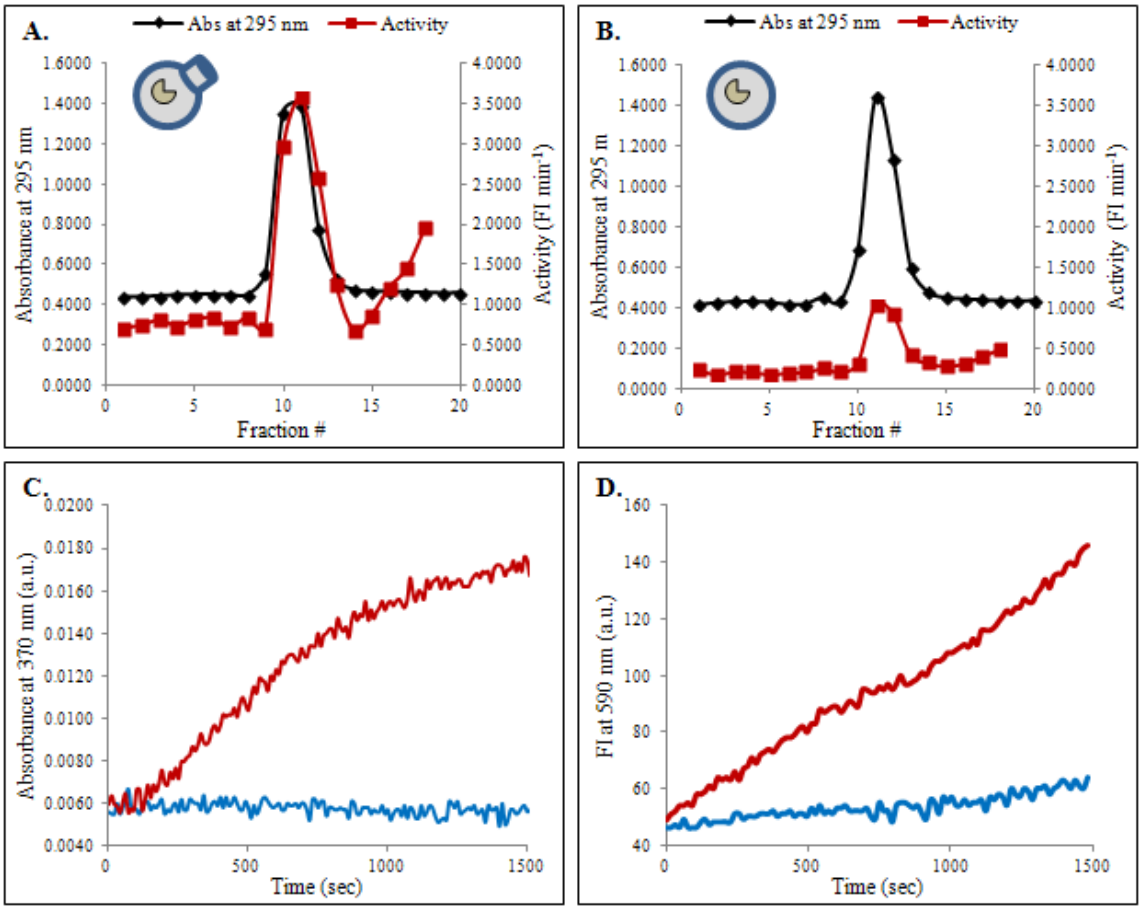

Figure 3.1. The absorbance at 295 nm and the peroxidase activity for each fraction of ABA polymer vesicles with OmpF channel proteins (**A**) and without OmpF channel proteins (**B**) collected from the Sepharose 4B column. The activity was measured as change in fluorescence emission at 590 nm min (FI min^{-1}). The schematic representation of the architecture of polymersome is shown on the top left corner. HRP enzyme activity in ABA vesicles with OmpF channel proteins (*red line*) compared to a blank without OmpF channel proteins (*blue line*) using either TMB substrate (**C**) or amplex red substrate (**D**).

The MC polymersomes with a vesicle-in-vesicle structure were prepared by direct dissolution method and purified by centrifugal filtration to remove the non-encapsulated GOx enzyme (**Scheme 3.1A**). The structures of the individual ABA polymersomes and multicompartmentalized polymersomes were confirmed by TEM (**Figure 3.2A** and **B**). The TEM images indicated that the multicompartmentalized polymersomes were successfully prepared. DLS measurements showed that the ABA vesicles sizes ranged in size from 50 to 250 nm, with an average diameter of approximately 106 nm, whereas the MC polymersomes ranged in size from 100 to 450 nm, with an average diameter of 295 nm (**Figure 3.2C**). These results were comparable with the results from the previous literature.[89] The smaller ABA vesicles caused their encapsulation into the PS-PIAT

polymersomes. More TEM and Cryo-TEM images are presented in Appendix A and B. Static light scattering (SLS) was used to measure the radius of gyration (R_G) and the ρ-value (R_G/R_H) was determined giving a value of ca. 1.0, confirming the vesicular structure of the polymersomes (See Appendix C).[96]

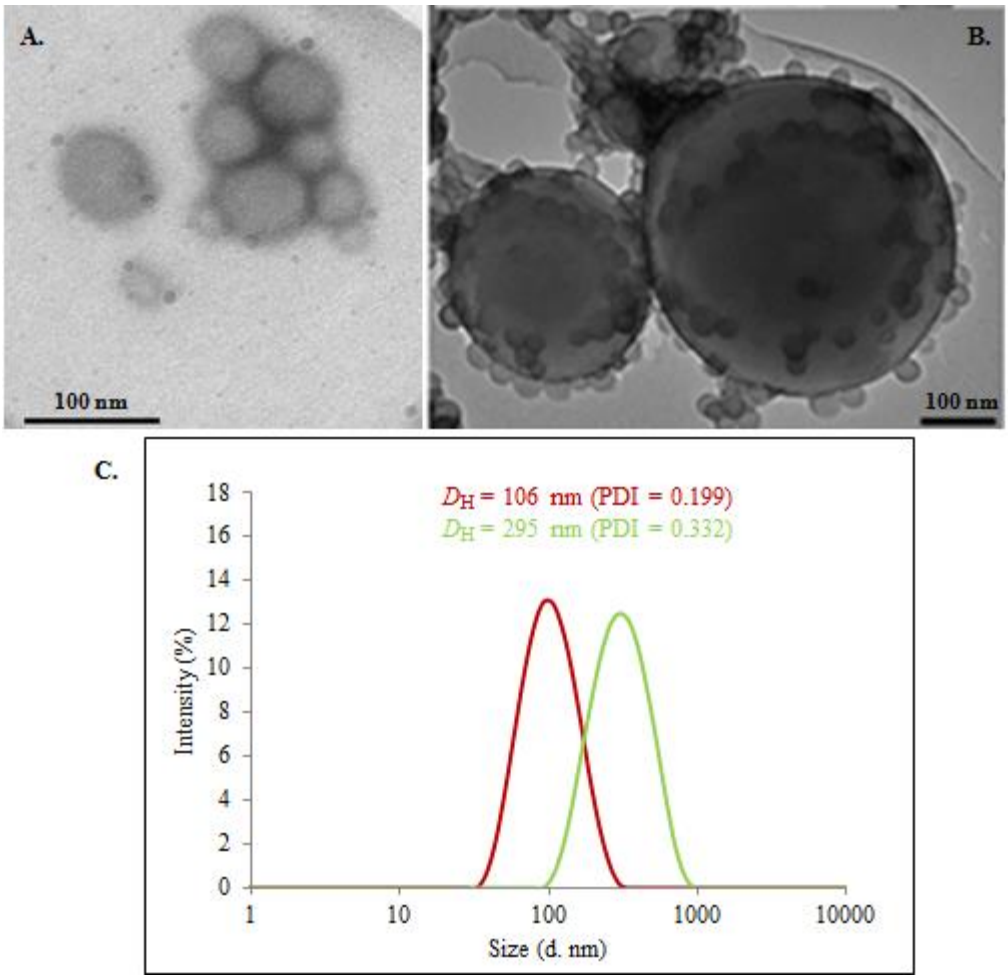

Figure 3.2. TEM images of individual ABA polymersomes (**A**) and multicompartmentalized polymersomes (**B**). The samples were stained with 1% phosphotungstic acid. Scale bars are 100 nm. The average size of ABA polymersomes (*red line*) and MC polymersomes (*green line*) measured with DLS (**C**).

In order to investigate the purification of MC polymersomes from free GOx enzymes, centrifugal filtration was performed by collecting the flow-throughs/filtrates and measuring the GOx activity. In this case, HRP (0.2 mg/mL) was added in excess to the solutions. The activities observed for each filtrate (as measured by the change in fluorescence emission at 590 nm minute (FI min^{-1})) are represented in a bar chart (**Figure**

3.3), showing a clear decrease after each filtration round, except for the activity of the first and second flow-through. This may result from the presence of THF, which could affect the performance of GOx.[97] For comparison, the activity of the MC polymersomes (i.e. the supernatant solution after 6 times centrifugal filtration) was also shown. This result not only proved that the enzymes were successfully encapsulated, but also showed that the GOx activity was retained inside the MC polymersomes.

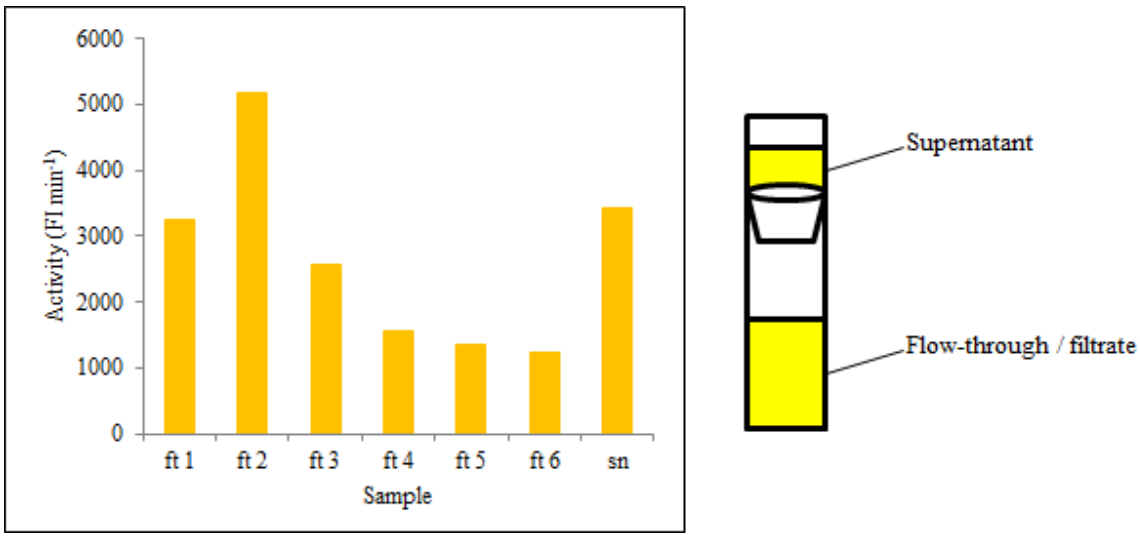

Figure 3.3. Activity of GOx enzyme (measured by addition of HRP) of the flow-throughs (ft 1-ft 6) from the centrifuge filtration compared to the MC polymersomes (i.e. the supernatant/sn). Activities were measured at 590 nm.

To probe the cascade reaction in the MC polymersomes, the activity was measured by the glucose/TMB cascade (370 nm) as well as glucose/Amplex red cascade (590 nm). Indeed, the multicompartmentalized polymersomes where OmpF porin was embedded into the inner ABA membranes showed accumulation of the product, indicating that exchange between the compartments was possible, whereas the control experiment where OmpF porins were omitted showed considerably lower enzymatic activity (**Figure 3.4A** and **B**). This is because, without the OmpF porins acting as a gate, neither substrate nor H_2O_2 is able to enter the inner vesicle, due to the non-permeability of the ABA membrane. Consequently, the encapsulated HRP cannot catalyze the oxidation

of the TMB or the amplex red. Hence, enzymatic activity is strongly reduced for the control experiment.

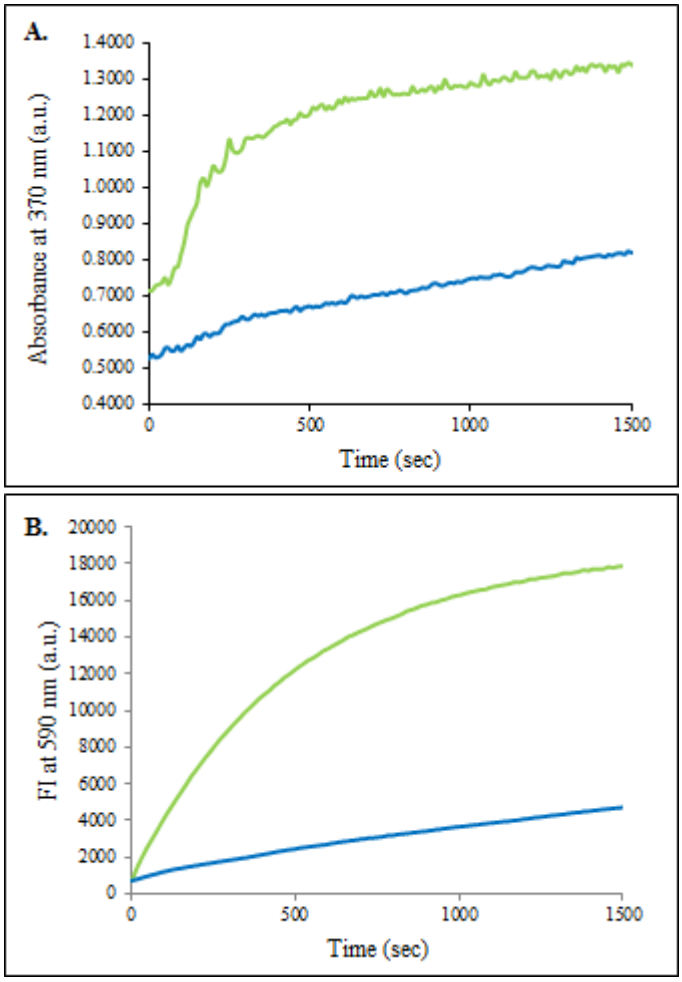

Figure 3.4. Activity of the cascade reactions in MC polymersomes (*green line*) compared to a blank where no OmpF channel proteins were embedded in the ABA vesicles (*blue line*) using TMB assay (**A**) or Amplex red assay (**B**).

Comparing the cascade activity of the MC polymersomes to the control experiments, such as ABA polymer vesicles in the presence of bulk GOx, blank MC polymersomes without OmpF present in the membrane and blank MC polymersomes with no HRP encapsulated inside, as in **Figure 3.5**, revealed that the conversion of amplex red was significantly higher for the MC polymersomes. The initial rate (v_0) of amplex red conversion for the MC polymersomes (v_0 = 22.2 au sec^{-1}) was considerably higher than for the blank MC polymersomes with no OmpF (v_0 = 3.6 au sec^{-1}) or no HRP

(v_0 = 3.3 au sec^{-1}). Since HRP and GOx are in close proximity in the MC polymersomes, it enhances the conversion of amplex red, given that OmpF is present to assist diffusion of the reactants.[98] The rate observed for the blank MC polymersomes without OmpF (v_0 = 3.6 au sec^{-1}) was almost equivalent to the blank MC vesicles without HRP (v_0 = 3.3 au sec^{-1}), implying that this activity is mostly happened because of the auto-oxidation of amplex red by the production of hydrogen peroxide. Auto-oxidation also influenced the single ABA polymer vesicles containing 0.3 mg mL^{-1} free GOx, roughly containing the same enzyme concentrations as the MC polymersomes. The final product yield for the ABA nanoreactors with free GOx, as can be seen from the fluorescence intensity at time = 2000 sec, was at least 2 times higher than for the blank MC polymersomes, indicating an involvement of the encapsulated HRP.

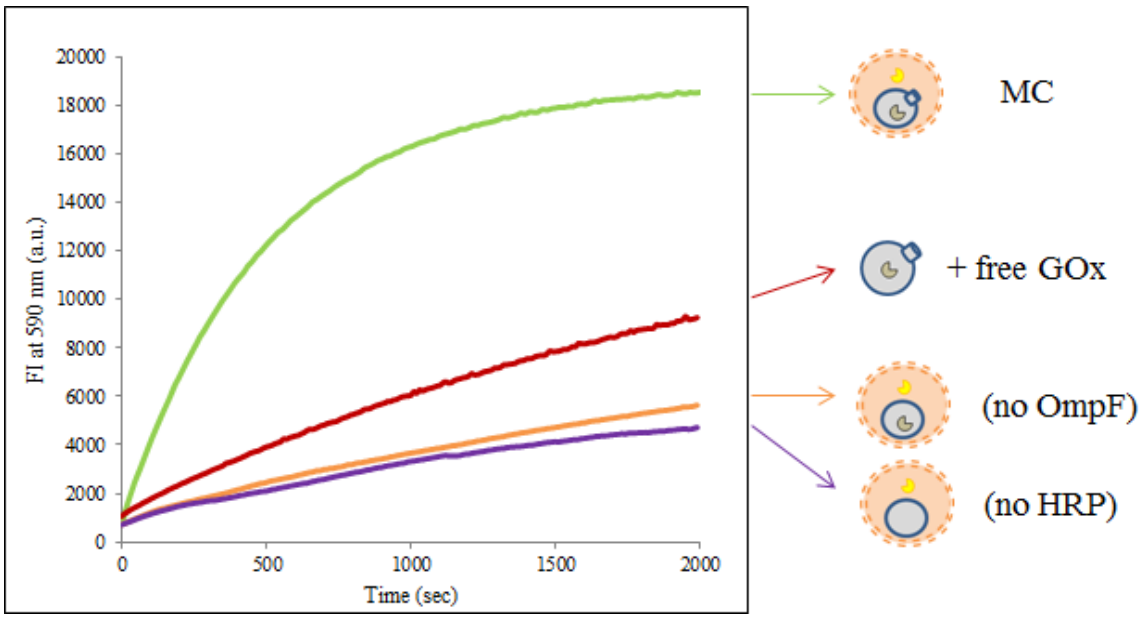

Figure 3.5. Cascade activity of the MC polymersomes as compared to the controls using Amplex red assay, showing an increased conversion of amplex red.

On the other hand, a series of measurements for enzymes in the bulk solution were prepared and their activities were measured by glucose/Amplex red cascade. For the bulk measurements, the concentration of GOx enzymes was fixed at 0.3 mg mL^{-1}, which was based on GOx encapsulation efficiency (ee) of about 38%, as estimated by measurement

of alexa-488 labeled GOx before and after encapsulation (See Appendix D), whereas the concentration of HRP was varied between 10 µg mL^{-1} (the theoretical HRP concentration at 100% ee) and 40 ng mL^{-1} (0.4% ee). It showed that the rate of resorufin formation increased with increasing HRP concentration (**Figure 3.6A**). Another observation was shown when the initial rate of the reaction (v_0) was plotted against HRP concentration (**Figure 3.6B**), the reaction rate increased linearly with HRP concentration below concentration of 5 µg mL^{-1}, which indicated that HRP catalysis was the rate determining factor. Above that concentration, GOx became rate determining.

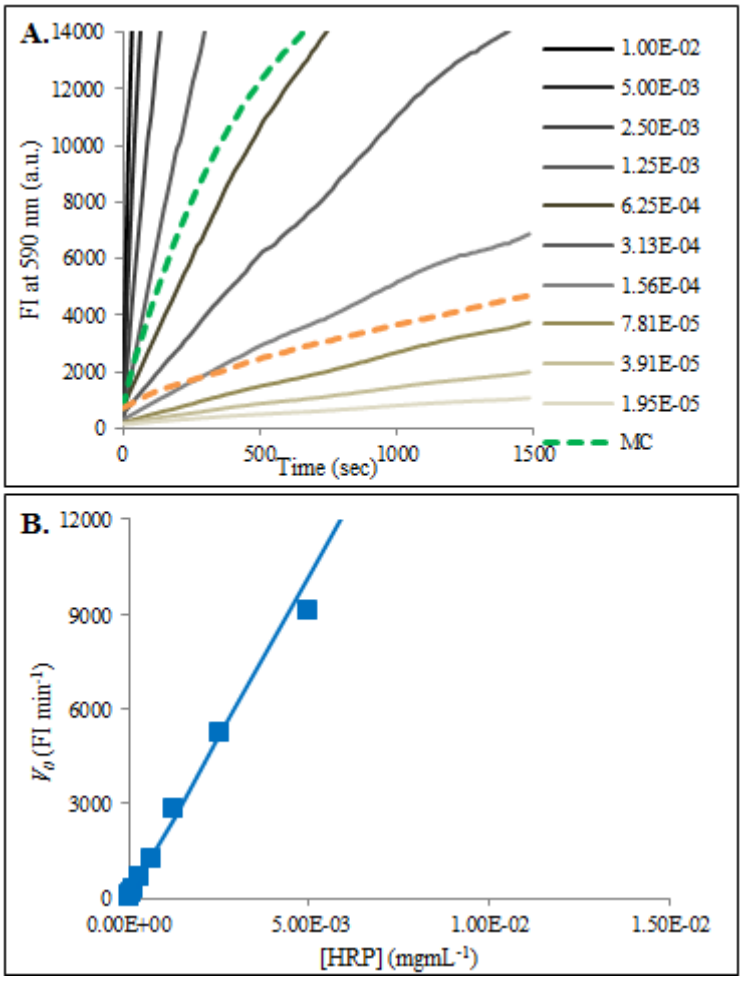

Figure 3.6. Bulk cascade measurements. Conversion of amplex red versus time by the GOx/HRP cascade, as measured by the increase of fluorescence at 590 nm (**A**). For comparison, the time trace of the reaction in the presence of MC polymersomes (orange dots), as well as that of ABA nanoreactors in the presence of free GOx (0.3 mg mL^{-1}) is also shown. Plot of initial velocities of the bulk reactions measured in **A** versus HRP concentration (**B**).

Judging that encapsulation is a statistical process, multiple species of polymersomes could be present in the MC polymersomes sample, such as single ABA and PS-PIAT polymersomes, apart from MC polymersomes. In order to distinguish between multiple species of polymersomes and to confirm if the enzymes are encapsulated separately in the two compartments, scanning confocal fluorescence microscopy was performed. Here, the inner compartment was stained by a reaction commonly used in histochemistry, so-called catalyzed reporter deposition.[99] This reaction makes use of the HRP-catalyzed oxidation of tyramides into radicals, which rapidly react with electron-rich amino acid moieties, mostly tyrosines (See **Scheme 3.2**). The use of tyramides carrying a fluorescent label leads to fluorescent staining. In our study, successful fluorescent staining will indicate that HRP is *active* in the OmpF-equipped MC polymersomes, while concomitant fluorescent labeling of GOx will show *colocalization* of the fluorescent signals.

Following this approach, MC polymersomes containing alexa-488 labeled GOx are prepared and incubated with tyramide alexa-647, and subsequently, the dye was removed by overnight dialysis. Visualizing and comparing the MC polymersomes samples with fluorescence microscopy in both blue channel and red channel (**Figure 3.7A-C**), we are able to distinguish the MC vesicles from single ABA and PS-PIAT polymersomes. As a control experiment, the blank MC polymersomes where OmpF porins were omitted in the inner compartment was used and imaged as well (**Figure 3.7E-G**). Both MC polymersomes with and without OmpF porins showed fluorescence signal at 488 nm, indicating that the labeled GOx was successfully encapsulated (**Figure 3.7B** and **F**). On the other hand, when visualizing those MC polymersomes in the red channel, a strong fluorescence signal was observed only for the MC polymersomes with OmpF porins (compare **Figure 3.7C** and **G**). This result proved that the OmpF channel would act as a gate which allowed the dye to enter into the inner compartment, and subsequently

catalyzed by HRP. By combining the images of the MC polymersomes in blue channel and red channel, the *colocalization* of the fluorescent signals at different wavelengths was demonstrated and represented in **Figure 3.7D**. This conclusion further supports our scheme that certain amount of enzymes is encapsulated in the multicompartmentalized polymersomes.

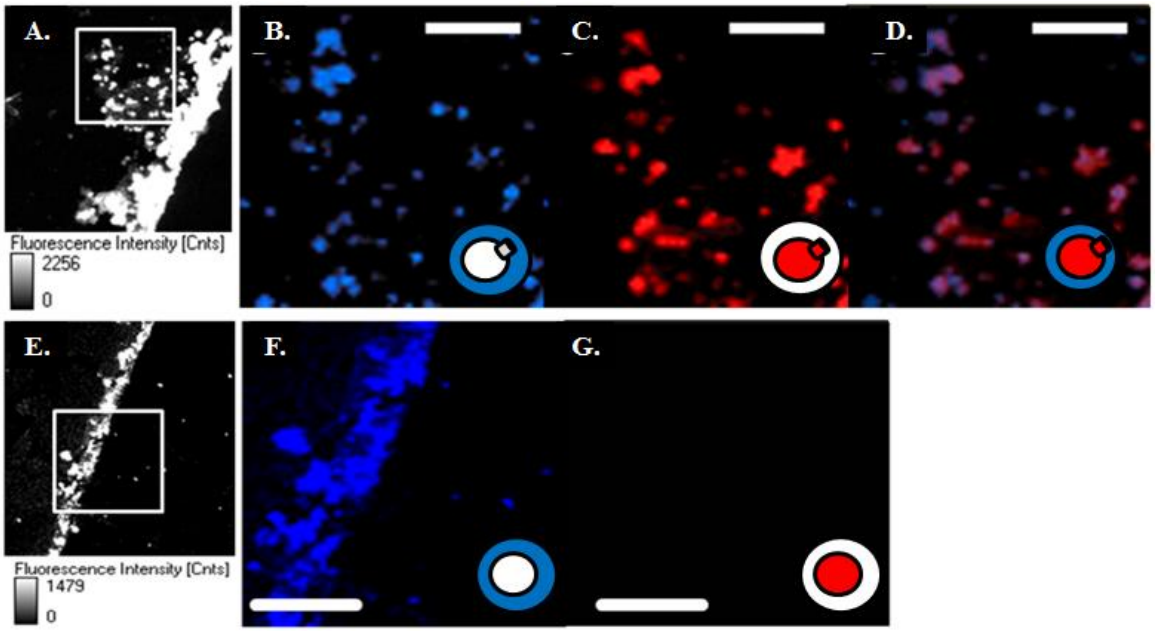

Figure 3.7. Confocal microscope images of MC polymersomes (**A**) and the blank MC polymersomes where no OmpF porins were embedded in the inner compartment (**E**). MC polymersomes and the blank MC polymersomes were prepared as described before. GOx was labeled with Alexa Fluor 488 and imaged in the blue channel (**B**; and **F** for the blank). After preparation of MC polymersomes, HRP was stained by its reaction with Alexa Fluor 647 tyramide and imaged in the red channel. (**C**). Fluorescence in the red channel was only observed when the OmpF porin was present in the inner compartment (compare **C** and **G**). The composite image of the blue and red channel which show the *colocalization* of the images (**D**). (**B, C, D** are the magnification of **A**, as specified by the white square; whereas **F, G** are magnification of **E**). The scale bars are 20 μm.

Furthermore, flow cytometry was also performed to the labeled MC polymersomes to investigate the distribution of enzymes in the MC polymersomes (**Figure 3.8**) and encapsulation efficiencies (See Appendix E). The measurements showed that out of the full population of polymersomes, 28% contained both alexa-647 labeled HRP and alexa-488 labeled GOx (i.e. MC polymersomes), while 5.7% and 16.2% contained alexa-647 labeled HRP (i.e. ABA polymersomes) and alexa-488 labeled GOx

(i.e. PS-PIAT polymersomes), respectively. By assuming that most GOx was labeled, upon addition of PS-PIAT, 44.2% of the resulting polymersome population contained GOx, which indicated that 63% of the population also included active HRP. Considering the ABA polymersomes, 83% of the total ABA population appeared to coexist with PS-PIAT, which is assigned to the filtration process, leading to disintegration of the single ABA nanoreactors. If the flow cytometry only detected the active enzymes of the polymersomes, hence, the outcome suggests that most of the cascade activity reactions are resulted from the MC polymersomes.

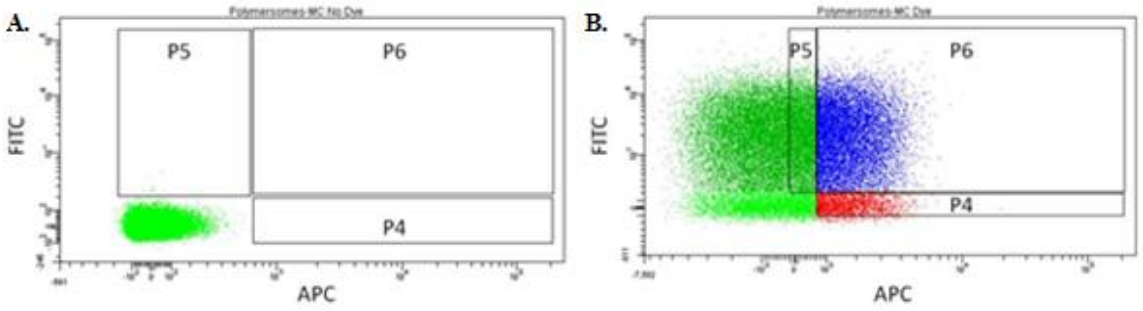

Figure 3.8. Flow cytometry analysis of the multicompartmentalized polymersomes. MC polymersomes containing unlabeled HRP and GOx enzymes, in which no fluorescence is detected in the sample (**A**). MC polymersomes containing alexa-674 labeled HRP and alexa-488 labeled GOx (**B**). Here, HRP is labeled with tyramide staining, in which only active HRP is observed. Regions P4 and P5 denote alexa-647 labeled HRP (i.e. ABA polymersomes, *red dots*) and alexa-488 labeled GOx (i.e. PS-PIAT polymersomes, *dark green dots*), respectively, whereas region P6 denote the double-labeled enzymes (i.e. MC polymersomes, *blue dots*). For a detailed discussion of the flow cytometry results, see **Appendix: Figure E1**.

In brief, eukaryotic cells are exceedingly complex membrane-delineated compartments whose internal organization makes possible the different functions that sustain their survival. In this work, we have demonstrated, on the most basic level, that we can develop higher-order architectures using fully synthetic amphiphilic block copolymers that mimic certain features of cells (compartmentalization of enzymes, and exchange of molecules). Upon detailed characterization of the formed architectures, their functionality is shown by a cascade reaction between separately encapsulated enzymes. This unique and stable higher-order architecture of polymer vesicles could serve as a

design principle for new generation of drug delivery vehicles, biosensors and protocell models.

3.4. Conclusion

Multicompartmentalized polymersomes with two different enzymes encapsulated separately in the two compartments were successfully prepared. By inserting the channel protein OmpF in the inner compartments' membrane, the exchange of molecules was made possible. Together with the intrinsic permeability of PS-PIAT, this allowed the construction of a bi-enzymatic cascade reaction. Functional multicompartments were shown by the encapsulation of HRP in the inner compartment and GOx in the outer compartment and measuring the conversion of either TMB or amplex red through the oxidation of glucose. The development of this multicompartmentalized structure gives rise to a new step in the mimicry of the compartmentalization of cells, and provides us the opportunity to study and understand the complexity of eukaryotic cells, opening the prospect of engineering very specific multicompartment polymersomes.

3.5. Output

This work was published on *Journal of Materials Chemistry B.*

Siti, W.; de Hoog, H. –P. M.; Fischer, O.; Shan, W. Y.; Tomczak, N.; Nallani, M.; Liedberg, B. An Intercompartmental Enzymatic Cascade Reaction in Channel-Equipped Polymersome-in-Polymersome Architectures, *J. Mater. Chem. B*, **2014**, *2*, 2733−2737.

CHAPTER 4

Synthesis & Assembly of Novel Functional Compartments from the New Building Blocks of Protein-Polymer Complexes

4.1. Introduction

In the previous chapter, we reported an enzymatic cascade reaction in the multicompartmentalized polymersomes catalyzed by two different enzymes encapsulated in different compartments. This functional multicompartmentalized structure was prepared by sequential self-assembly approach using synthetic amphiphilic block copolymers, i.e. PMOXA-PDMS-PMOXA (ABA) and PS-PIAT polymers. Apart from these synthetic amphiphilic block copolymers, peptide-based and protein-based block copolymers as building blocks have been used to prepare vesicles, known as peptosomes[45-48] (See **Section 2.3.1**) and proteinosomes,[60-62] (See **Section 2.4**) respectively. Using polypeptides and proteins as building blocks offer advantages compared to the amphiphilic block copolymers, especially in terms of biocompatibility, biodegradability and biofunctionality of the membranes. Another type of semi-permeable polymeric vesicles formed from a so-called polyion complex membrane was developed by Kataoka group recently by mixing a pair of oppositely charged polypeptides block copolymers in aqueous medium.[50-52] These vesicles were termed as PICsomes (See **Section 2.3.2**). In contrast to other polymersomes, the advantages of PICsomes are the absence of the use of organic solvent during preparation, the facile encapsulation of water-soluble macromolecules, and the semi-permeability of the vesicle wall.[50] Furthermore, they show pH sensitive self-assembly,[51] and are resistant to protease degradation.[52]

In order to extend the development of novel functional compartments which are self-assembled without any traditional methods of polymer vesicles self-assembly, a new method of forming protein-polymer conjugate was designed and the protein-polymer conjugate was synthesized to facilitate the self-assembly. In this chapter, we present the facile route using bio-orthogonal chemistry[100-105] for developing new supramolecules consisting of poly(ethylene glycol) (PEG) connected to the major bovine milk protein β-lactoglobulin (BLG). Here, BLG is chosen as a protein of interest due to having fascinating self-assembly behavior[106] and its availability in pure form. These protein-polymer complexes are self-assembled eventually into fluorescent novel functional nanoscale compartments in an aqueous solution (**Figure 4.1**). We term these nano-compartments as 'proteinionosomes', and demonstrate how their structural and functional characterization would allow them to be used as cell mimics, capable of encapsulate molecules and furthermore they are permeable for smaller molecules.

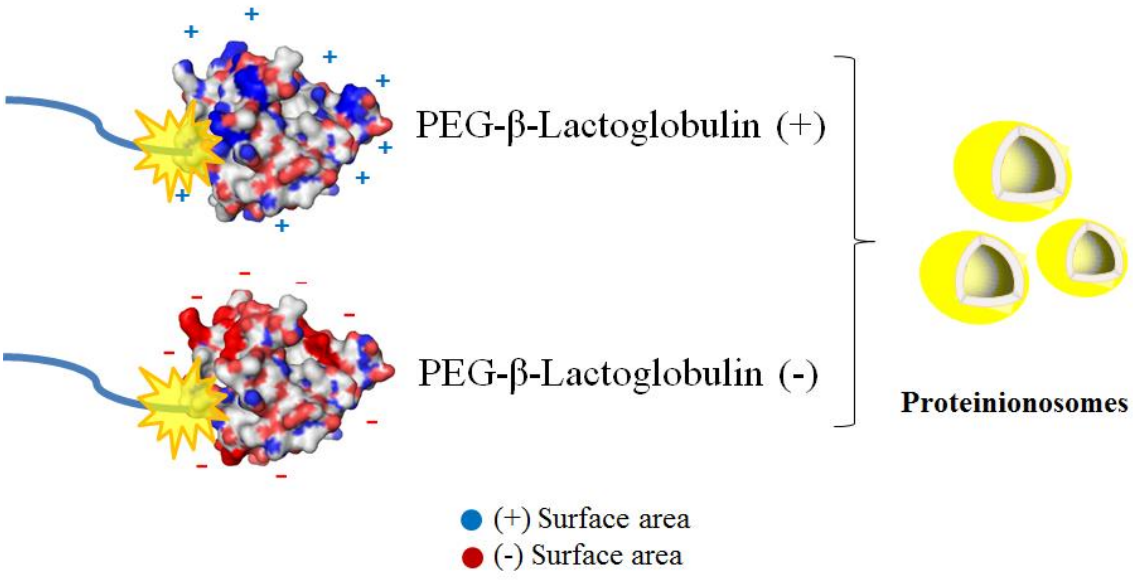

Figure 4.1. Self-assembly of fluorescent proteinionosomes from new building blocks of oppositely charged PEG-BLG complexes that are fluorescent.

For the preparation of the protein-polymer conjugates, bio-orthogonal chemistry using mild-intensity UV light (302 nm), which involves tetrazoles[107] and alkenes is utilized in the construction of PEG-BLG conjugates.[100-105] Upon UV irradiation, the tetrazole expels N_2 and forms a relatively stable nitrile imine intermediate, which reacts spontaneously with a dipolarophile, such as an alkene to generate a fluorescent pyrazoline cycloadduct (**Scheme 4.1**).[100-101] Apart of getting high yield of product, several advantages of this reaction are the simplicity of preparing the starting material with tetrazole functionality, no catalyst and organic solvent being involved in the system, as well as a fast approach (15-20 minutes) to generate fluorescent cycloadduct. Such fluorescent product may be beneficial; especially it can be measured simply by fluorescence spectroscopy. As a result, the final proteinionosomes will be fluorescent as well.

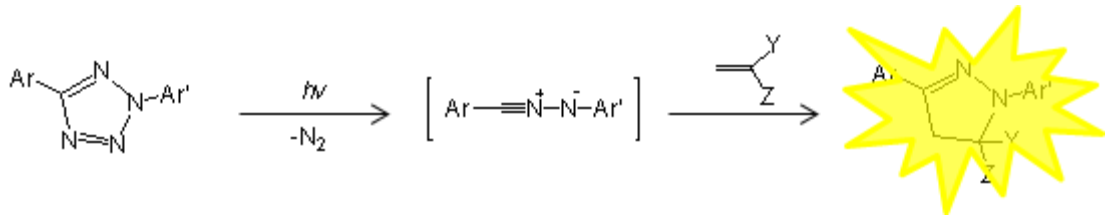

Scheme 4.1. Photoinduced cycloaddition reaction involves tetrazole and alkene to generate pyrazoline cycloadduct, which is fluorescent. Reproduced with permission from ref.[100] Copyright © 2008 WILEY-VCH Verlag GmbH & Co. KGaA, Weinheim.

In order to make BLG suitable for the photo-click chemistry, we adopt a strategy to site-specifically introduce a PEG-chain at the only free cysteine residue of BLG, i.e. Cys-121,[106,108] in which cysteine is derivatized to an alkene by reacting with allyl chloride as reported by Chalker *et al.*[109] Following that, the positive and negative groups of allyl-appended BLG (BLG-allyl) are prepared by reacting the glutamate or lysine residues of BLG with ethylene diamine or succinic anhydride respectively.[110-112] Since each BLG has 16 glutamate residues and 15 lysine residues, the ratio for the positive and negative

groups should be about 1:1, and therefore, BLG seems to be a good choice to be used in developing the new building blocks of protein-polymer complexes. Tetrazole-functionalized PEG (PEG-tetrazole) is prepared following procedure reported in the literature,[100-101] which later undergoing photoinduced cycloaddition chemistry with both positive and negative group of BLG-allyl to form charged PEG-BLG conjugates which are fluorescent (See **Scheme 4.2**).

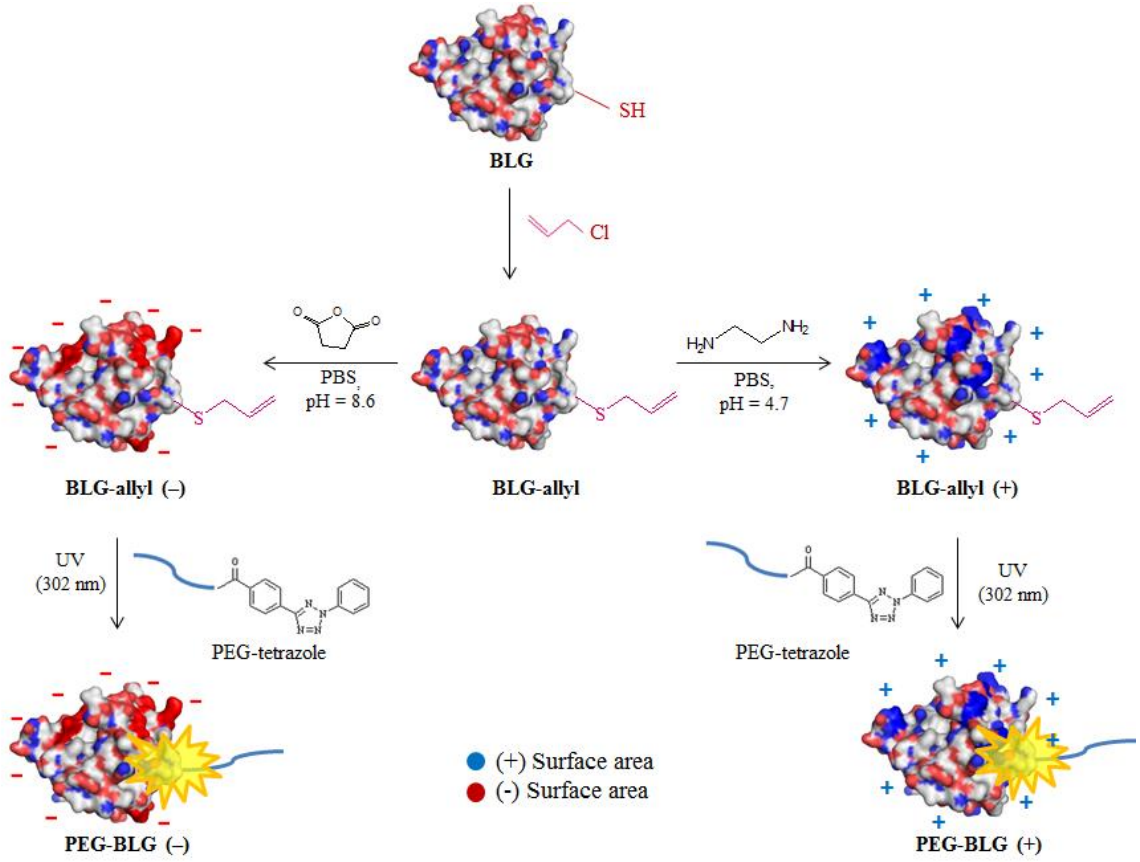

Scheme 4.2. Schematic representation for the chemical modification of BLG at the free cysteine residue at Cys-121 to the formation of positive and negative charged of PEG-BLG conjugates under photoinduced cycloaddition chemistry. The positive and negative groups of BLG-allyl were introduced by reacting the glutamate and lysine residues with suitable reagents, respectively.

4.2. Experimental

4.2.1. Materials and Methods

Terephthaldehydic acid, benzenesulfonyl hydrazide, aniline, succinic anhydride, allyl chloride, 4-dimethylaminopyridine (DMAP), and 1-Ethyl-3-(3-dimethylaminopropyl) carbodiimide hydrochloride (EDC) were bought from TCI. Poly(ethylene glycol)monomethyl ether-3300 (PEG-3300) was purchased from Polymer Source. Sodium nitrite, sodium chloride, hydrochloric acid, pyridine, ethylene diamine dihydrochloride and bovine milk β-lactoglobulin isoform A (BLG-A) were bought from Sigma-Aldrich. Phosphate buffer saline (PBS, 1X, pH 7.4) was purchased from Invitrogen. Absolute ethanol and dimethylformamide (DMF) were from Merck. Ethyl Acetate and dichloromethane were from Alfa Aesar. All reagents, buffers and solvents were used as received, without further purification.

UV-Vis measurements were performed on a Perkin-Elmer Lambda 35 UV/Vis spectrometer. Absorbance and fluorescence measurements were performed on a Tecan Infinite M200 pro plate reader using 96-well plates (Corning). Dynamic Light Scattering (DLS) and Zeta Potential measurements were performed on a Malvern Nano Sizer. Nuclear Magnetic Resonance (NMR) spectra were obtained from 300-MHz Bruker Avance Ultrashield. UV irradiation was conducted using a UVP UVM-57 Handheld UV lamp at 302 nm (6 Watt, 0.16 Amps). SDS-PAGE was performed using Bio-Rad Mini-PROTEAN Tetra Cell. MALDI-TOF was performed on a Shimadzu Kratos Axima TOF2 using 4-hydroxy-3,5-dimethoxycinnamic acid as matrix. Fast Protein Liquid Chromatography (FPLC) was performed with ÄKTA purifier UPC-900. Transmission Electron Microscopy (TEM) was carried out on a FEI Tecnai G^2 200 kV TEM.

4.2.2. Preparation of 4-(2-phenyl-2*H*-tetrazol-5-yl)benzoic acid (1; Tetrazole)

Tetrazole (**1**) was prepared following literature procedures.[100-101,107] The mixture of benzenesulfonyl hydrazide (0.86 g, 25 mmol) and terephthaldehydic acid (0.75 g, 5.0 mmol) in 50.0 mL of ethanol was stirred for 30 minutes, followed by the addition of 100 mL water. The white precipitate that formed was collected in a funnel, yielding the phenylsulfonyl hydrazone. At the same time, about 2.0 mL of aqueous sodium nitrite solution (2.5 M) was added dropwise to a cooled mixture of 1.3 mL concentrated HCl and aniline (0.47 g, 5.0 mmol) dissolved in 8.0 mL of ethanol-water (1:1). Subsequently, this yellow solution was added slowly to 30.0 mL of phenylsulfonyl hydrazone in pyridine cooled in an ice-salt bath, resulting in an orange or red solution. The reaction mixture was then extracted with ethyl acetate (50.0 mL x 3). The organic layers were collected and combined, followed by addition of 250.0 mL of 3M HCl. The pinkish precipitates that formed were collected and purified by recrystallization with hot ethanol to yield 0.40 g (30.2 %) of product.

^{1}H-NMR (300 MHz, DMSO-d_6): δ 13.35 (s, 1H), 8.36 (d, 2H), 8.22 (m, 4H), 7.77 (m, 2H), 7.69 (m, 1H) (See Appendix F).

4.2.3. Preparation of Tetrazole-functionalized Poly(ethylene glycol), PEG-3300-Tetrazole

Briefly, a solution of EDC (10.9 mg, 57.2 μmol) in 0.5 mL of dichloromethane was added dropwise to a mixture of PEG-3300 (100.0 mg, 28.6 μmol) and tetrazole (**1**) (9.7 mg, 34.3 μmol), and DMAP (0.8 mg, 2.86 μmol) in 1.0 mL of dichloromethane at -20 °C. After complete addition, the reaction mixture was allowed to stir for 20 hours at room temperature. Then, the reaction mixture was extracted with 0.1 M HCl (1.5 mL x 2), followed by saturated sodium chloride (1.5 mL x 2). The organic layer was dried with

magnesium sulfate before rotary-evaporation and drying under high vacuum overnight. The orange crystallines solid was then dissolved in milliQ and centrifuged at 14,000 rpm for 10 minutes to remove non-dissolved material. The filtrate was freeze-dried overnight to yield 79.9 mg (74.5%) of a white powder.

^{1}H-NMR (300 MHz, $CDCl_3$): δ 8.31 (d, 2H), 8.18 (m, 4H), 7.56 (m, 2H), 7.48 (m, 1H), 4.48 (t, 2H), 3.83 (t, 2H), 3.51 (m, 296H), 3.36 (s, 3H) (See Appendix F). MALDI-TOF: m/z 3,140 Da.

4.2.4. Preparation of Allyl-functionalized β-Lactoglobulin, BLG-allyl

Allyl-functionalized BLG was prepared as detailed in literature by mixing 2.0 mL of 2.0 mg/mL BLG (0.11 mM) in 5.0 mM of PBS, pH 7.5 with 200 µL of allyl chloride (0.65 M) in DMF.[109] The mixture was incubated under agitation using a thermomixer (VWR 5355, Eppendorf) at 37 °C for 2.0 hours, followed by removal of the small molecules using a PD-10 column, eluting with 5.0 mM PBS, pH 7.5. An Ellman's test[113-115] was performed to determine the yield of the reaction (See Appendix G, Table G1). The product was freeze-dried overnight to yield white powder.

4.2.5. Preparation of Positively Charged Allyl-functionalized β-Lactoglobulin, BLG-allyl (+)

The positively charged BLG-allyl was prepared by reacting the glutamate residues of BLG with ethylene diamine. [110-112] About 120 µL of 0.1 M of ethylene diamine of pH 4.7 (12.0 µmol, 10.0 equiv.) was added to 1.0 mL of 2.0 mg/mL BLG-allyl (0.11 µmol) in 0.1 M PBS, pH 4.7, followed by addition of 1.1 mg of EDC (5.8 µmol). The reaction mixture was incubated at room temperature for 2.0 hours, followed by removing the low mass components using a PD-10 column, eluting with milliQ. The collected fractions were

freeze-dried overnight to yield a white powder. MALDI-TOF: m/z 19,679 Da. Average zeta potential measurements: +27.7 mV.

4.2.6. Preparation of Negatively Charged Allyl-functionalized β-Lactoglobulin, BLG-allyl (–)

The negatively charged BLG-allyl was prepared by reacting lysine residues of BLG with excess succinic anhydride.[110-112] Briefly, 1.22 mg of succinic anhydride (12.2 μmol, 10.0 equiv.) was added to 1.0 mL of 2.0 mg/mL BLG-allyl (0.11 μmol) in 0.1 M PBS, pH 8.6 in a glass vial under shaking. The pH was maintained between 8.0 and 9.0 by pH indicator paper. The reaction was incubated at room temperature for 2.0 hours, followed by removing the excess low mass components using a PD-10 column, eluting with milliQ. The collected fractions were freeze-dried overnight to yield a light yellow powder. MALDI-TOF: m/z 19,946 Da. Average zeta potential measurements: -29.9 mV.

4.2.7. Preparation of Positively Charged Protein-Polymer Conjugates, PEG-BLG (+) using Photoinduced Cycloaddition Chemistry

The positively charged protein-polymer conjugates were prepared by the UV irradiation method using the BLG-allyl (+) and the PEG-tetrazole. Shortly, 1.0 mL of 1.5 mg/mL BLG-allyl (+) (0.08 μmol, 1.0 equiv.) in milliQ was mixed with 0.3 mL of 5.0 mg/mL mPEG-3300-Tetrazole (0.43 μmol, 5.0 equiv.) in milliQ in a quartz cuvette (10 mm pathlength). Under stirring, the mixture was irradiated at 302 nm with a handheld UV-lamp at about 5 cm distances from above for 15 minutes, resulting in light yellow solution. For purification, the mixture was filtered three times through Vivaspin 10 kDa centrifuge filter at 10,000 rpm for 10 minutes each time (Legend Micro 21 Centrifuge, Thermo Scientific, Sorvall) to remove excess PEG-tetrazole. The resulting PEG-BLG (+) was redispersed in 1.0 mL of milliQ, and freeze-dried overnight yielding a white/ light

yellowish powder. The product was characterized by fluorescence spectroscopy, SDS-PAGE and MALDI-TOF. Furthermore, FPLC with Sepharose SP HP column (Sigma Aldrich) was used for purification to get a pure PEG-BLG (+) product (See Appendix H for the chromatogram). MALDI-TOF: m/z 23,315 Da. Average zeta potential measurements: +21.3 mV.

4.2.8. Preparation of Negatively Charged Protein-Polymer Conjugates, PEG-BLG (–) using Photoinduced Cycloaddition Chemistry

Same procedure and purification step as the preparation of positively charged protein-polymer conjugates, the negatively charged protein-polymer conjugates were prepared by the UV irradiation method using the BLG-allyl (-) and the PEG-tetrazole. The product was characterized by fluorescence spectroscopy, SDS-PAGE and MALDI-TOF. Furthermore, FPLC with Sepharose Q FF column (Sigma Aldrich) was used for purification to get a pure PEG-BLG (-) product (See Appendix H for the chromatogram). MALDI-TOF: m/z 23,569 Da. Average zeta potential measurements: -20.8 mV.

4.2.9. Self-Assembly of Proteinionosomes

Proteinionosomes were prepared by mixing a pair of oppositely charged protein-polymer conjugates in equal concentration of charged (1:1 $–NH_3^+$ units : $–COO^-$ units) in an aqueous solution. Since we have a ratio of 16:15 of positive to negative groups (~1:1), 0.5 mL of 1.0 mg/mL PEG-BLG (+) and 0.5 mL of 1.0 mg/mL PEG-BLG (–) in milliQ were mixed. The reaction mixture was vortexed for 30 seconds, before being incubated at room temperature overnight. DLS was used to measure the size of proteinionosomes formed. Further characterization was performed with TEM to confirm the structure of the novel compartments.

4.3. Results and Discussion

BLG-allyl was prepared by allylation of the only accessible free cysteine residue of BLG, i.e. Cys-121. For characterization, Ellman's test was performed to determine the concentration of free thiols to the unmodified BLG (See Appendix G). The test showed that there were not any free thiols left after the reaction with allyl chloride. This means that all of the free thiols had been derivatized into alkene groups. Subsequently, the oppositely 'charged' BLG-allyl was introduced by modifying the glutamate and lysine residues of BLG with suitable reagents. MALDI-TOF analysis was carried out to confirm the presence of charged BLG-allyl; whereas zeta potential measurements were performed to identify the surface charged of the protein. The average zeta potential for BLG-allyl (+) was measured to be +27.7 mV and BLG-allyl (-) was measured to be -29.9 mV. Both of these values were in agreement with the ratio of glutamate and lysine residues (1:1).

Following that, the charged BLG-allyl was then conjugated to PEG-tetrazole under irradiation with UV light at wavelength of 302 nm for15 minutes. In our case, the photoinduced cycloaddition reaction would give rise to a protein-polymer conjugate with a pyrazoline moiety as the connecting group between PEG and BLG. Since the pyrazoline shows strong fluorescence emission between 470-540 nm,[100] the conversion of tetrazole to pyrazoline was analyzed by the accompanying changes in the fluorescence spectra. As can be seen in **Figure 4.2**, the fluorescence emission after UV irradiation (*red line*) showed a maximum at 510 nm, indicating the presence of pyrazoline cycloadducts, whereas no visible peak was seen before UV irradiation (*blue line*) at that particular wavelength.

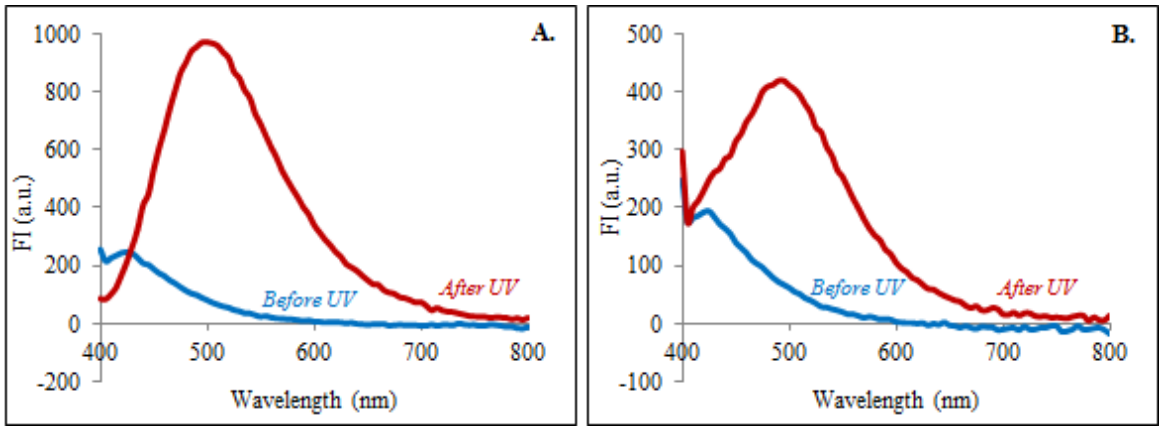

Figure 4.2. Schematic representation for the chemical modification of BLG at the free cysteine residue at Cys-121 to the formation of positive (**A**) and negative (**B**) charged of PEG-BLG conjugates under photoinduced cycloaddition chemistry. The positive and negative groups of BLG-allyl were introduced by reacting the glutamate and lysine residues with suitable reagents, respectively.

To purify the oppositely charged PEG-BLG conjugates from excess or unreacted PEG-tetrazole, the reaction mixture was purified using Vivaspin 10 kDa MWCO centrifuge filters. These conjugates were further characterized with SDS-PAGE and MALDI-TOF (**Figure 4.3**). From SDS-PAGE, it is clear that all charged BLG-allyl had conjugated with PEG-tetrazole, since no band was visible at the lower band, supposedly at ~19-20 kDa that corresponding to the charged BLG-allyl. However, a smear was observed between 23-50 kDa. To confirm the mass of the charged PEG-BLG conjugates, MALDI-TOF analysis was conducted. Both positively charged and negatively charged PEG-BLG conjugates showed three peaks, apart from the unreacted modified protein peak. Those three conjugation peaks were roughly 3 kDa differences, suggesting singly, doubly and triply conjugated BLG. In theory, conjugation using bio-orthogonal chemistry only involved tetrazole and alkene, in our case, tetrazole-functionalized PEG would only react with allyl-modified BLG to form singly PEG-BLG conjugates at around 23 kDa. Furthermore, we have also discovered that under photoirradiation, PEG-tetrazole would react with native BLG to form PEG-BLG conjugates (results will be discussed in Chapter 5). This discovery gave rise to a question what is actually reacting with tetrazoles, and extended our study on the sequence of proteins, together with the chemistry behind the

photoinduced cycloaddition reaction. Further investigations on the side reactions between tetrazoles and native proteins will be reported in details in the following **Chapter 5**.

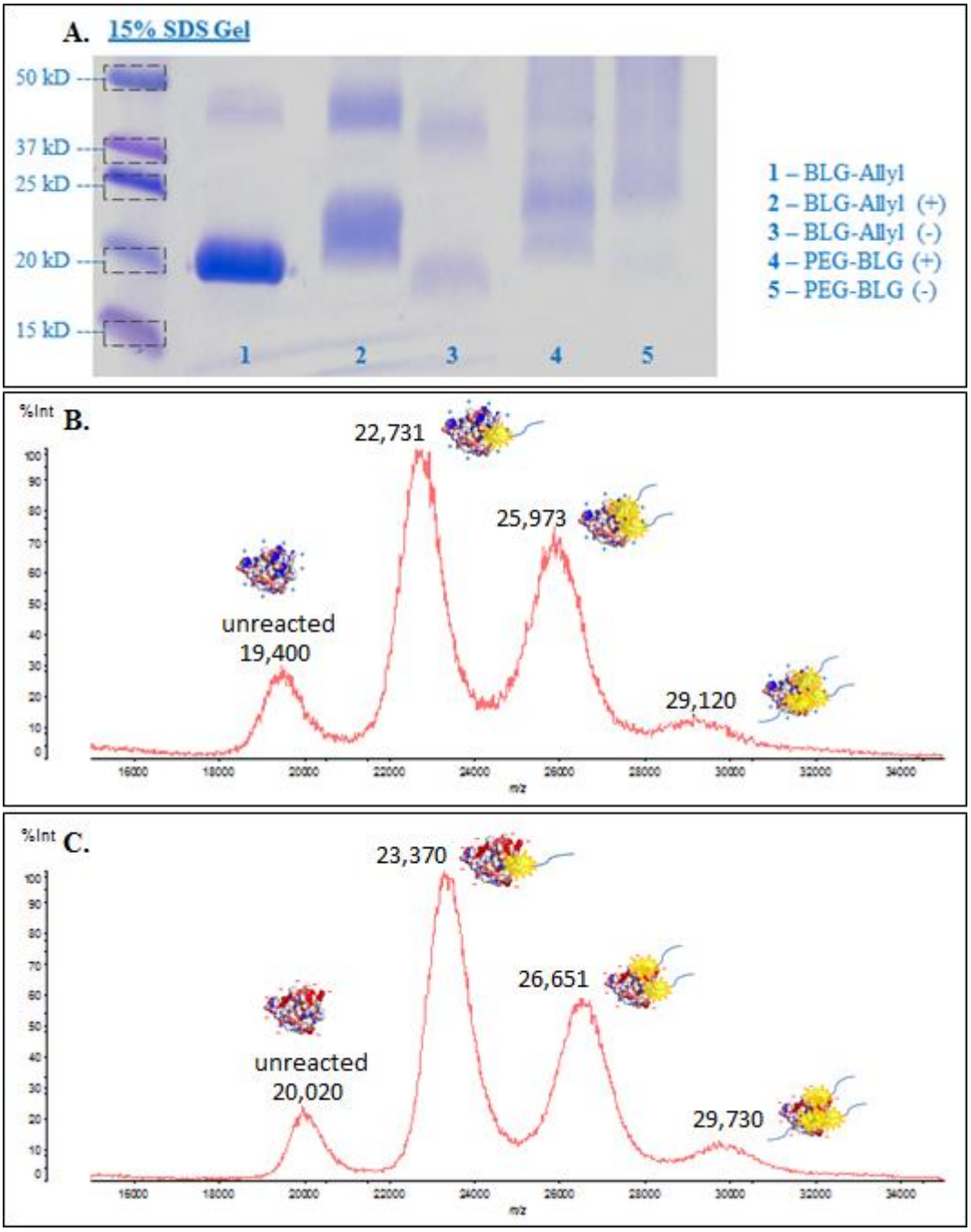

Figure 4.3. SDS-PAGE gel for each different purified products (**A**). MALDI-TOF spectra for the positively charged PEG-BLG conjugates (**B**) and negatively charged PEG-BLG conjugates (**C**) showing the presence of singly, doubly and triply conjugated BLG, apart from the unreacted modified BLG.

In order to purify these oppositely charged PEG-BLG conjugates, fast protein liquid chromatography (FPLC) via ionic-exchange chromatography were carried out.

Sepharose SP HP column and Sepharose Q FF column were used to purify the positive charged and negative charged PEG-BLG conjugates respectively, and their fractions were collected (See Appendix H) and characterized by MALDI-TOF and DLS (**Figure. 4.4**). At the same time, the average zeta potential measurements were performed to confirm the surface charged of the conjugates. The average zeta potential value for the positive conjugate is +21.3 mV, whereas the average zeta potential value for the negative conjugate is about -20.8 mV. The similar value from the zeta potential for the positive and negative conjugates also indicated that this approach agrees with the ratio of glutamate and lysine residues that were involved in the reaction to give about 1:1 ratio (based on charge).

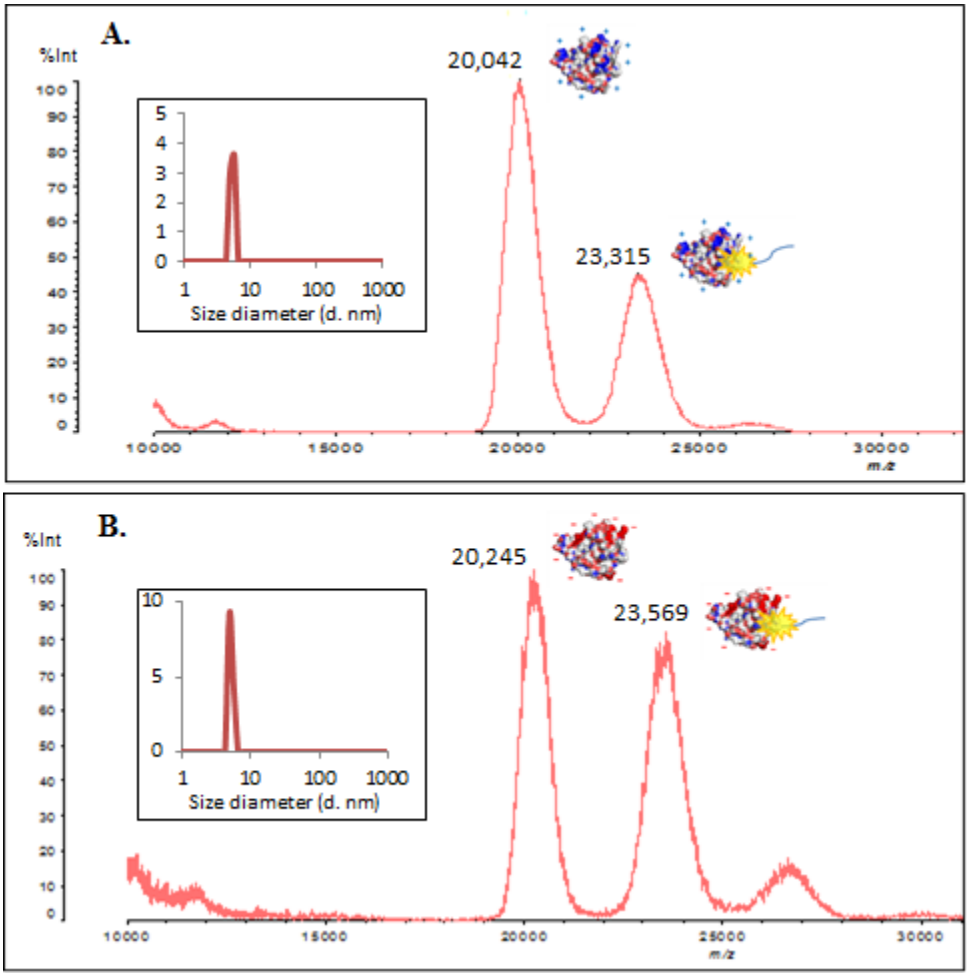

Figure 4.4. MALDI-TOF spectra for the positively charged PEG-BLG conjugates (**A**) and negatively charged PEG-BLG conjugates (**B**) after purification by FPLC via ionic-exchange column chromatography. Inset is the DLS data showing that the size of the charged conjugates is about 8 nm.

Finally, the purified charged PEG-BLG conjugates were mixed in a 1:1 ratio (based of charge) in an aqueous solution to form novel compartments, named 'proteinionosomes', which are fluorescent and have average size of about 80 nm in diameter (**Figure 4.5**). The structure of proteinionosomes can be seen clearly with TEM.

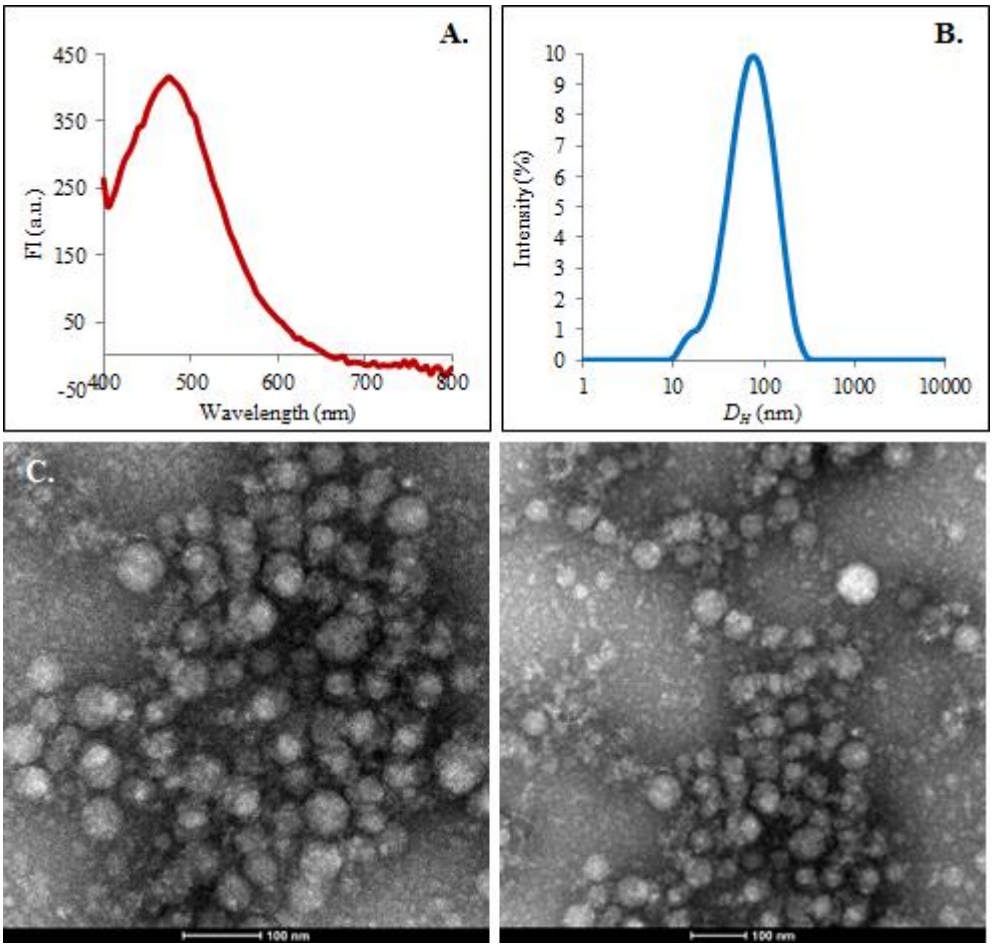

Figure 4.5. Fluorescence measurement shows that the proteinionosomes are fluorescent with strong fluorescence emission at 490 nm (**A**). DLS data shows the hydrodynamic diameter (D_H) of the proteinionosomes is about 80 nm (**B**). TEM images of the proteinionosomes (**C**), stained with 2% uranyl acetate. Scale bars are 100 nm.

The self-assembly of proteinionosomes is not only induced by electrostatic interactions from the oppositely charged BLG conjugates, but also by the presence of an apparent hydrophilic-hydrophobic balance. This was confirmed by the mixing of positively and negatively charged BLG (without any conjugation of PEG) where no aggregates or vesicles were observed using TEM or DLS (data not shown). Since it is

known that aggregation of BLG occurs mainly via a denatured intermediate with a hydrophobic character, we tentatively suggest that, in our case as well, the BLG is slightly hydrophobic, hence making the overall conjugate amphiphilic.

Furthermore, with the purpose to study the structural and functional characterization of these novel compartments to be used as cell mimics, we encapsulated molecules, i.e. HRP enzymes. The activity of the enzyme encapsulated proteinionosomes was investigated by adding amplex red and hydrogen peroxide extraneously, and the conversion of amplex red to resorufin (See **Chapter 3**) was compared with the free enzymes, having roughly same concentration (0.1 mg mL^{-1}) and the blank compartments (**Figure 4.6**). Comparison of the activity of the proteinionosomes indicated that the initial rate (v_0) of amplex red conversion is three times higher for the HRP encapsulated proteinionosomes (v_0 = 0.31 au s^{-1}) than the blank (v_0 = 0.10 au s^{-1}), and much lower than the free HRP enzymes (v_0 = 22.4 au s^{-1}). This suggests that HRP might be encapsulated inside the compartments. However, this has to be investigated further for the encapsulation efficiency and the semi-permeability of the reactants and products.

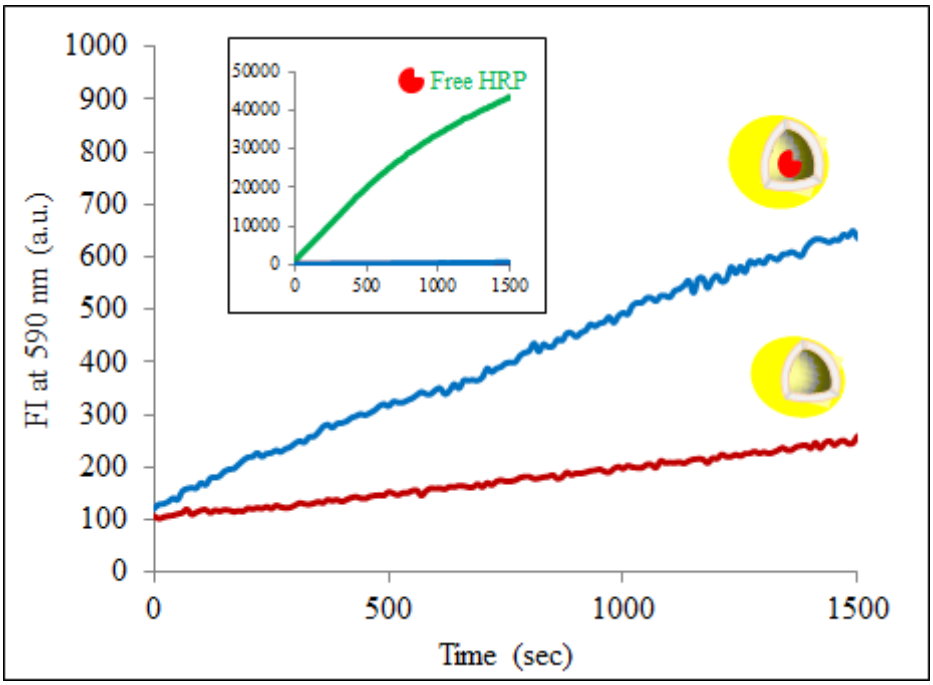

Figure 4.6. Enzyme activity inside the proteinionosomes was compared with the free HRP enzymes (roughly having similar concentration, i.e. 0.1 mg/mL) and the blank (without HRP). The enzyme encapsulated proteinionosomes shows an increased conversion of amplex red, indicating that the enzyme is active

4.4. Conclusion

We demonstrate the design and synthesis of proteinionosomes, novel functional compartments based on the new supramolecule based on protein-polymer conjugates derived from the major milk protein BLG and PEG. The PEG-BLG complexes can be prepared using a bio-orthogonal chemistry that involved tetrazoles and alkenes to form pyrazoline moiety as the connecting group between PEG and BLG. The oppositely charged PEG-BLG complexes will undergo self-assembly in an aqueous solution to form novel semi-permeable nano-compartments, capable of encapsulating molecules and are fluorescent. These novel compartments provide an opportunity for scientists and engineers to develop model systems for cellular mimicking.

4.5. Output

Siti, W.; de Hoog, H. –P. M.; Liedberg, B.; and Nallani, M., Synthesis and Assembly of Vesicles from Protein-Polymer Complexes through Photoclick Chemistry, *in preparation*.

CHAPTER 5

Photoinduced Cycloaddition Reaction of Tetrazoles to Proteins in a Conjugation System

5.1. Introduction

The conjugation of polymers to proteins or peptides has been demonstrated to enhance their physical stability and promote their self-assembly, which represents an interesting aspect of research, especially in developing protein-based therapeutics.[116-120] The use of bio-orthogonal chemistry has been widely applied for the conjugation of two macromolecules, in which it will give a single product in high yield under biological conditions without any side reaction.[102-105] One of the most essential reactions is the reaction that involved strained alkynes and azides.

Another approach in the bio-orthogonal chemistry that requires a relatively simple conjugation system is based on the photoinduced cycloaddition of tetrazole-functionalized molecules to alkene moieties that generate fluorescent pyrazoline moiety as a linker.[100-105] This approach has shown to be advantageous in term of its rate, photoinducibility and fluorescence of the resulting pyrazoline molecule.

At the same time, we have also used this approach to construct protein-polymer conjugates as new building blocks for developing novel functional compartments, where simple PEG chains were attached to a protein of interest (i.e. BLG), which was reported in **Chapter 4**. Nevertheless, the initial discoveries during the course of our experimental process to construct protein-polymer conjugates, gave rise to a significant side reaction (**Scheme 5.1**), which we considered noteworthy to investigate further in details. Here, in this chapter, we will focus on the investigation of the side reaction of the photoinduced cycloaddition of tetrazoles to several proteins, the chemistry behind it and its significance in the conjugation of polymers to proteins.

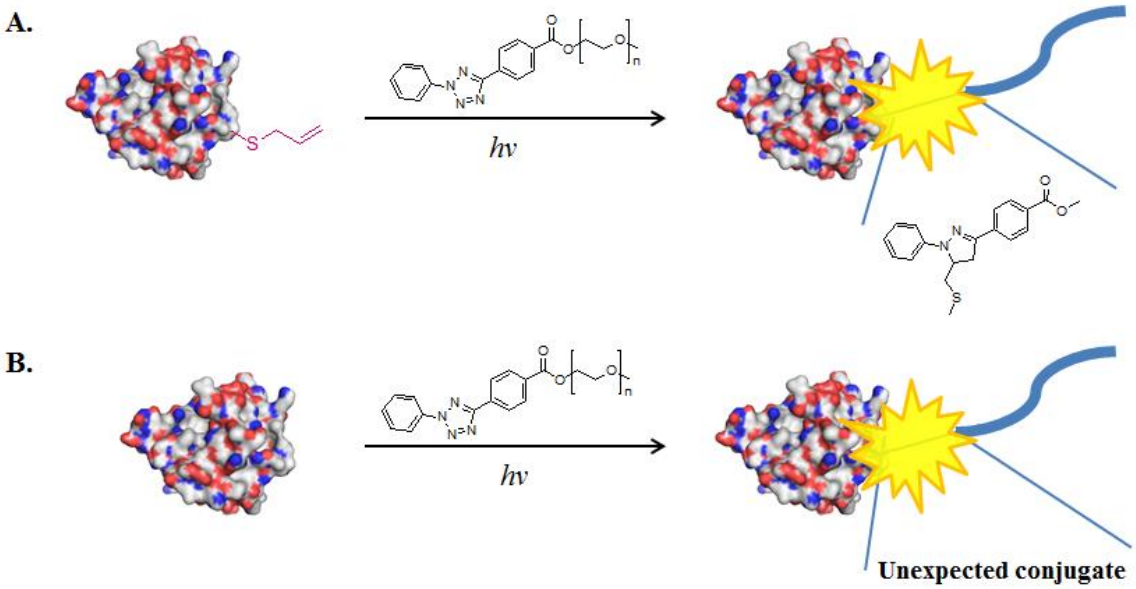

Scheme 5.1. Preparation of PEG-BLG conjugates by the photoinduced cycloaddition reaction of PEG-tetrazole. Apart from the procedure outlined (**A**), which involves reaction of BLG with allyl chloride, a significant side reaction occurs when performing the photoinduced cycloaddition reaction in the presence of native protein (**B**).

5.2. Experimental

5.2.1. Materials and Methods

Allyl chloride and L-tryptophan were bought from TCI. Bovine milk β-lactoglobulin isoform A (BLG-A), horseradish peroxidase Type I (HRP), *Candida Antarctica* lipase B recombinant from *Aspergillus oryzae* (CalB), and lysozyme from chicken egg white were purchased from Sigma-Aldrich. The polypeptides JR2EC was provided by the group of Prof. Daniel Aili, Linköping University, Sweden.[121-122] Phosphate buffer saline (PBS, 1X, pH 7.4) was purchased from Invitrogen. Dimethylformamide (DMF) was from Merck. All reagents, buffers and solvents were used as received, without further purification.

Absorbance and fluorescence measurements were performed on a Tecan Infinite M200 pro plate reader using 96-well plates (Corning). UV irradiation was conducted using a UVP UVM-57 Handheld UV lamp at 302 nm (6 Watt, 0.16 Amps). SDS-PAGE was performed using Bio-Rad Mini-PROTEAN Tetra Cell. MALDI-TOF measurements were performed on a Shimadzu Kratos Axima TOF2 using 4-hydroxy-3,5-dimethoxycinnamic acid as a matrix.

5.2.2. Photoinduced Cycloaddition Reaction of PEG-tetrazole with Native Proteins

The synthesis of tetrazole, PEG-tetrazole and BLG-allyl were described in details in **Sections 4.2.2 – 4.2.4**.

Shortly, 1.0 mL of 2.0 mg/mL native BLG (0.11 μmol, 1.0 equiv.) in milliQ was mixed with 0.40 mL of 5.0 mg/mL PEG-3300-Tetrazole (0.57 μmol, 5.0 equiv.) in milliQ in a quartz cuvette (10 mm pathlength). Under stirring, the mixture was irradiated at 302 nm with a handheld UV-lamp at about 5 cm distance for 15 minutes. For purification, the mixture was filtered three times through Vivaspin 10 kDa centrifuge filter at 10,000 rpm

for 10 minutes (Legend Micro 21 Centrifuge, Thermo Scientific, Sorvall) to remove excess PEG-tetrazole. The resulting product was redispersed in 1.0 mL of PBS, before being characterized by fluorescence measurements, SDS-PAGE and MALDI-TOF.

Similar procedure was performed for the conjugation of PEG with other unmodified proteins (Lysozyme, HRP and CalB), polypeptides JR2EC and L-tryptophan.

5.2.3. Preparation of Allyl-functionalized JR2EC Polypeptides, JR2EC-allyl

Similar procedure, purification and characterization were carried out as the preparation of BLG-allyl described in **Section 4.2.4**, but using polypeptides JR2EC instead.

5.3. Results and Discussion

As it can be seen from **Chapter 4**, our original study using charged allyl-functionalized BLG (BLG-allyl) and PEG-tetrazole to prepare charged PEG-BLG conjugates under photoclick chemistry (mild-intensity UV lamp at 302 nm), gave a broad band between 23-50 kDa on SDS-PAGE gel, and more than 1 conjugated peaks on MALDI-TOF (See **Chapter 4**: **Figure 4.3**). In order to investigate what was actually reacting with tetrazoles, we repeated the photoinduced cycloaddition reaction using PEG-tetrazole and only BLG-allyl (**Scheme 5.1A**). Since the pyrazoline shows strong fluorescence emission between 470-540 nm,[99] the conjugation of PEG-tetrazole to BLG-allyl was analyzed by fluorescence spectroscopy (**Figure 5.1A**). As a control experiment, BLG without allyl group (native BLG) was exposed to photoirradiation at 302 nm for 15 minutes in the presence of PEG-tetrazole (**Scheme 5.1B**), followed by analysis with fluorescence spectroscopy. Interestingly, both reactions gave rise to a fluorescent adducts, as confirmed by SDS-PAGE gel (**Figure 5.1B**), showing a clear band at 22 kDa and a minor band at 25 kDa, the latter band possibly indicating formation of doubly conjugated BLG. By looking at the shape of the fluorescence spectrum, the conjugation of 'BLG-allyl + PEG-tetrazole' represents a different species than that of the "direct" conjugate of 'native BLG + PEG-tetrazole'. The single peak of the 'BLG-allyl + PEG-tetrazole' conjugate is significant for pyrazoline formation, and therefore most likely shows the successful addition of PEG-tetrazole to BLG-allyl. Nevertheless, the nature of this "direct" conjugate was ambiguous. Since the reaction was happening under bio-orthogonal conditions, we considered it useful to study its occurrence in more details and explore the protein site involved.

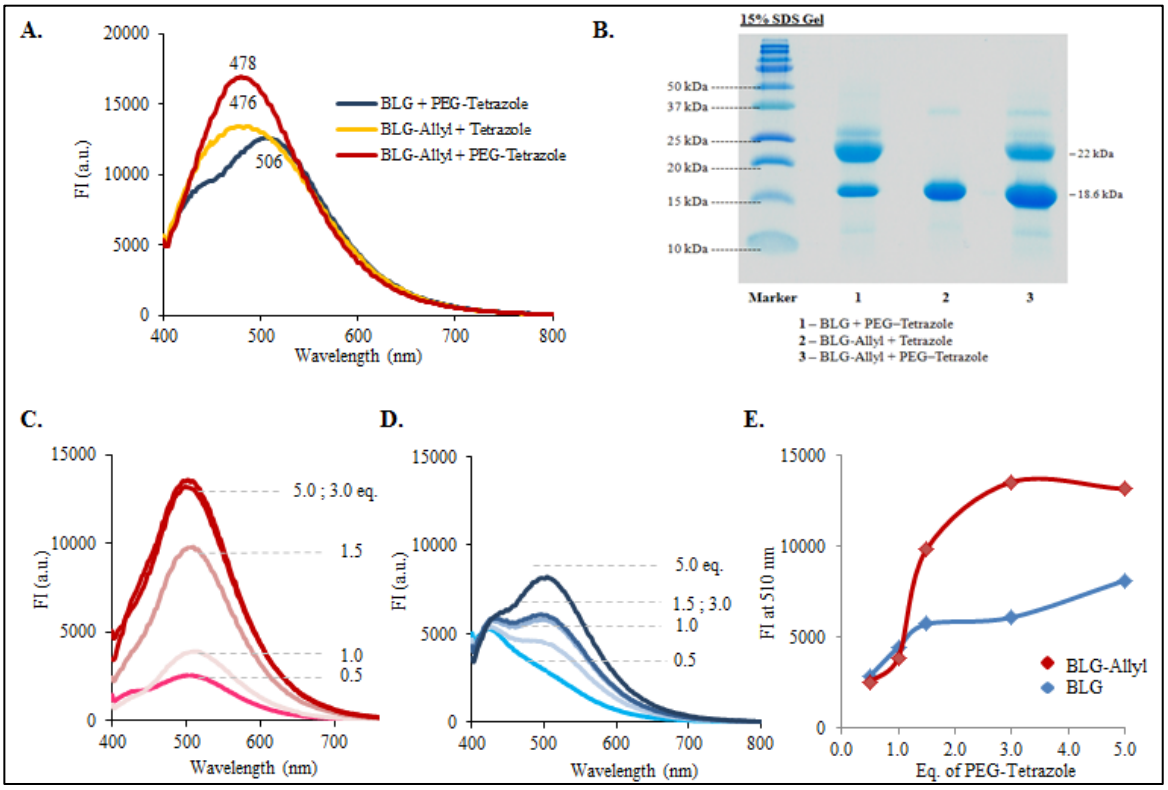

Figure 5.1. Characterization of the products formed by photoinduced cycloaddition of PEG-tetrazole (5.0 equiv.) with BLG-allyl and native BLG by fluorescence spectroscopy (**A**) and SDS-PAGE gel (**B**), showing the formation of PEG-BLG conjugate. Fluorescence spectra after photoirradiation of increasing equivalents of PEG-tetrazole (0.5 – 5.0 eqs) with BLG-allyl (**C**) and native BLG (**D**) show formation of chemically distinct conjugates. Chart representation of the fluorescence intensity at 510 nm versus increasing equivalents of PEG-tetrazole used with BLG-allyl (*red line*) and native BLG (*blue line*) (**E**).

First, the efficiency of the conjugation was investigated by reacting increasing equivalents of PEG-tetrazole (0.5 – 5.0 eqs) with BLG. The relevant mixtures were then irradiated for 15 minutes and the resulting conjugated products were evaluated by SDS-PAGE (Appendix I: Figure I1). The analysis implied an increase in conjugate formation with increasing concentration of PEG-tetrazole, with 5.0 eqs of PEG-tetrazole showing over 50% conversion, which is significantly high given the short reaction time and the macromolecular nature of the proteins. The fluorescence spectra of the conjugation of 'BLG + PEG-tetrazole' showed an interesting growth with increasing equivalents of PEG-tetrazole when compared to that of the conjugation of 'BLG-allyl + PEG-tetrazole' (**Figure 5.1C-E**). For the conjugation of 'BLG + PEG-tetrazole' at low concentration (0.5 eq of PEG-tetrazole), a peak was visible at 415 nm, which was not observed for BLG-

allyl. This peak increased only slightly in intensity at higher concentrations of PEG-tetrazole; whereas the peak at 510 nm showed a steady increase. This observation may be assigned to reaction of PEG-tetrazole at multiple sites of BLG, dependent on the concentration of the protein. At the same time, MALDI-TOF analysis for both photoinduced cycloaddition reactions of PEG-tetrazole to native BLG and PEG-tetrazole to BLG-allyl were carried out (**Figure 5.2**). The results showed the occurrence of two additional peaks at around m/z 21.9 kDa and 25.3 kDa for the reaction between PEG-tetrazole and native BLG, representing singly conjugated BLG and doubly conjugated BLG; whereas three additional peaks for the reaction between PEG-tetrazole and BLG-allyl. In general, the experiments demonstrate that PEG-tetrazole, which is a fully water-soluble tetrazole derivative, directly reacts to a considerable extent with a site on the protein, without the presence of an externally introduced dipolaraphile, i.e. the alkene or allyl group.

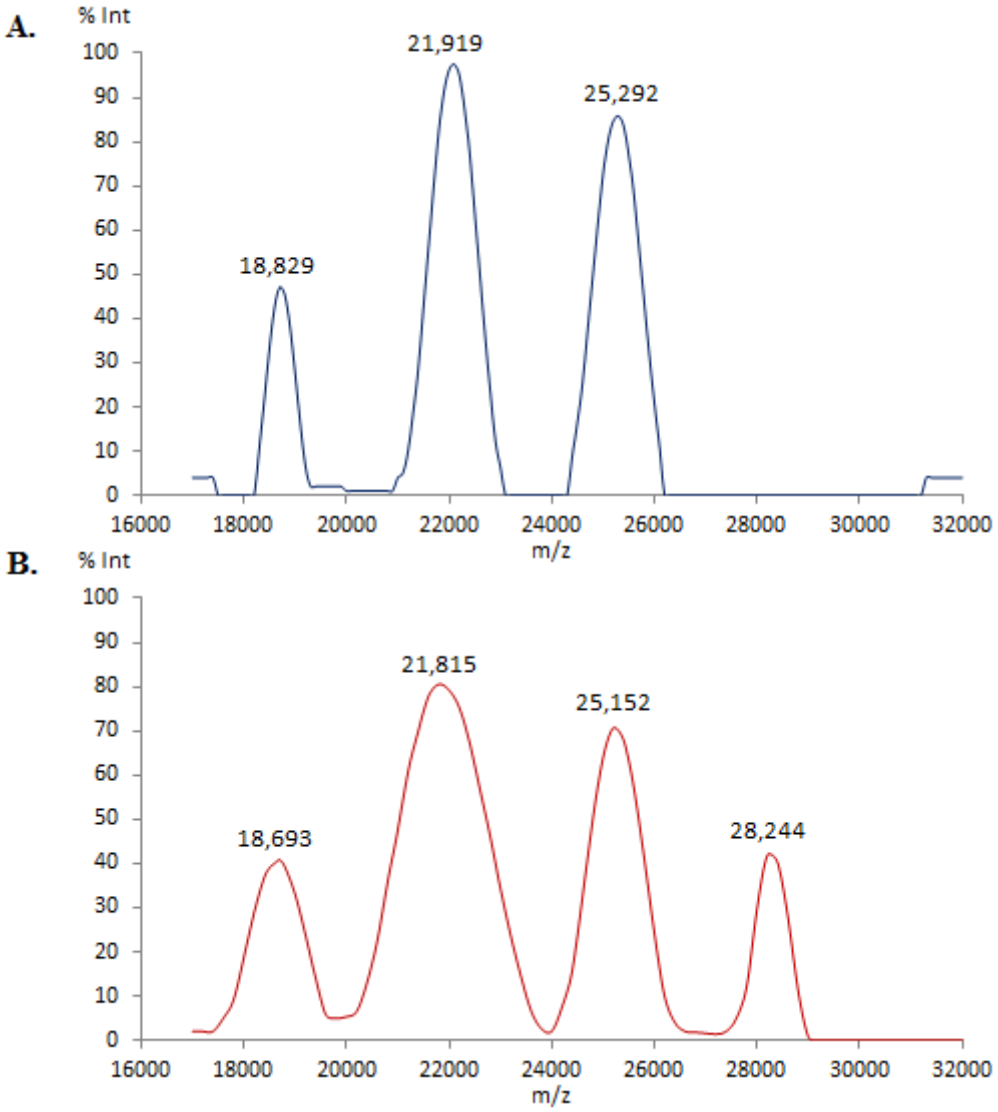

Figure 5.2. MALDI-TOF spectra for the photoinduced cycloaddition reactions of PEG-tetrazole to native BLG (**A**) and PEG-tetrazole to BLG-allyl (**B**), showing the presence of multiple site conjugates of BLG, apart from the externally introduced dipolaraphile.

Because of the simplicity of the observed side reaction, we then explored the reaction with other proteins or enzymes – horseradish peroxidase (HRP), *Candida antarctica* lipase (CalB) and lysozyme – used commonly in bionanotechnology. All the reactions were performed in PBS, and native proteins or enzymes were used without any modification, incubated with PEG-tetrazole at various concentrations under photoirradiation at 302 nm for 15 minutes. Interestingly, all the enzymes showed formation of a conjugate with PEG-tetrazole as shown from the fluorescence

spectroscopy of the reaction products (**Figure 5.3**). This suggested that the observed side reaction is common and occurs readily with a diverse subset of enzymes.

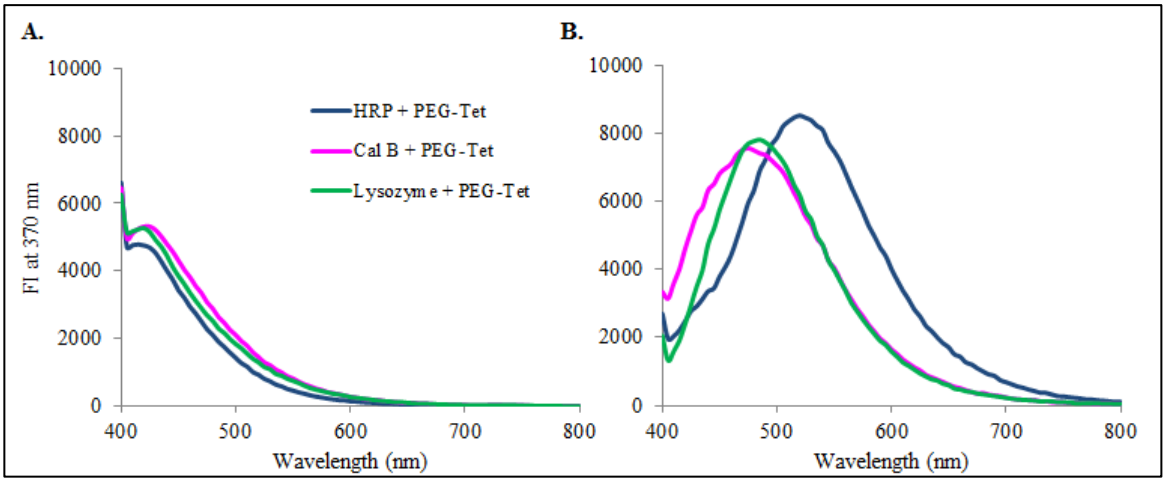

Figure 5.3. Fluorescence spectra for the photoinduced cycloaddition reaction of PEG-tetrazole to native HRP, CalB and lysozyme before (**A**) and after (**B**) UV irradiation.

First, looking at lysozyme's fluorescence spectrum as a function of PEG-tetrazole after photoirradiation, it displayed similar behaviour as that observed for BLG, with emission peak at around 500 nm and an increasing extent of conjugate formation with increasing equivalents of PEG-tetrazole (See **Figure 5.4A**). SDS-PAGE showed the clear formation of the PEG-lysozyme conjugate, which was confirmed by MALDI-TOF spectrum, showing a peak at 17.8 kDa, although it did not fully correlate with that observed by SDS-PAGE. This inconsistency was also obvious for the PEG-BLG conjugates, we believe it might be due to the decreased desorption or ionization tendency of the PEG-protein conjugate as compared to the free protein. The observed rapid conjugation of PEG-tetrazole to the unmodified lysozyme is particularly remarkable, since earlier studies have shown no apparent conjugation of unmodified lysozyme with PEG-tetrazole.[100,123]

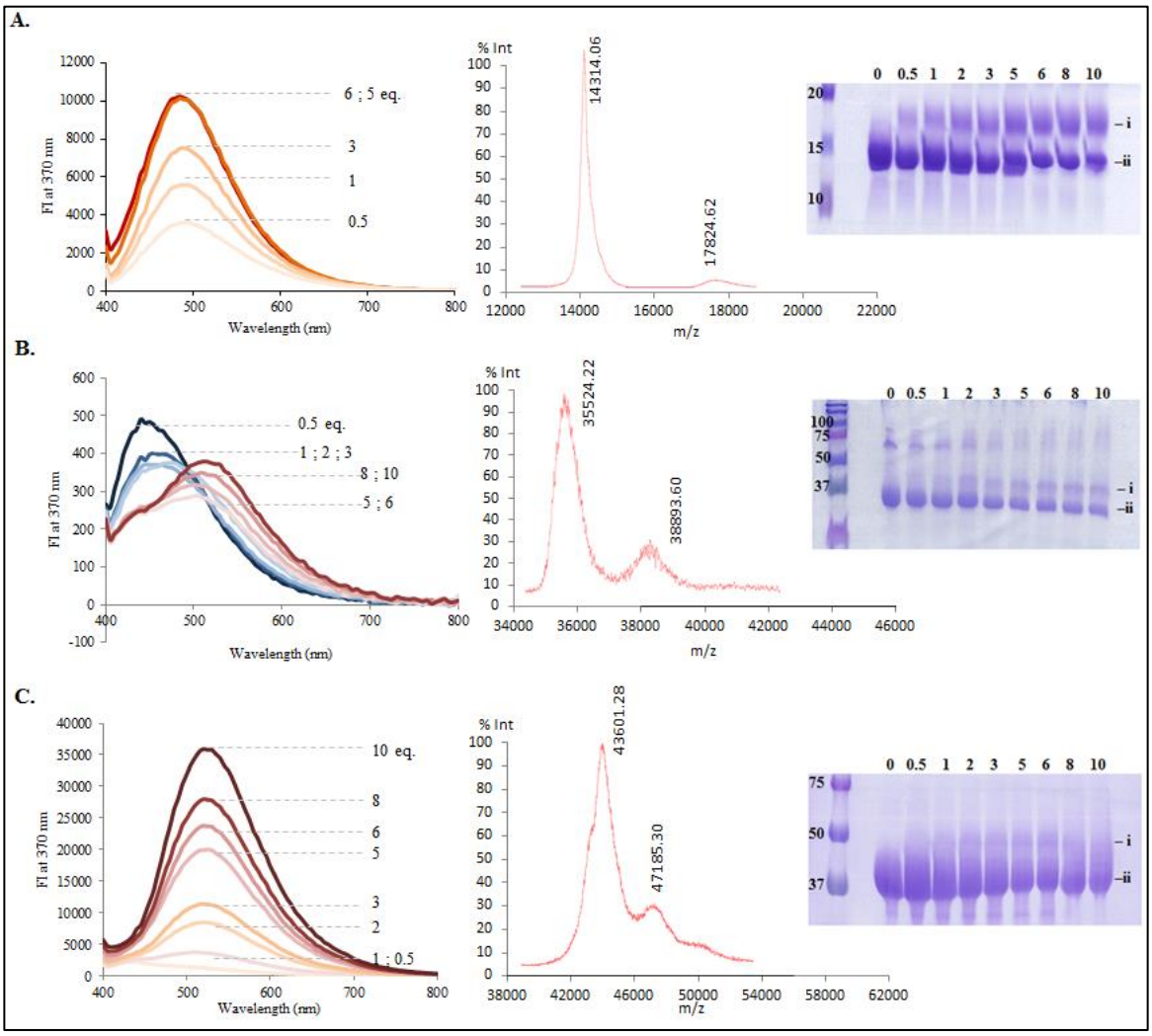

Figure 5.4. Fluorescence spectra, MALDI-TOF and SDS-PAGE gel for the photoirradiation of increasing equivalents of PEG-tetrazole to unmodified lysozyme (**A**), CalB (**B**), and HRP (**C**), respectively. For SDS-PAGE, bands indicated by i represents the conjugated product, while ii represents the free enzyme.

On the other hand, the fluorescence spectrum of CalB (**Figure 5.4B**) displayed somewhat dissimilar behavior than the fluorescence spectrum of BLG. At low concentrations of PEG-tetrazole (0.5 – 3.0 eqs), an intense peak was observed at 450 nm for Cal B, which resembled to BLG, despite the initial decreased and later shifted steadily to a bimodal peak with a maximum of 515 nm at higher concentrations of PEG-tetrazole. SDS-PAGE and MALDI-TOF clearly showed the reaction at a single site on the protein.

Likewise, the fluorescence spectrum of HRP (**Figure 5.4C**) displayed a very different behaviour than the fluorescence spectra of BLG, CalB and lysozyme, since it showed relatively high fluorescence intensity and a regularly increasing single emission

peak at 525 nm with increasing equivalents of PEG-tetrazole. We tentatively suggest that this observation might come from the presence of the heme prosthetic group in HRP. In fact, the heme comprises a chemically flexible double bond, which might be the site of reaction.[124] With regard to the amount of conjugation, a mainly singly conjugated product was observed with MALDI-TOF, in addition to a small peak at 51 kDa, indicating of the double conjugated product. Here, SDS-PAGE was not fully convincing because of the relatively broad bands of the native HRP, probably due to the presence of apo-HRP in the sample.[124]

In short, the various fluorescence behaviour of the conjugates in the photoinduced cycloaddition reaction, pointed to the role of an amino acid with dipolaraphile characteristics. Investigation of possible reactive side groups showed the most likely contender to be tryptophan, since it carries possibly reactive double bonds and its photoreactivity is well documented. It is furthermore fluorescent which might explain the fluorescence spectra that could suggest contribution from multiple fluorescent moieties. The contribution of tryptophan to the side reaction was confirmed by the following lines of evidence. First, the reaction between a small polypeptide JR2EC (sequence shown in **Figure 5.5A**)[121-122] and PEG-tetrazole did not show conjugation as can be seen from the fluorescence spectra, indicating absence of a fluorescent product with increasing equivalents of PEG-tetrazole (**Figure 5.5B-C**). However, strong fluorescence was observed for JR2EC, upon modifying the only cysteine with allyl chloride. The JR2EC sequence revealed the absence of tryptophan residues in the polypeptide, indicating that a role of the amino acid in the conjugation reaction. Indeed, photoirradiation of PEG-tetrazole with tryptophan led to significant fluorescence as well, while reaction with a control amino acid (histidine) did not show visible fluorescence (data not shown).

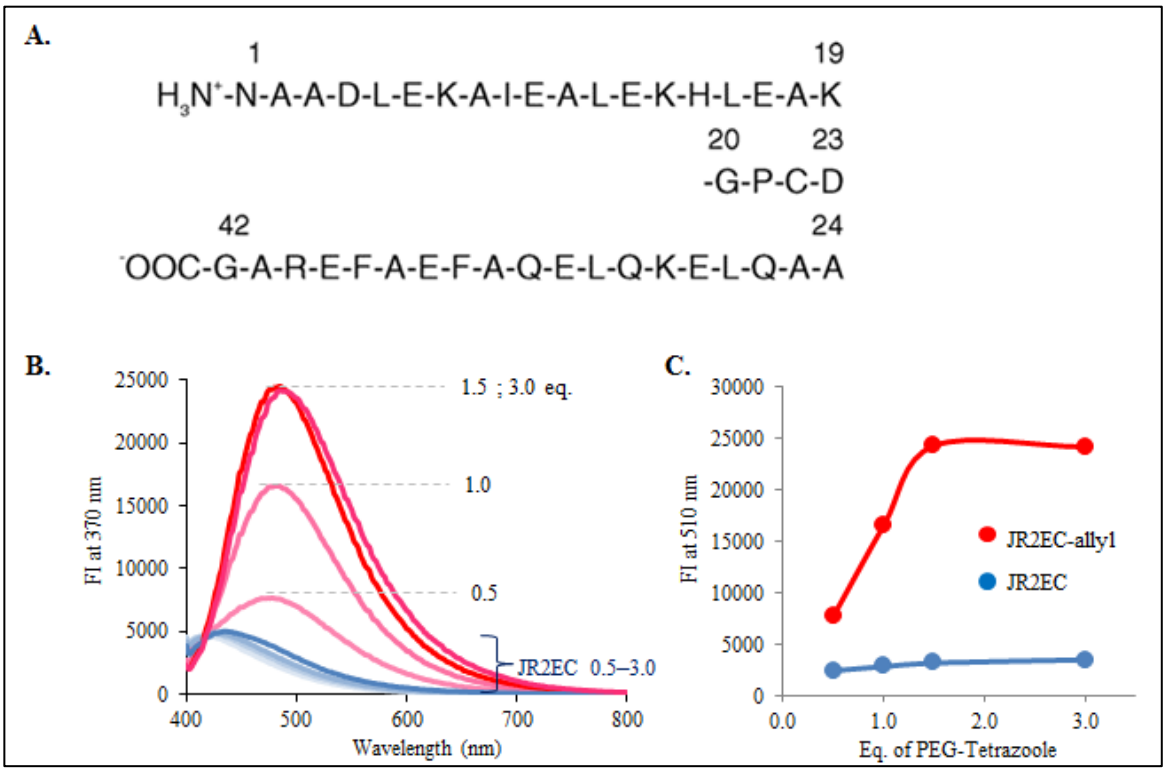

Figure 5.5. Amino acid sequence of JR2EC (**A**). A cysteine is present at position 22. Reproduced with permission from ref.[122] Copyright © 2008 WILEY-VCH Verlag GmbH & Co. KGaA, Weinheim. Fluorescence spectra of the photoirradiation of increasing equivalents of PEG-tetrazole (0.5–3.0 eqs) with unmodified polypeptide JR2EC (*blue line*) and JR2EC-allyl (*red line*), showing absence of fluorescent product for unmodified polypeptide JR2EC (**B-C**).

Since we could not extract the structural information of the cycloadduct from the photoirradiation of PEG-tetrazole and tryptophan (where tryptophan was added in excess) by 1H-NMR, we obtained MALDI-TOF spectra before and after irradiation. The spectra showed a clear shift in m/z values between PEG-tetrazole before and after irradiation, with a mass difference of 176.89 (**Figure 5.6**). Assuming loss of dinitrogen (28.01) during irradiation of PEG-tetrazole, the mass difference of 176.89 is close to the expected theoretical value of 176.21 (i.e. the molecular weight of tryptophan (204.23) minus that of dinitrogen (28.01)), indicating the presence of tryptophan to the nitrilimine. It should be noticed that the MALDI-TOF analysis does not allow differentiation between quenching of the nitrilimine by the amine or cycloaddition, so that either pathway remains open.[125] Nevertheless, the formation of a fluorescent moiety suggests the generation of pyrazoline after photoirradiation.

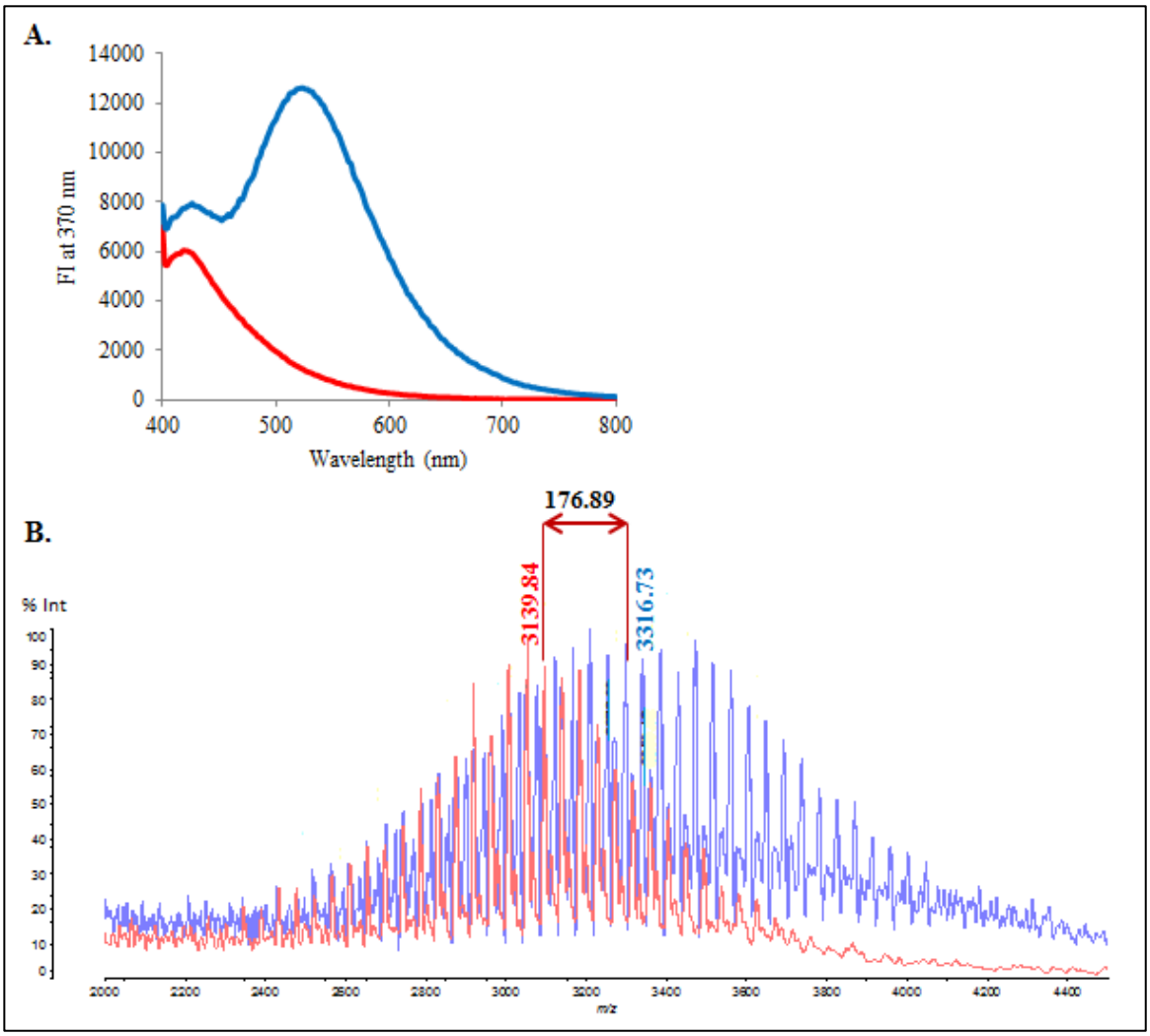

Figure 5.6. Fluorescence spectra (**A**) and MALDI-TOF analysis (**B**) for the reaction of PEG-tetrazole with excess tryptophan before irradiation (*red line*) and after irradiation (*blue line*), indicating addition of amino acid to the PEG polymer.

In general, the results strongly imply the involvement of tryptophan in the direct photoinduced cycloaddition reaction of tetrazoles to proteins as observed here in our study, in which all enzymes studied have one or more tryptophan residues present (See Appendix J: Figure J1). With this convincing evidence for the direct reaction of tryptophan with photo-activated nitrilimines, it is significant that this reaction has not been observed earlier by others or even us.[100-101,126-128] In our study, this result might come from the experimental design, in which we modified the protein with a double bond, instead of a tetrazole. Judging from other reports, [100-101,126-128] the existence of an

alkene-modified amino acid of high reactivity may direct the alkene being modified, which prevents the reaction of tetrazole with tryptophan. Since lots of papers have been reported regarding such alkene-modified amino acids, it seems that it is indeed the case. Besides, it should be noted that the reaction in this study involves excitation at 302 nm, which induces the photo-activation of tryptophan. Nitrilimines produced from tetrazoles excitable at higher wavelengths may be less, or not at all, susceptible to the reaction with tryptophan.

Study on the late report before the introduction of bio-orthogonal chemistry, reveals that direct reaction of nitrilimines to tryptophan is not exceptional. In fact, Ruccia *et al.* reported the reaction of nitrilimines with indole (functional group of tryptophan) in 1973.[129] For the most closely related indole, cycloadduct (**1**) was observed, although it was in a very low yield. This is the most possible product of our current investigation. Beside this cycloadduct, a bisadduct (**2**) was observed for indole carrying one free nitrogen at the 3-position (**Scheme 5.2**). This might explain our observation for the formation of doubly conjugated protein with HRP (having only one tryptophan) and triply conjugated allyl-modified BLG (having only two tryptophans).

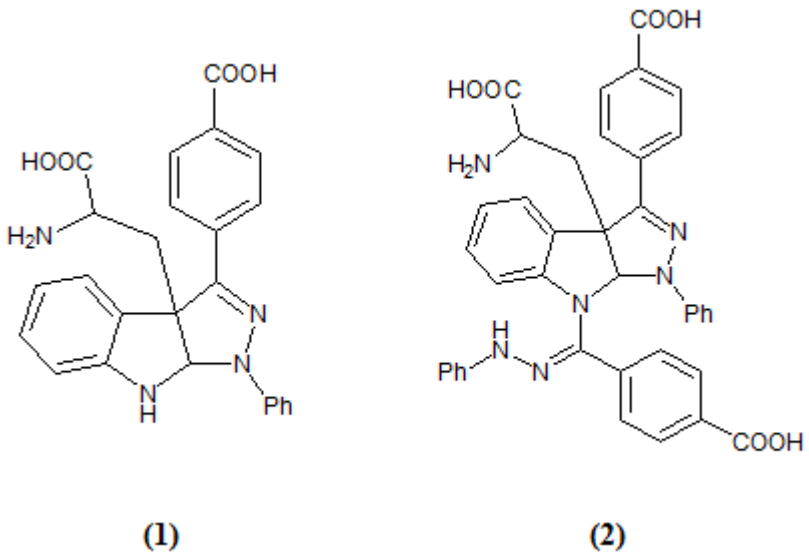

Scheme 5.2. Proposed structure (**1**) of the possible conjugate formed by photoinduced cycloaddition reaction of PEG-tetrazole to tryptophan residues in proteins. Structure (**2**) shows a possible bisadduct of the PEG-tetrazole. The amide back bone of the protein is shown as a single residue.

In addition, the reaction in our study seems to be different than that reported by Zhao *et al.*,[125] who explained quenching of nitrilimine by the amine moiety of amino acids, a reaction that was observed irrespective to the nature of the amino acid. In our case, the photoinduced cycloaddition reaction appears to be specific to tryptophan, and hence, does not be affected by quenching by amines. We suggest that this may be due to the reaction stoichiometry (using an excess amount of nucleophile in the case of Zhao *et al.* versus equimolar or excess amount of tetrazole in our study), and the use of aqueous buffer, which is known to accelerate the cycloaddition.[125]

On the other hand, the nature of the protein may play a role in the photoinduced cycloaddition reaction as well. In our case, BLG consists of a tryptophan residue in its active site, and it may be predicted that the PEG-tetrazole interacts with this site, as the tetrazole itself carries some hydrophobic character. The close proximity may support the relatively high yield and speed of the reaction, with roughly 75% of the protein having reacted after 15 minutes irradiation. Another proof for an effect of the protein structure on reactivity can be seen by the reactions with CalB and lysozyme. Both enzymes contain

multiple tryptophan residues, with lysozyme carrying three solvent-exposed residues, and therefore, mainly singly conjugated proteins were visible which indicate the presence of a single tryptophan with optimal reactivity.

5.4. Conclusion

During our investigation of the photoinduced cycloaddition reaction of tetrazole-functionalized PEG (PEG-tetrazole) to alkene-modified proteins, we observed quite substantial fluorescent product formation for the photoirradiation of PEG-tetrazole to native protein. Study of the reaction with unmodified BLG showed the side reaction to be nearly as efficient and high-yielding as the usual photoinduced cycloaddition reaction of tetrazoles to alkenes. Similar observations were found on the reactions with other proteins (HRP, Cal B and lysozyme), except for a small polypeptide (JR2EC) that lacked tryptophan. Further investigation showed that, indeed, the PEG-tetrazole reacts rapidly with tryptophan to form a fluorescent product. In brief, if the bio-orthogonal reaction is carried out at low UV wavelengths, consideration should be taken when analyzing conjugation merely on the generation of fluorescent products in conditions where tryptophan might be present.

5.5. Output

This work was published on *Organic & Biomolecular Chemistry*.

Siti, W.; Khan, A. K.; de Hoog, H. –P. M.; Liedberg, B.; and Nallani, M., Photo-induced Conjugation of Tetrazoles to Modified and Native Proteins, *Org. Biomol. Chem.*, **2015**, *13*, 3202-3206.

CHAPTER 6

Conclusion & Future Perspectives

Several different types of higher order architectures have been reported in the literature for mimicking cell structure, including capsosomes, vesosomes, and multicompartmentalized polymersomes. All of these architectures were prepared using emulsion techniques, which resulted in microscale compartments. Our simple self-assembly approach using synthetic amphiphilic block copolymers comprising of PMOXA-PDMS-PMOXA (ABA) and PS-PIAT block copolymers led to the formation of novel multicompartments in nanoscale range. By encapsulating different functional molecules (i.e. enzymes) separately in the multicompartmentalized polymersomes and performing cascade reaction, we have demonstrated the interactions between the compartments, and therefore, these novel higher-order structures is shown to mimic the complexity of cells.

In order to build novel functional architectures for cell mimicking, we had expanded our study on synthesizing new building blocks of protein-polymer complexes, consisting of PEG and BLG, which self-assembled into stable, nano-compartments, named as proteinionosomes. Since photoinduced cycloaddition chemistry were used for the preparation of PEG-BLG conjugates, the proteinionosomes generated have shown to be fluorescent, capable of encapsulating molecules and semi-permeable. This observation is particularly interesting since permeability is one of the essential features of cell membrane.

In addition, the self-assembly of proteinionosomes opens up a new branch of building blocks using protein-polymer complexes, where globular proteins are involved (i.e. BLG in our case). In fact, the self-assembly of globular protein-polymer diblock copolymers to form nanostructures (such as cylinders, lamellae and micelles) has been

reported extensively by Olsen *et al.*[130-131] Their experimental design involved the presence of malemeide and thiol groups for conjugation, was different from our experimental design using bio-orthogonal chemistry that involved tetrazole and alkene group. Moreover, the self-assembly of proteinionosomes is not only induced by electrostatic interaction, in which different charges are introduced on the BLG, but also the amphiphilicity of the block copolymers, i.e. from PEG and BLG.

In brief, we can use these proteinionosomes in future to build novel multicompartments architectures for mimicking cellular compartments. The assembly and disassembly of the compartments can be controlled upon subjected to different external conditions, such as pH or salt concentration, can be studied in the future. These types of novel higher order architectures would provide opportunities for scientists and engineers to study and understand the complexity of living cells.

Last but not least, the nano-sized proteinionosomes have a potential in therapeutic applications and diagnostic imaging. Different proteins or enzymes can be conjugated with PEG to form varieties of proteinionosomes for specific therapeutic applications. And since proteinionosome itself is already fluorescent, we can use it directly for diagnostic imaging without additional steps to encapsulate the dyes or fluorescent molecules inside the compartment, or to embed them on the membrane. In this way, the proteinionosomes would aid the work of the physicians and health professionals.

LIST OF PUBLICATIONS & CONFERENCES

Papers published / submitted / in preparation

1. Siti, W.; de Hoog, H. –P. M.; Fischer, O.; Shan, W. Y.; Tomczak, N.; Nallani, M.; Liedberg, B. An Intercompartmental Enzymatic Cascade Reaction in Channel-Equipped Polymersome-in-Polymersome Architectures. *J. Mater. Chem. B*, **2014**, *2*, 2733−2737.

2. Siti, W.; de Hoog, H. –P. M.; Liedberg, B.; and Nallani, M., Synthesis and Assembly of Vesicles from Protein-Polymer Complexes through Photoclick Chemistry, *in preparation*.

3. Siti, W.; Khan, A. K.; de Hoog, H. –P. M.; Liedberg, B.; and Nallani, M., Photo-induced Conjugation of Tetrazoles to Modified and Native Proteins, *Org. Biomol. Chem.*, **2015**, *13*, 3202-3206.

International Conferences and Workshops

1. Development of Enzymatic Cascade Reactions in Polymersomes with Multicompartmentalized Architectures, International Conference on Materials for Advanced Technologies (ICMAT), 2013, Singapore.

2. Synthesis & Assembly of Polyion Complex Vesicles (PICsomes) from Protein-Polymer Complexes, Koala-NTU International Workshop on Materials for Smart Wound Dressings, 2013, Singapore.

3. Polymersome Architectures as Novel Biosensing Interfaces, International Conference on Materials for Advanced Technologies (ICMAT), 2011, Singapore.

BIBLIOGRAPHY

1 Alberts, B.; Johnson, A.; Lewis, J.; Raff, M.; Roberts, K.; and Walter, P., Molecular Biology of the Cell, 4th Edition, Garland Science, New York, **2002**.

2 Lodish, H. F.; Berk, A.; Matsudaira, P.; Kaiser, C. A.; Krieger, M.; Scott, M. P.; Zipursky, L.; Darnell, J., Molecular Cell Biology, 5th Edition, W. H. Freeman, New York, **2003**.

3 De Duve, C., The origin of eukaryotes: a reappraisal, *Nature Reviews Genetics*, **2007**, ***8***, 395-403.

4 Hartman, H.; Fedorov, A., The origin of the eukaryotic cell: A genomic investigation, *PNAS*, 2002, *99*, 1420-1425.

5 Bangham, A. D., Liposomes: the Babraham connection, *Chem. Phys. Lipids*, **1993**, *64*, 275-285.

6 Vemuri, S.; Rhodes, C. T., Preparation and characterization of liposomes as therapeutic delivery systems: a review, *Pharmaceutica Acta Helvetiae*, **1995**, 95-111.

7 Bangham, A. D.; Horne, R. W., Negative Staining of Phospholipids and Their Structural Modification by Surface-Active Agents as Observed in the Electron Microscope, *J. Mol. Biol.*, **1964**, *8*, 660-668.

8 Walde, P.; Cosentino, K.; Engel, H.; and Stano, P., Giant Vesicles: Preparations and Applications, *ChemBioChem*, **2010**, *11*, 848-865.

9 Akbarzadeh, A.; Sadabady, R. R.; Davaran, S.; Joo, S. W.; Zarghami, N.; Hanifehpour, Y.; Samiei, M.; Kouhi, M.; and Koshki, K. N., Liposomes: Classification, Preparation and Application, *Nanoscale Research Letters*, **2013**, *8*, 102-110.

10 Lasic, D. D., Novel Applications of Liposomes, *Trends Biotechnol.*, **1998**, *16*, 307-321.

11 Kisel, M. A.; Kulik, L. N.; Tsybovsky, I. S.; Vlasov, A. P.; Vorob'yov, M. S.; Kholodova, E. A.; Zabarovskaya, Z. V., Liposomes with phosphatidylethanol as a carrier for oral delivery of insulin: studies in the rat, *Intl. J. Pharm.*, **2001**, *216*, 105-114.

12 Banerjee, R., Liposomes: Applications in Medicine, *J. Biomater. Appl.*, **2001**, *16*, 3-21.

13 Edwards, K. A.; Baeumner, A. J., Review: Analysis of Liposomes, *Talanta*, **2006**, *68*, 1432-1441.

14 Torchilin, V. P., Recent advances with liposomes as pharmaceutical carriers, *Nature Reviews Drug Discovery*, **2005**, ***4***, 145-160.

15 Allen, T. M.; Cullis, P. R., Liposomal drug delivery systems: From concept to clinical applications, *Adv. Drug Delivery Rev.*, **2013**, *65*, 36–48.

16 Nasseau, M.; Boublik, Y.; Meier, W.; Winterhalter, M.; and Fournier, D., Substrate-permeable encapsulation of enzymes maintains effective activity, stabilizes against denaturation, and protects against proteolytic degradation, *Biotechnol. Bioeng.*, **2001**, *75 (5)*, 615-618.

17 Walde, P.; Ichikawa, S., Enzymes inside lipid vesicles: preparation, reactivity and applications, *Biomol. Eng.*, **2001**, *18*, 143–177.

18 Mecke, A.; Dittrich, C.; and Meier, W., Biomimetic membranes designed from amphiphilic block copolymers, *Soft Matter*, **2006**, *2*, 751-759.

19 Tanner, P.; Baumann, P.; Enea, R.; Onaca, O.; Palivan, C.; Meier, W., Polymeric Vesicles: From Drug Carriers to Nanoreactors and Artificial Organelles, *Acc. Chem. Res.*, **2011**, *44 (10)*, 1039-1049.

20 Meng, F.; Zhong, Z.; Feijen, J., Stimuli-Responsive Polymersomes for Programmed Drug Delivery, *Biomacromolecules*, **2009**, *10*, 197-209.

21 Discher, B. M.; Won, Y. –Y.; Ege, D. S.; Lee, J. C. –M.; Bates, F. S.; Discher, D. E.; Hammer, D. A., Polymersomes: Tough Vesicles Made from Diblock Copolymers, *Science*, **1999**, *284*, 1143-1146.

22 Discher, D. E.; and Eisenberg, A., Polymer Vesicles, *Science*, **2002**, *297*, 967-973.

23 Nardin, C.; Widmer, J.; Winterhalter, M.; Meier, W., Amphiphilic block copolymer nanocontainers as bioreactors, *Eur. Phys. J. E.*, **2001**, *4*, 403-410.

24 Taubert, A.; Napoli, A.; Meier, W., Self-assembly of reactive amphiphilic block co-polymers as mimetics for biological membranes, *Current Opinion in Chemical Biology*, **2004**, *8*, 598-603.

25 Blanazs, A.; Armes, S. P.; Ryan, A. J., Self-Assembled Block Copolymer Aggregates: From Micelles to Vesicles and their Biological Applications, *Macromol. Rapid Commun.*, **2009**, *30*, 267-277.

26 Van Dongen, S. F. M.; Nallani, M.; Cornelissen, J. J. L. M.; Nolte, R. J. M.; Van Hest, J. C. M., A Three-Enzyme Cascade Reaction through Positional Assembly of Enzymes in a Polymersome Nanoreactor, *Chem. Eur. J.*, **2009**, *15*, 1107-1114.

27 Massignani, M.; Lomas, H.; Battaglia, G., Polymersomes: A Synthetic Biological Approach to Encapsulation and Delivery, *Adv. Polym. Sci.*, **2010**, *229*, 115-154.

28 Van Dongen, S. F. M.; de Hoog, H. –P. M.; Peters, R. J. R. W.; Nallani, M.; Nolte, R. J. M.; Van Hest, J. C. M., Biohybrid Polymer Capsules, *Chem. Rev.*, **2009**, *109*, 6212-6274.

29 Vriezema, D. M.; Garcia, P. M. L.; Oltra, N. S.; Hatzakis, N. S.; Kuiper, S. M.; Nolte, R. J. M.; Rowan, A. E.; Van Hest, J. C. M., Positional Assembly of Enzymes in Polymersome Nanoreactors for Cascade Reactions, *Angew. Chem. Int. Ed.*, **2007**, *46*, 7378-7382.

30 Delaittre, G.; Reynhout, I. C.; Cornelissen, J. J. L. M.; Nolte, R. J. M., Cascade Reactions in an All-Enzyme Nanoreactor, *Chem. Eur. J.*, **2009**, *15*, 12600-12603.

31 Van Dongen, S. F. M.; Nallani, M.; Schoffelen, S.; Cornelissen, J. J. L. M.; Nolte, R. J. M.; Van Hest, J. C. M., A Block Copolymer for Functionalization of Polymer Surfaces, *Macromol. Rapid Commun.*, **2008**, *29*, 321-325.

32 Lee, H. J.; Yang, S. R.; An, E. J.; and Kim, J. –D., Biodegradable Polymersomes from Poly(2-hydroxyethyl aspartamide) Grafted with Lactic Acid Oligomers in Aqueous Solution, *Macromolecules*, **2006**, *39*, 4938-4940.

33 Shi, Z; Zhou, Y.; Yan, D., Facile Fabrication of pH-Responsive and Size-Controllable Polymer Vesicles From a Commercially Available Hyperbranched Polyester, *Macromol. Rapid Commun.*, **2008**, *29*, 412-418.

34 Discher, D. E.; and Ahmed, F., Polymersomes, *Annu. Rev. Biomed. Eng.*, **2006**, *8*, 323-341.

35 LoPresti, C.; Lomas, H.; Massignani, M.; Smart, T.; and Battaglia, G., Polymersomes: nature inspired nanometer sized compartments, *J. Mater. Chem.*, **2009**, *19*, 3576-3590.

36 Li, M. –H.; and Keller, P., Stimuli-responsive polymer vesicles, *Soft Matter*, **2009**, *5*, 927-937.

37 Choucair, A.; Lavigueur, C.; and Eisenberg, A., Polystyrene-*b*-poly(acrylic acid) Vesicle Size Control Using Solution Properties and Hydrophilic Block Length, *Langmuir*, **2004**, *20*, 3894-3900.

38 Meng, F.; Engbers, G. H. M.; Feijen, J., Biodegradable polymersomes as a basis for artificial cells: encapsulation, release and targeting, *J. Control. Release*, **2005**, *101*, 187-198.

39 Shum, H. C.; Kim, J. W.; and Weitz, D. A., Microfluidic Fabrication of Monodisperse Biocompatible and Biodegradable Polymersomes with Controlled Permeability, *J. Am. Chem. Soc.*, **2008**, *130*, 9543-9549.

40 Lorenceau, E.; Utada, A. S.; Link, D. R.; Cristobal, G.; Joanicot, M.; and Weitz, D. A., Generation of Polymerosomes from Double-Emulsions, *Langmuir*, **2005**, *21*, 9183-9186.

41 Shum, H. C.; Zhao, Y. –J.; Kim, S. –H.; and Weitz, D. A., Multicompartment Polymersomes from Double Emulsions, *Angew. Chem. Int. Ed.*, **2011**, *50*, 1648-1651.

42 Mabrouk, E.; Cuvelier, D.; Pontani, L. –L.; Xu, B.; Levy, D.; Keller, P.; Wyart, F. B.; Nassoy, P.; and Li, M. –H., Formation and material properties of giant liquid crystal polymersomes, *Soft Matter*, **2009**, *5*, 1870-1878.

43 Garcia, R. R.; Mell, M.; Montero, I. L.; Netzel, J.; Hellweg, T.; and Monroy, F., Polymersomes: smart vesicles of tunable rigidity and permeability, *Soft Matter*, **2011**, *7*, 1532-1542.

44 Lensen, D.; Vriezema, D. M.; Van Hest, J. C. M., Polymeric Microcapsules for Synthetic Applications, *Macromol. Biosci.*, **2008**, *8*, 991-1005.

45 Fujita, K., Kimura, S., and Imanishi, Y., Spherical self-assembly of a synthetic R-helical peptide in water, *Langmuir*, **1999**, *15*, 4377–4379.

46 Kimura, S., Kim, D. H., Sugiyama, J., and Imanishi, Y., Vesicular self-assembly of a helical peptide in water, *Langmuir*, **1999**, *15*, 4461–4463.

47 Tanisaka, H.; Kondoh, S. K.; Makino, A.; Tanaka, S.; Hiraoka, M.; and Kimura, S., Near-Infrared Fluorescent Labeled Peptosome for Application to Cancer Imaging, *Bioconjugate Chem.*, **2008**, *19*, 109-117.

48 Makino, A.; Kimura, S., Preparation of peptide- and protein-based molecular assemblies and their utilizations as nanocarriers for tumor imaging, *Reactive & Functional Polymers*, **2011**, *71*, 272-279.

49 Holowka, E. P.; Pochan, D. J.; and Deming, T. J., Charged polypeptide vesicles with controllable diameter, *J. Am. Chem. Soc.*, **2005**, *127*, 12423-12428.

50 Koide, A.; Kishimura, A.; Osada, K.; Jang, W. – D.; Yamasaki, Y.; Kataoka, K., Semipermeable Polymer Vesicle (PICsome) Self-Assembled in Aqueous Medium from a Pair of Oppositely Charged Block Copolymers: Physiologically Stable Micro-/Nano- containers of Water-Soluble Macromolecules, *J. Am. Chem. Soc.*, **2006**, *128*, 5988-5989.

51 Anraku, Y.; Kishimura, A.; Oba, M.; Yamasaki, Y.; Kataoka, K., Spontaneous Formation of Nanosized Unilamellar Polyion Complex Vesicles with Tunable Size and Properties, *J. Am. Chem. Soc.*, **2010**, *132*, 1631-1636.

52 Kishimura, A.; Koide, A.; Osada, K.; Yamasaki, Y.; Kataoka, K., Encapsulation of Myoglobulin in PEGylated Polyion Complex Vesicles Made from a Pair of Oppositely Charged Block Ionomers: A Physiologically Available Oxygen Carrier, *Angew. Chem. Int. Ed.*, **2007**, *46*, 6085-6088.

53 Chuanoi, S.; Kishimura, A.; Dong, W. –F.; Anraku,Y.; Yamasaki, Y.; and Kataoka, K., Structural factors directing nanosized polyion complex vesicles (Nano-PICsomes) to form a pair of block aniomer/homo catiomers: studies on the aniomer segment length and the catiomer side-chain structure, *Polymer Journal*, **2013**, 1-6.

54 Anraku, Y.; Kishimura, A.; Yamasaki, Y.; and Kataoka, K., Living Unimodal Growth of Polyion Complex Vesicles via Two-Dimensional Supramolecular Polymerization, *J. Am. Chem. Soc.*, **2013**, *135*, 1423-1429.

55 Kishimura, A., Development of polyion complex vesicles (PICsomes) from block copolymers for biomedical applications, *Polymer Journal*, **2013**, *45*, 892-897.

56 Kokuryo, D.; Anraku, Y.; Kishimura, A.; Tanaka, S.; Kano, M. R.; Kershaw, J.; Nishiyama, N.; Saga, T.; Aoki, I.; Kataoka, K., SPIO-PICsome: Development of a highly sensitive and stealth-capable MRI nano-agent for tumor detection using SPIO-loaded unilamellar polyion complex vesicles (PICsomes), *J. Control. Release*, **2013**, *169 (3)*, 220-227.

57 Oana, H.; Kishimura, A.; Yonehara, K.; Yamasaki, Y.; Washizu, M.; and Kataooka, K., Spontaneous Formation of Giant Unilamellar Vesicles from Microdroplets of a Polyion Complex by Thermally Induced Phase Separation, *Angew. Chem. Int. Ed.*, **2009**, *48*, 4613-4616.

58 Oana, H.; Morinaga, M.; Kishimura, A.; Kataoka, K.; and Washizu, M., Direct formation of giant unilamellar vesicles from microparticles of polyion complexes and investigation of their properties using a microfluidic chamber, *Soft Matter*, **2013**, *9*, 5448-5458.

59 Schrage, S.; Sigel, R.; and Schlaad, H., Formation of Amphiphilic Polyion Complex Vesicles from Mixtures of Oppositely Charged Block Ionomers, *Macromolecules*, **2003**, *36 (5)*, 1417-1420.

60 Huang, X.; Li, M.; Green, D. C.; Williams, D. S.; Patil, A. J.; and Mann, S., Interfacial assembly of protein-polymer nano-conjugates into stimulus-responsive biomimetic protocells, *Nat. Commun.*, **2013**, *4*, 2239.

61 Huang, X.; Patil, A. J.; Li, M.; and Mann, S., Design and Construction of Higher-Order Structure and Function in Proteinosome-Based Protocells, *J. Am. Chem. Soc.*, **2014**, *136*, 9225-9234.

62 Huang, X.; Li, M.; and Mann, S., Membrane-mediated cascade reactions by enzyme-polymer proteinosomes, *Chem. Commun.*, **2014**, *50*, 6278-6280.

63 Wang, L.; Chierico, L.; Little, D.; Patikarnmonthon, N.; Yang, Z.; Azzouz, M.; Madsen, J.; Armes, S. P.; and Battaglia, G., Encapsulation of Biomacromolecules within Polymersomes by Electroporation, *Angew. Chem. Int. Ed.*, **2012**, *51*, 11122-11125.

64 Yildiz, U. H.; De Hoog, H. –P. M.; Fu, Z.; Tomczak, N.; Parikh, A. N.; Nallani, M.; and Liedberg, B., Third-Party ATP Sensing in Polymersomes: A Label-Free Assay of Enzyme Reactions in Vesicular Compartments, *Small*, **2014**, *10 (3)*, 442-447.

65 Onaca, O.; Nallani, M.; Ihle, S.; Schenk, A.; Schwaneberg, U., Functionalized nanocompartments (Synthosomes): Limitations and prospective applications in industrial biotechnology, *Biotechnol. J.*, **2006**, *1*, 795-805.

66 Malinova, V.; Belegrinou, S.; Ouboter, D. de B.; Meier, W., Biomimetic Block Copolymer Membranes, *Adv. Polym. Sci.*, **2010**, *224*, 113-166.

67 Nallani, M.; Benito, S.; Onaca, O.; Graff, A.; Lindemann, M.; Winterhalter, M.; Meier, W.; Schwaneberg, U., A nanocompartment system (Synthosome) designed for biotechnological applications, *J. Biotechnol.*, **2006**, *123*, 50-59.

68 Nardin, C.; Widmer, J.; Winterhalter, M.; Meier, W., Amphiphilic block copolymer nanocontainers as bioreactors, *Eur. Phys. J. E.*, **2001**, *4*, 403-410.

69 Axthelm, F.; Casse, O.; Koppenol, W. H.; Nauser, T.; Meier, W.; Palivan, C. G., Antioxidant nanoreactor based on superoxide dismutase encapsulated in superoxide-permeable vesicles, *J. Phys. Chem. B*, **2008**, *112*, 8211-8217.

70 Kim, Y.; Tewari, M.; Pajerowski, J. D.; Cai, S.; Sen, S.; Williams, J.; Sirsi, S.; Lutz, G.; and Discher, D. E., Polymersome delivery of siRNA and antisense oligonucleotides, *J. Controlled Release*, **2009**, *134 (2)*, 132-140.

71 Levine, D. H.; Ghoroghchian, P. P.; Freudenberg, J.; Zhang, G.; Therien, M. J.; Greene, M. I.; Hammer, D. A.; Murali, R., Polymersomes: A new multi-functional tool for cancer diagnosis and therapy, *Methods*, **2008**, *46*, 25-32.

72 De Hoog, H. –P. M.; Vriezema, D. M.; Nallani, M.; Kuiper, S.; Cornelissen, J. J. L. M.; Rowan, A. E.; Nolte, R. J. M., Tuning the properties of PS–PIAT block copolymers and their assembly into polymersomes, *Soft Matter*, **2008**, *4*, 1003-1010.

73 Vriezema, D. M.; Kros, A.; De Gelder, R.; Cornelissen, J. J. L. M.; Rowan, A. E.; Nolte, R. J. M., Electroformed Giant Vesicles from Thiophene-Containing Rod-Coil Diblock Copolymers, *Macromolecules*, **2004**, *37*, 4736-4739.

74 Vriezema, D. M.; Hoogboom, J.; Velonia, K.; Takazawa, K.; Christianen, P. C. M.; Maan, J. C.; Rowan, A. E.; Nolte, R. J. M., Vesicles and Polymerized Vesicles from Thiophene-Containing Rod–Coil Block Copolymers, *Angew. Chem. Int. Ed.*, **2003**, *42*, 772-776.

75 Ahmed, F.; Pakunlu, R. I.; Brannan, A.; Bates, F.; Minko, T.; Discher, D. E., Biodegradable polymersomes loaded with both paclitaxel and doxorubicin permeate and shrink tumors, inducing apoptosis in proportion to accumulated drug, *J. Controlled Release*, **2006**, *116*, 150-158.

76 Ahmed, F.; Pakunlu, R. I.; Srinivas, G.; Brannan, A.; Bates, F.; Klein, M. L.; Minko, T.; and Discher, D. E., Shrinkage of a Rapidly Growing Tumor by Drug-Loaded Polymersomes: pH-Triggered Release through Copolymer Degradation, *Molecular Pharmaceutics*, **2005**, *3 (3)*, 340-350.

77 Discher, D. E.; Ortiz, V.; Srinivas, G.; Klein, M. L.; Kim, Y.; Christian, D.; Cai, S.; Photos, P.; Ahmed, F., Emerging applications of polymersomes in delivery: From molecular dynamics to shrinkage of tumors, *Prog. Polym. Sci.*, **2007**, *32*, 838-857.

78 Anraku, Y.; Kishimura, A.; Kobayashi, A.; Oba, M.; and Kataoka, K., Size-controlled long-circulating PICsome as a ruler to measure critical cut-off disposition size into normal and tumor tissues, *Chem. Commun.*, **2011**, *47*, 6054-6056.

79 Christian, N. A.; Benencia, F.; Milone, M. C.; Li, G.; Frail, P. R.; Therien, M. J.; Coukos, G.; Hammer, D. A., In Vivo Dendritic Cell Tracking Using Fluorescence Lifetime Imaging and Near-Infrared-Emissive Polymersomes, *Mol. Imaging Biol.*, **2009**, *11*, 167-177.

80 Zhou, W.; Meng, F.; Engbers, G. H. M.; Feijin, J., Biodegradable polymersomes for targeted ultrasound imaging, *J. Controlled Release*, **2006**, *116 (2)*, e62-e64.

81 Nahire, R.; Haldar, M. K.; Paul, S.; Ambre, A. H.; Meghnani, V.; Layek, B.; Katti, K. S.; Gange, K. N.; Singh, J.; Sarkar, K.; Mallik, S., Multifunctional polymersomes for cytosolic delivery of gemcitabine and doxorubicin to cancer cells, *Biomaterials*, **2014,** *35*, 6482-6497.

82 Wong, B.; Boyer, C.; Steinbeck, C.; Peters, D.; Schmidt, J.; van Zanten, R.; Chmelka, B.; Zasadzinski, J. A., Design and In Situ Characterization of Lipid Containers with Enhanced Drug Retention, *Adv. Mater.*, **2011**, *23*, 2320–2325.

83 Kisak, E. T.; Coldren, B.; Evans, C. A.; Boyer, C.; and Zasadzinski, J. A., The Vesosome – A Multicompartment Drug Delivery Vehicle, *Curr. Med. Chem.*, **2004**, *11*, 1241-1253.

84 Hosta -Rigau, L.; Chung, S. F.; Postma, A.; Chandrawati, R.; Städler, B.; Caruso, F., Capsosomes with "Free-Floating" Liposomal Subcompartments, *Adv. Mater.*, **2011**, *23*, 4082–4087.

85 Chandrawati, R.; Hosta-Rigau, L.; Vanderstraaten, D.; Lokuliyana, S. A.; St ädler, B.; Albericio, F.; and Caruso, F., Engineering Advanced Capsosomes: Maximizing the Number of Subcompartments, Cargo Retention, and Temperature-Triggered Reaction, *ACS Nano*, **2010**, *4 (3)*, 1351-1361.

86 Hosta-Rigau, L.; York-Duran, M. J.; Zhang, Y.; Goldie, K. N.; and Städler, B., Confined Multiple Enzymatic (Cascade) Reactions within Poly(dopamine)-based Capsosomes, *ACS Appl. Mater. Interfaces*, **2014**, *6 (15)*, 12771-12779.

87 Marguet, M.; Edembe, L.; and Lecommandoux, S., Polymersomes in Polymersomes: Multiple Loading and Permeability Control, *Angew. Chem. Int. Ed.*, **2012**, *51*, 1173-1176.

88 Marguet, M.; Samdre, O.; and Lecommandoux, S., Polymersomes in "Gelly" Polymersomes: Toward Structural Cell Mimicry, *Langmuir*, **2012**, *28*, 2035-2043.

89 Fu, Z.; Ochsner, M. A.; de Hoog, H. –P. M.; Tomczak, N.; Nallani, M., Multi-compartmentalized polymersomes for selective encapsulation of biomacromolecules, *Chem. Commun.*, **2011**, *47*, 2862-2864.

90 De Hoog, H. –P. M.; Nallani, M.; and Tomczak, N., Self-assembled architectures with multiple aqueous compartments, *Soft Matter*, **2012**, *8*, 4552-4561.

91 Chandrawati, R.; and Caruso, F., Biomimetic Liposome- and Polymersome-Based Multicompartmentalized Assemblies, *Langmuir*, **2012**, *28*, 13798-13807.

92 Harada, T.; and Discher, D. E., Bubble wrap of cell-like aggregates, *Nature*, **2011**, *471*, 172-173.

93 Kim, S. –H.; Shum, H. C.; Kim, J. W.; Cho, J. –C.; and Weitz, D. A., Multiple Polymersomes for Programmed Release of Multiple Components, *J. Am. Chem. Soc.*, **2011**, *133*, 15165-15171.

94 Chiu, H. –C.; Lin, Y. –W.; Huang, Y. –F.; Chuang, C. –K.; and Chern, C. –S., Polymer Vesicles Containing Small Vesicles within Interior Aqueous Compartments and pH-Responsive Transmembrane Channels, *Angew. Chem. Int. Ed.*, **2008**, *47*, 1875-1878.

95 Peters, R. J. R. W.; Marguet, M.; Marais, S.; Fraaije, M. W., van Hest, J. C. M.; and Lecommandoux, S., Cascade Reactions in Multicompartmentalized Polymersomes, *Angew. Chem. Int. Ed.*, **2014**, *53*, 146-150.

96 Burchard, W., Static and Dynamic Light Scattering from Branched Polymers and Biopolymers, Springer, Berlin, **1983**, 1-124.

97 Kuiper, S. M.; Nallani, M.; Vriezema, D. M.; Cornelissen, J. J. L. M.; Van Hest, J. C. M.; Nolte, R. J. M.; Rowan, A. E., Enzymes containing porous polymersomes as nano reaction vessels for cascade reactions, *Org. Biomol. Chem.*, **2008**, *6*, 4315-4318.

98 Velde, F.V.D.; Rantwijk, F.V.; and Sheldon, R.A. Improving the catalytic performance of peroxidases in organic synthesis, *Trends in Biotechnology*, **2001**, *19*, 73-80.

99 Bobrow, M.N.; Harris, T.D.; Shaughnessy, K.J.; and Litt, G.J., Catalyzed reporter deposition, a novel method of signal amplification, *Application to immunoassay: Journal of Immunological Methods*, **1989**, *125*, 279-285.

100 Song, W.; Wang, Y.; Qu, J.; Madden, M. M.; Lin, Q., A Photoinducible 1,3-Dipolar Cycloaddition Reaction for Rapid, Selective Modification of Tetrazole-Containing Proteins, *Angew. Chem. Int. Ed.*, **2008**, *47*, 2832-2835.

101 De Hoog, H. –P. M.; Nallani, M.; and Liedberg, B., A facile and fast method for the functionalization of polymersomes by photoinduced cycloaddition chemistry, *Polym. Chem.*, **2012**, *3*, 302-306.

102 Ramil, C. P.; and Lin, Q., Bioorthogonal chemistry: strategies and recent developments, *Chem. Commun.*, **2013**, *49*, 11007-11022.

103 Lim, R. K. V.; and Lin, Q., Bioorthogonal chemistry: recent progress and future directions, *Chem. Commun.*, **2010**, *46*, 1589-1600.

104 Lim, R. K. V.; and Lin, Q., Photoinducible Bioorthogonal Chemistry: A Spatiotemporally Controllable Tool to Visualize and Perturb Proteins in Live Cells, *Acc. Chem. Res.*, **2011**, *44 (9)*, 828-839.

105 Lang, K.; and Chin, J. W., Bioorthogonal Reactions for Labeling Proteins, *ACS Chem. Biol.*, **2014**, *9 (1)*, 16-20.

106 Sakai, K.; Sakurai, K.; Sakai, M.; Hoshino, M.; and Goto, Y., Conformation and stability of thiol-modified bovine β-lactoglobulin, *Protein Science*, **2000**, *9*, 1719-1729.

107 Ito, S.; Tanaka, Y.; Kakehi, A.; Kondo, K., A facile synthesis of 2,5-disubstituted tetrazoles by the reaction of phenylsulfonylhydrazones with arenediazonium salts, *Bull. Chem. Soc. Jpn.*, **1976**, *49*, 1920-1923.

108 Kitabatake, N.; Wada, R.; Fujita, Y., Reversible Conformational Change in β-Lactoglobulin A Modified with N-Ethylmaleimide and Resistance to Molecular Aggregation on Heating, *J. Agric. Food Chem.*, **2001**, *49*, 4011-4018.

109 Chalker, J. M.; Lin, Y. A.; Boutureira, O.; Davis, B. G., Enabling olefin metathesis on proteins: chemical methods for installation of *S*-allyl cysteine, *Chem. Commun.*, **2009**, 3714-3716.

110 Hermanson, G. T., Bioconjugate Techniques, 2nd Edition, Academic Press, Massachusetts, **2008**.

111 Wu, Y.; Pramanik, G.; Eisele, K.; and Weil, T. Convenient Approach to Polypeptide Copolymers Derived from Native Proteins, *Biomacromolecules*, **2012**, *13*, 1890-1898.

112 Eisele, K.; Gropeanu, R. A.; Zehendner, C. M.; Rouhanipour, A.; Ramanathan, A.; Mihov, G.; Koynov, K.; Kuhlmann, C. R. W.; Vasudevan, S. G.; Luhmann, H. J.; and Weil, T. Fine-tuning DNA/albumin polyelectrolyte interactions to produce the efficient transfection agent cBSA-147, *Biomaterials*, **2010**, *31*, 8789-8801.

113 Ellman, G. L., Tissue Sulfhydryls Groups, *Arch. Biochem. Biophys.*, **1959**, *82*, 70-77.

114 Bulaj, G.; Kortemme, T.; Goldenberg, D. P., Ionization-Reactivity Relationships for Cysteine Thiols in Polypeptides, *Biochemistry*, **1998**, *37*, 8965-8972.

115 Riddles, P. W.; Blakeley, R. L.; and Zerner, B., Reassessment of Ellman's Reagent, *Methods Enzymol.*, **1983**, *91*, 49-60.

116 Duncan, R., The dawning era of polymer therapeutics, *Nat. Rev. Drug Discovery*, **2003**, *2*, 347-360.

117 Broyer, R. M.; Grover, G. N.; Maynard, H. D., Emerging synthetic approaches for protein–polymer conjugations, *Chem. Commun.*, **2011**, *47*, 2212-2226.

118 Wonganan, P.; Croyle, M. A., PEGylated Adenoviruses: From Mice to Monkeys, *Viruses*, **2010**, *2*, 468-502.

119 Börner, H. G.; Schlaad, H., Bioinspired functional block copolymers, *Soft Matter*, **2007**, *3*, 394-408.

120 Gauthier, M. A.; Klok, H. –A., Peptide/protein–polymer conjugates: synthetic strategies and design concepts, *Chem. Commun.*, **2008**, *23*, 2591-2611.

121 Aili, D.; Selegard, R.; Baltzer, L.; Enander, K.; and Liedberg, B., Colorimetric Protein Sensing by Controlled Assembly of Gold Nanoparticles Functionalized with Synthetic Receptors, *Small*, **2009**, *5 (21)*, 2445–2452.

122 Aili, D.; Tai, F.–I,; Enander, K.; Baltzer, R.; Liedberg, B., Self-Assembly of Fibers and Nanorings from Disulfide-Linked Helix–Loop–Helix Polypeptides, *Angew. Chem. Int. Ed.*, **2008**, *47*, 5554-5556.

123 Yu, Z.; Lim, R. K. V.; Lin, Q., Synthesis of Macrocyclic Tetrazoles for Rapid Photoinduced Bioorthogonal 1,3-Dipolar Cycloaddition Reactions, *Chem. Eur. J.*, **2010**, *16*, 13325-13329.

124 Huang, L.; Wojciechowski, G.; de Montellano, P. R. O., Role of Heme-Protein Covalent Bonds in Mammalian Peroxidases: Protection of the Heme by a Single Engineered Heme-Protein Link in Horseradish Peroxidase, *J. Biol. Chem.*, **2006**, *281*, 18983-18988.

125 Zhang, Y.; Liu, W.; and Zhao, Z. K., Nucleophilic Trapping Nitrilimine Generated by Photolysis of Diaryltetrazole in Aqueous Phase, *Molecules*, **2014**, *19*, 306-315.

126 Lee, Y.–J.; Wu, B.; Raymond, J. E.; Zeng, Y.; Fang, X.; Wooley, K. L.; Liu, R., Fluorogenic, Two-Photon-Triggered Photoclick Chemistry in Live Mammalian Cells, *ACS Chem. Biol.*, **2013**, *8*, 1664-1670.

127 Yu, Z.; Pan, Y.; Wang, Z.; and Lin, Q., Genetically Encoded Cyclopropene Directs Rapid, Photoclick-Chemistry-Mediated Protein Labeling in Mammalian Cells, *Angew. Chem. Int. Ed.*, **2012**, *51*, 10600-10604.

128 An, P.; Yu, Z.; and Lin, Q., Design of oligothiophene-based tetrazoles for laser-triggered photoclick chemistry in living cells, *Chem. Commun.*, **2013**, *49*, 9920-9922.

129 Ruccia, M.; Vivona, N.; Cusmano, G.; Marino, M. L.; Piozzi, F., Addition reactions of heterocycles—IV : Indoles and nitrilimines, *Tetrahedron*, **1973**, *29*, 3159-3164.

130 Thomas, C. S.; Xu, L.; and Olsen B. D., Kinetically Controlled Nanostructure Formation in Self-Assembled Globular Protein-Polymer Diblock Copolymers, *Biomacromolecules*, **2012**, *13*, 2781-2792.

131 Lam, C. N.; Kim, M.; Thomas, C. S.; Chang, D.; Sanoja, G. E.; Okwara, C. U.; and Olsen, B. D., The Nature of Protein Interactions Governing Globular Protein-Polymer Block Copolymer Self-Assembly, *Biomacromolecules*, **2014**, *15*, 1248-1258.

132 Berry, G. C., Thermodynamic and conformational properties of polystyrene. I. Light-Scattering Studies on Dilute Solutions of Linear Polystyrenes, *J. Chem. Phys.*, **1966**, *44*, 4550-4564.

APPENDIX A:

Transmission Electron Microscope (TEM) Imaging

TEM was performed with a Carl Zeiss Libra 120 Plus TEM, operated at 120 kV at the Facility for Analysis, Characterization, Testing, and Simulation (FACTS) in Nanyang Technological University, Singapore. The samples were prepared by dispensing 15 µL of a vesicle suspension on a holey-carbon coated copper grid followed by 30 min of incubation and removal of excess solution with a piece of filter paper. The adsorbed vesicles were then stained by dispensing and incubating 10 µL of 1% phosphotungstic acid on the copper grid for 1 min, before removal of excess solution.

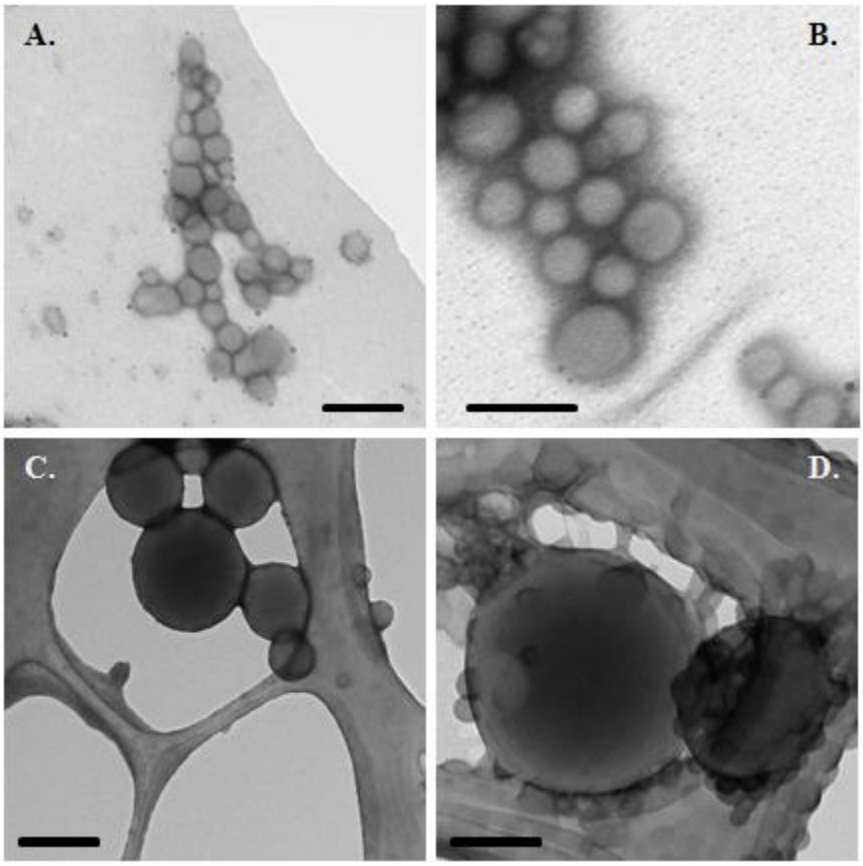

Figure A1. TEM images of individual ABA polymersomes encapsulating HRP and OmpF incorporated in the membrane before (**A**) and after addition of THF (**B**), individual PS-PIAT polymersomes (**C**), and the multicompartmentalized polymersomes (**D**). The samples were stained with 1% phosphotungstic acid. Scale bars are 100 nm.

APPENDIX B:

Cryo-TEM Imaging

For cryo-TEM, 4 µL of sample containing nanoreactors was adsorbed onto a holey carbon-coated grid (Quantifoil, Germany). The grid was afterwards blotted with Whatman filter paper for 2 seconds and then was vitrified into the liquid ethane at -178°C using a Vitrobot (FEI company, Netherlands). Frozen grids were transferred into a Titan Krios microscope (80-300 kV, FEG, LN2-cooled stage for 12 grids, Ultrascan 4000 (4k CCD), Tridiem GIF (Ultrascan 1000, 2k CCD)) (FEI company, Netherlands).

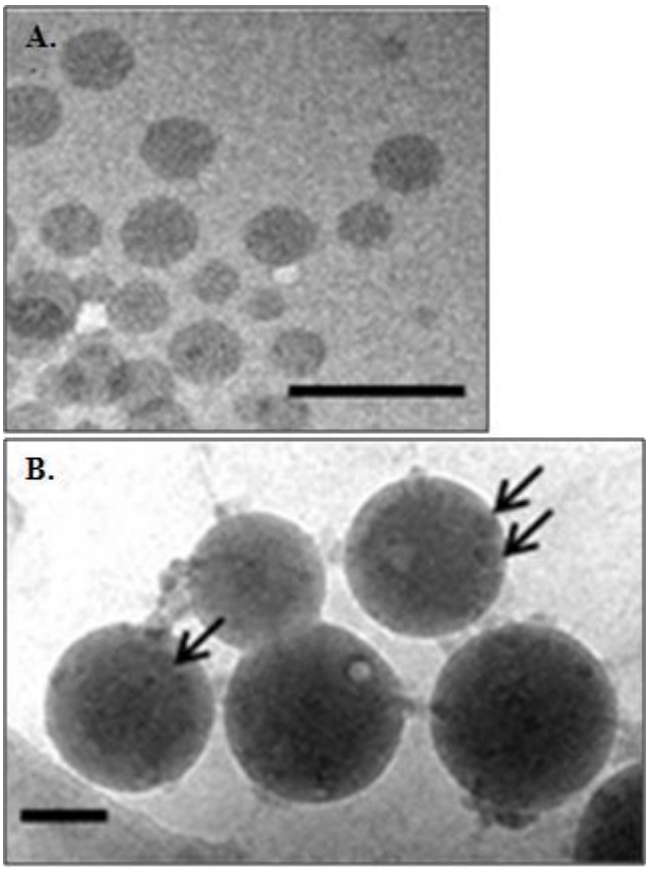

Figure B1. Cryo-TEM images of individual ABA polymersomes (**A**) and multicompartmentalized polymersomes (**B**). Arrows indicate the presence of inner compartments. Scale bars are 100 nm and 200 nm respectively.

APPENDIX C:

Static Light Scattering (SLS) Measurements

SLS measurements are performed with Brookhaven Instruments BI-200 SM at temperature of 20°C. Approximately 200 µL samples at different concentrations were diluted in 8.0 mL of milli-Q water (filtered 5 times over 0.2 µm filters). The sample was then placed in a glass round cell and positioned inside the Brookhaven Instruments BI-200 SM. The measurement angles for the large angular were set from 50° to 150° with 15° increments. By using the companion software, a Berry plot for the scattering measurements at various concentrations was then constructed,[132] and radius of gyration (R_G) value were calculated.

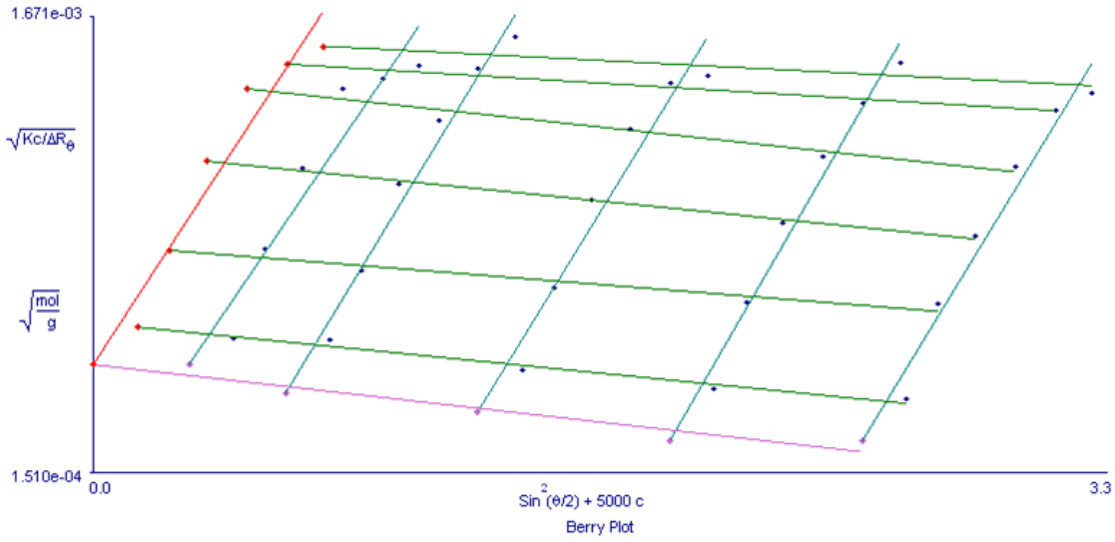

Figure C1. Berry plot of the MC polymersomes at various concentrations. A concentration range of 62.5–500 µg mL^{-1} was employed in the static light scattering measurements. Static light scattering measurements provided a radius of gyration of 163 nm (± 28), as determined from slope and intercept of the linear fit at different measurement angles, resulting in a R_G/R_H (ρ-value) of 1.10, indicative of the vesicular structure. [96]

APPENDIX D:

Labeling of GOx with Alexa-488

For confocal microscopy, flow cytometry, and estimation of the encapsulation efficiency, GOx was labeled with alexa-488 using an alexa fluor 488 protein labeling kit (Life technologies), following the protocol supplied. The labeling efficiency was calculated from the ratio of the absorbance at 280 nm ($\varepsilon_{protein}$ = 267,200 M^{-1} cm^{-1}) and 495 nm (ε_{dye} = 71,000 M^{-1} cm^{-1}) yielding a labeling efficiency of 3.77. For (crude) estimation of the encapsulation efficiency, the absorbance of alexa-488 labeled GOx before and after encapsulation at 488 nm was measured. The scattering of the polymersomes was corrected by fitting the spectra to a first-order exponential decay function using GraphPad Prism 6.01 for Windows (**Figure D1**). After correction, the relative areas before and after filtration were determined, allowing calculation of the concentration (Table D1).

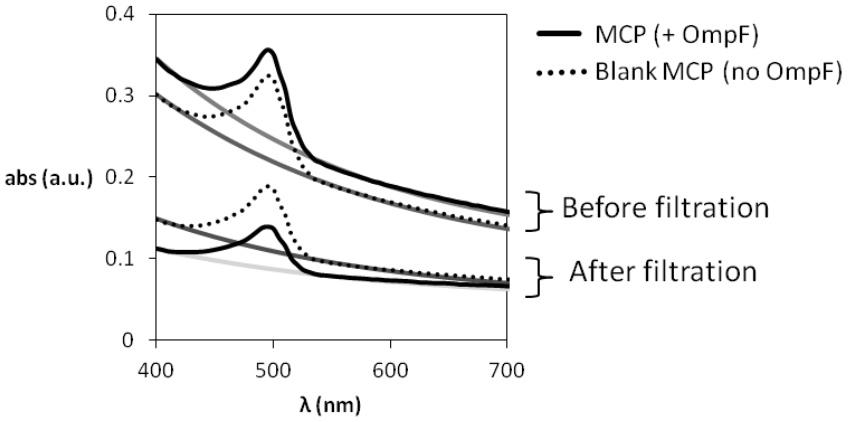

Figure D1. Absorption spectra of alexa-488 labeled Gox encapsulated in the multicompartmentalized polymersomes (MCPs). Spectra were acquired before and after filtration, with (black line), and without OmpF (dotted line) present in the ABA membrane. Although the absorption spectra are obscured by scattering from the polymersomes, a clear signal from the dye is observed.

Table D1. Calculation of encapsulation efficiency. Area of the alexa-488 absorption peak in the UV-Vis spectra of MCPs, before and after filtration, and estimation of the GOx concentration. The scattering has been substracted by fitting to an exponential decay function.

Sample	Area under the curve (AU cm)	Encapsulation efficiency	GOx concentration (mg mL^{-1})
Before filtration			
MCP (+OMPF)	14.7	NA [a]	0.80
Blank MCP (no OmpF)	15.8	NA	0.80
After filtration			
MCP (+ OMPF)	7.4	50.2	0.40
Blank MCP (no OmpF)	6.0	37.8	0.30

a) Not applicable

APPENDIX E:

Flow Cytometry Analysis

Polymersomes were analyzed using a BD FACSCanto II flow cytometer. Alexa-488 conjugated GOx was detected using a 530 ± 15 nm (FITC) bandpass filter, while alexa-647 conjugated HRP was detected using a 660 ± 10 nm (APC) bandpass filter. Data is presented as a two dimensional dot plot between alexa-647 and alexa-488 using forward- and side-angle scatter (FSC/SSC) gating to capture the majority of the polymersomes and to exclude background from PBS. 50,000 Gated events were recorded for each set of measurements.

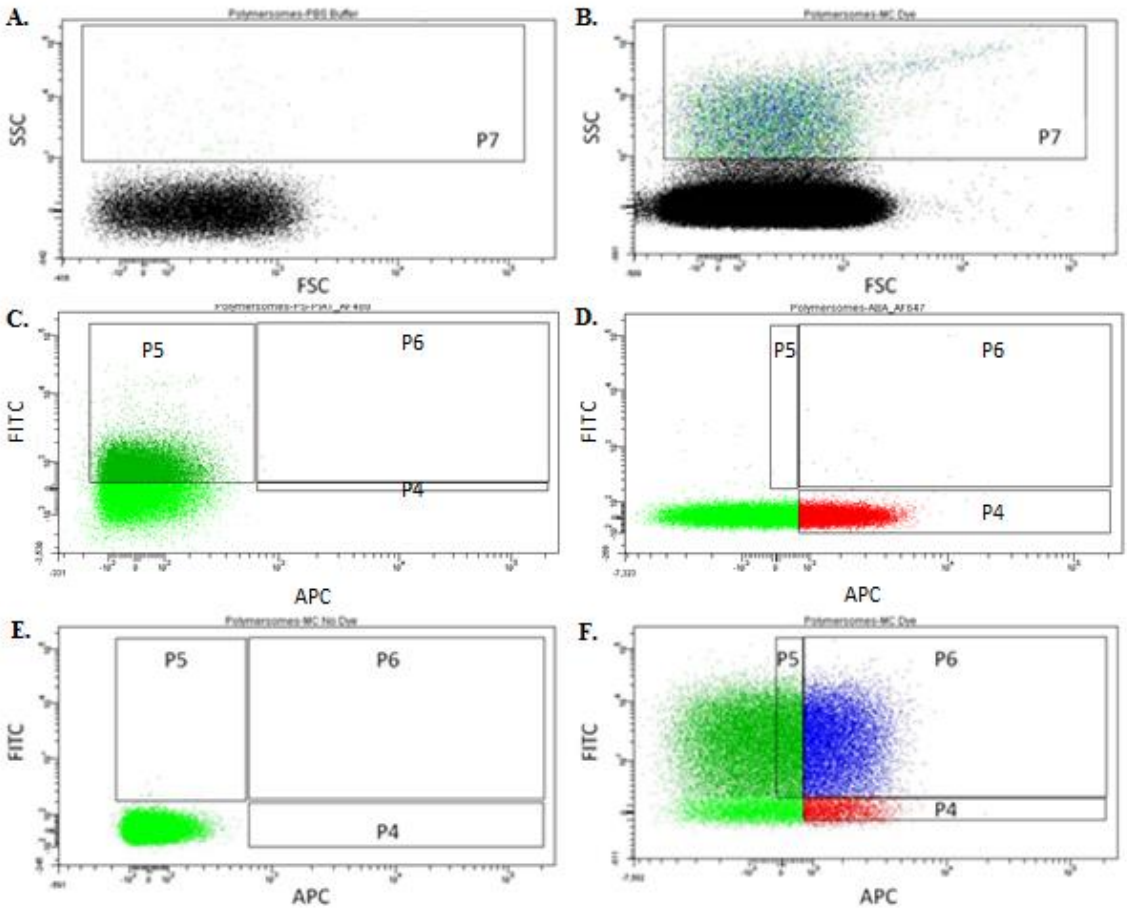

Figure E1. Flow cytometry analysis of the multicompartmentalized polymersomes. FSC/SSC dot plots of PBS (**A**) and MC polymersomes (**B**) respectively. Gating was applied (region P7) to capture the majority of the polymersomes and to exclude background from PBS. Dot plot of FITC (530 ± 15 nm for detection of alexa-488) against APC (660 ± 10 nm for detection of alexa-647) for PS-PIAT polymersomes with alexa-

488 labeled GOx (**C**), ABA polymersomes with alexa-647 labeled HRP (**D**), and MC polymersomes containing unlabeled enzymes (**E**) after applying gate P7. Regions P4, P5, and P6 were selected to reflect polymersomes containing alexa-647 only (*red dots*), polymersomes containing alexa-488 only (*dark green dots*), and polymersomes containing both alexa-647 and alexa-488 (*blue dots*) respectively. Dot plot of FITC/APC for MC polymersomes containing labeled enzymes (**F**) after applying gate P7. Note that region P5 was narrowed to exlcude intrinsic fluorescence of individual PS-PIAT polymersomes (as observed in **C)**. MC polymersomes containing alexa-647 and alexa-488 make up 28% of the total polymersome population, while individual ABA polymersomes containing alexa-647 and individual PS-PIAT polymersomes containing alexa-488 make up 5.7% and 16.2% of the total polymersome population respectively. The remainder of the polymersome population does not contain labeled enzymes.

Table E1. Encapsulation efficiencies as calculated from Figure E1.F.

Sample ID	Gating number	Fluorescence events a	% encapsulation (based on fluorescence counts)
ABA (AF647)	P4	2812	5.7
PS-PIAT (AF488)	P5	7991	16.2
MCPs (AF647+ AF488)	P6	13778	27.9

a: Total fluorescence events is 49,454

Table E2. Encapsulation efficiencies as calculated from Table E1.

	Fluorescence events				% encapsulation (based on fluorescence counts)
	Active HRP or AF647 (in MCPs)	Labeled GOx or AF488 (in PS-PIAT and MCPs)	Active HRP or AF647 (in ABA and MCPs)	Total	
Polymersomes population contained GOx	-	21769	-	49454	44.2
Polymersomes population with active HRP	13778	21769	-	-	63.0
Total ABA population that coexist with PS-PIAT	13778	-	16590	-	83.0

APPENDIX F:

1H-NMR Spectra

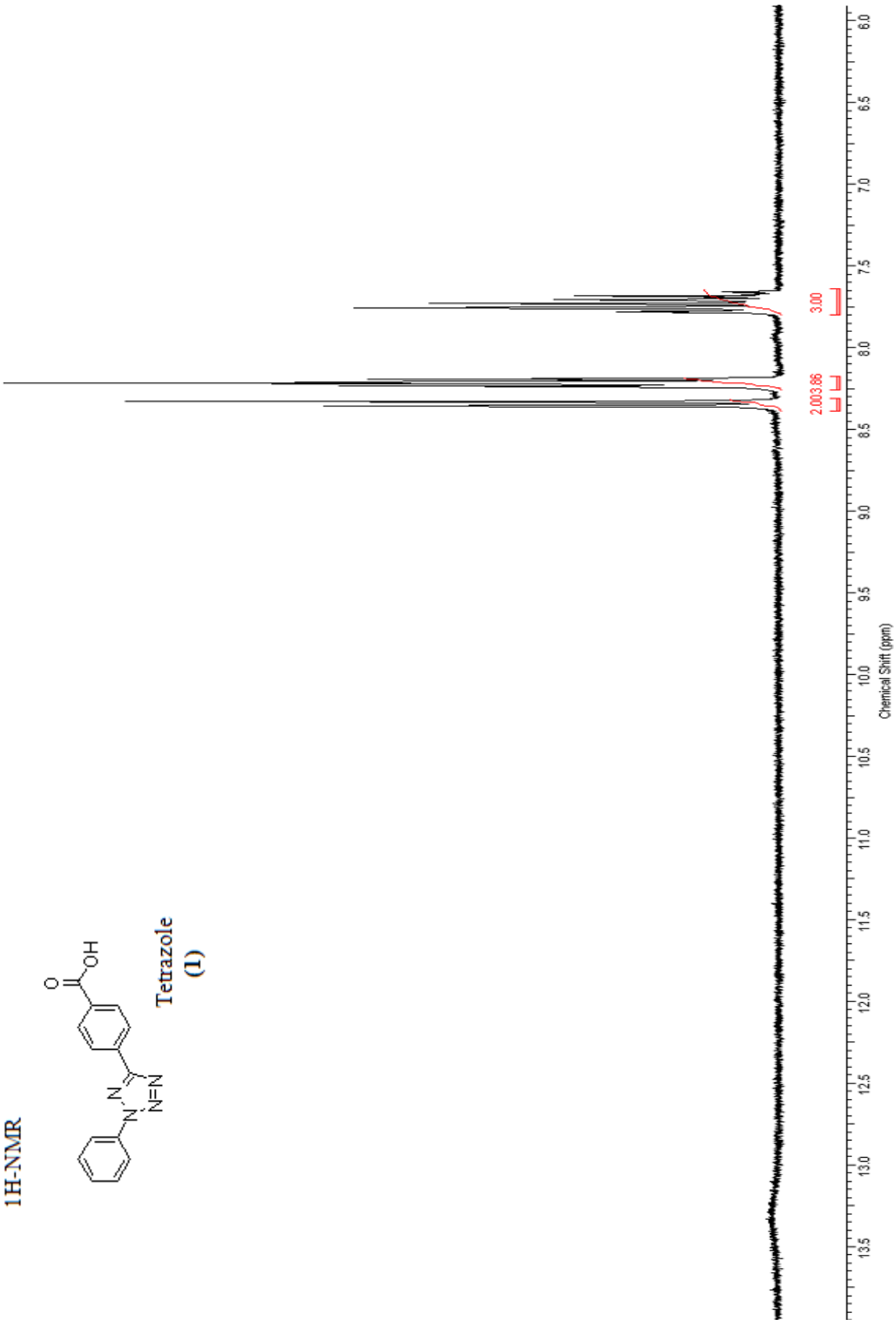

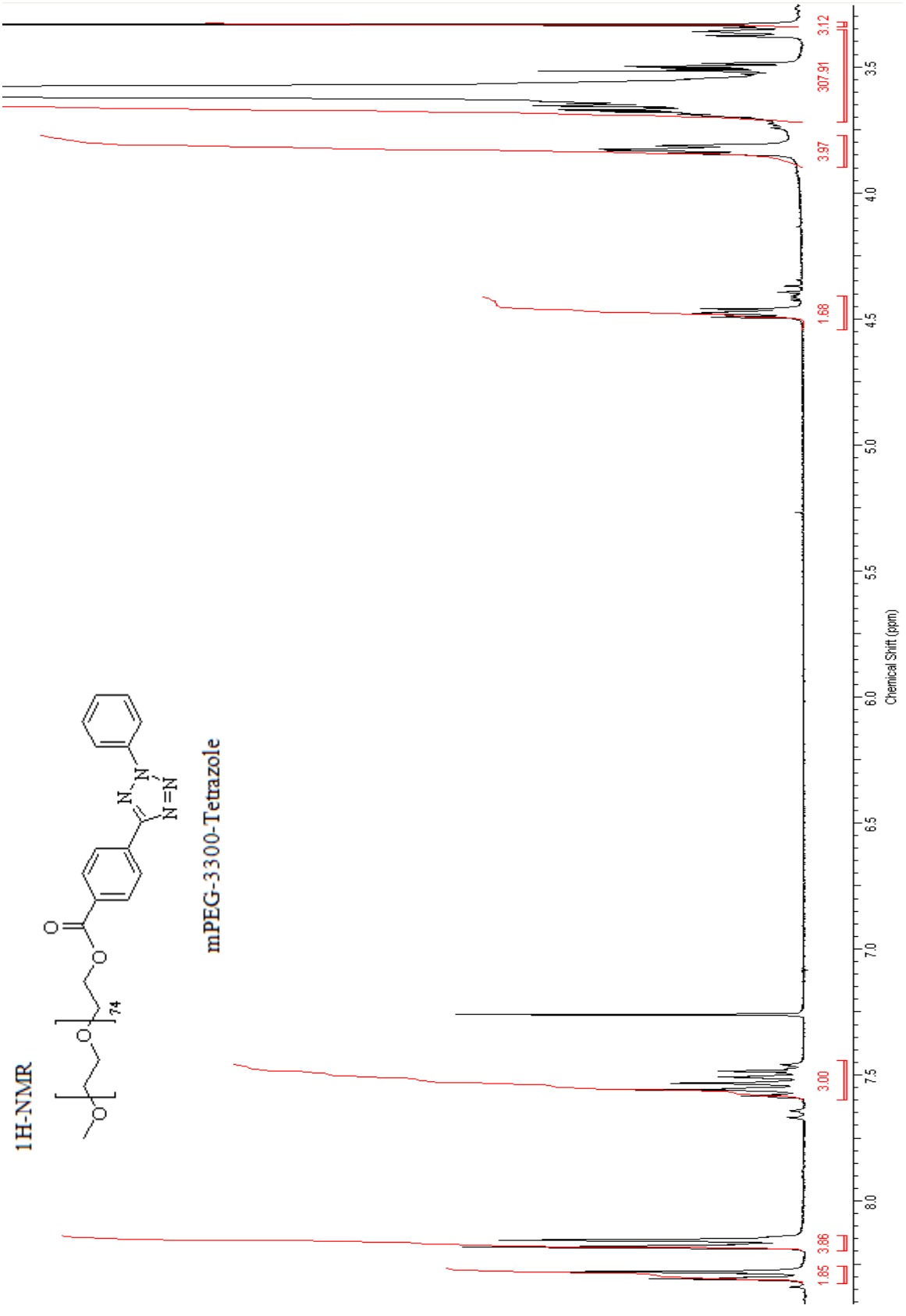
1H-NMR
mPEG-3300-Tetrazole
74
Chemical Shift (ppm)
3.5
4.0
4.5
5.0
5.5
6.0
6.5
7.0
7.5
8.0
3.12
307.91
3.97
1.68
3.00
3.86
1.85

APPENDIX G:
Ellman's Test

The Ellman's reagent, 5,5'-dithio-bis-(2-nitrobenzoic acid) (DTNB) was used to determine the amount or concentration of free thiol groups in proteins. The Ellman's test is based on the fast and sensitive reaction of DTNB with thiol to give the mixed disulfide and 2-nitro-5-thiobenzoate (TNB^-), which ionizes to TNB^{2-} dianion in water at both neutral and alkaline pH (**Figure G1**).[113-115] This TNB^{2-} dianion is yellow color and can be quantified easily by its absorbance of visible light at 412 nm using UV/Vis spectrophotometer with molar absorption coefficient, ε_{412} of 14,150 M^{-1} cm^{-1} for dilute buffer.[115]

Figure G1. The reaction of DTNB with thiol group. Reprinted with permission from ref.[115] Copyright © 1983 Elsevier Ltd.

In Section 4.3, for the preparation of BLG-allyl, Ellman's test was used to quantify the concentration of the remaning thiols to unmodified BLG (**Table G1**). After reaction, all the free thiols had been derivatized into alkene groups.

Table G1. Ratio of free thiols to BLG molecule before and after reaction.

	Conc. of BLG-A (mg/mL) [a,b]	**Conc. of Free -SH (μM)[b]**	**Free -SH / BLG-A (mole/mole)**
BLG-A before reaction	2.5 (± 0.3)	3.3 (± 0.1)	1.3
BLG-A after reaction with allyl chloride	0.41 (± 0.04)	-0.1 (± 0.2)	-0.03

a) BLG-A concentration was determined by the absorbance of protein at 280 nm using UV/Vis spectrometer.

b) Average of three independent measurements

APPENDIX H:

Fast Protein Liquid Chromatography (FPLC)

FPLC was conducted using ÄKTA purifier UPC-900. For the purification of positively charged PEG-BLG conjugates and negatively charged PEG-BLG conjugates, FPLC via ionic-exchange column chromatography was performed with Sepharose SP HP column and Sepharose Q FF column respectively.

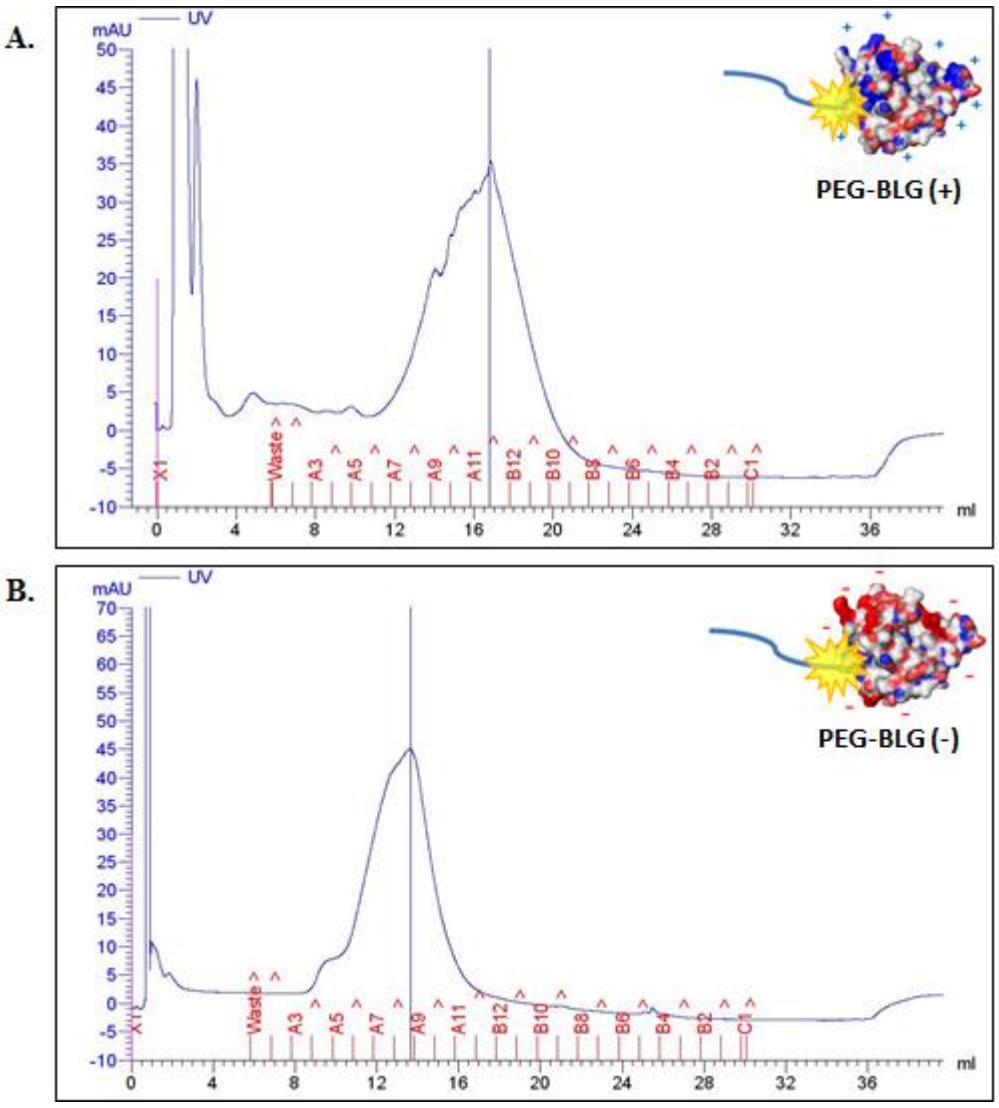

Figure H1. FPLC chromatograms following the purification of positively charged PEG-BLG conjugates (**A**) and negatively charged PEG-BLG conjugates (**B**) via ionic-exchange column chromatography.

APPENDIX I:

SDS-PAGE

SDS-PAGE was performed using Bio-Rad Mini-PROTEAN Tetra Cell.

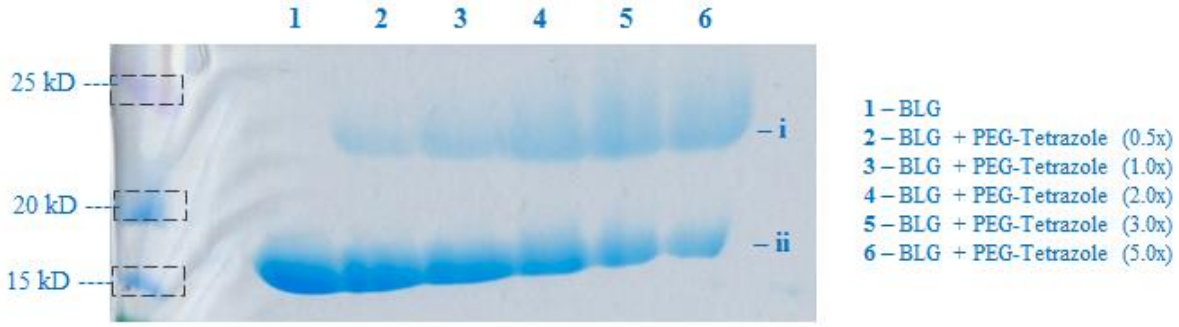

Figure I1. SDS-PAGE of the product of PEG-tz and native BLG, after photoirradiation at increasing equivalents of PEG-tz (0.5, 1.0, 2.0, 3.0 and 5.0 eqs). Bands indicated by **i** represent the conjugated product, while **ii** represents native BLG.

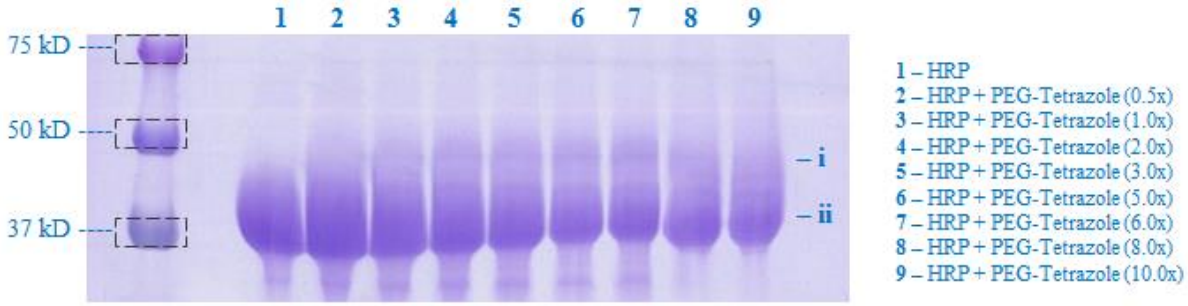

Figure I2. SDS-PAGE of the product of PEG-tz and native HRP, after photoirradiation at increasing equivalents of PEG-tz (0.5 – 10.0 eqs). Bands indicated by **i** represent the conjugated product, while **ii** represents native HRP.

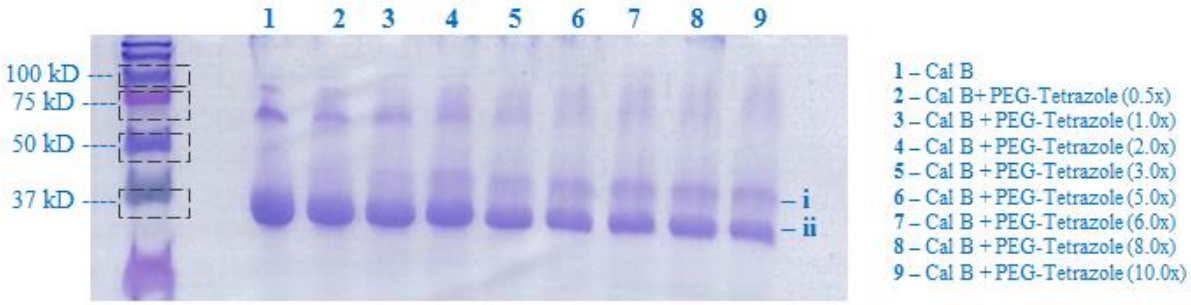

Figure I3. SDS-PAGE of the product of PEG-tz and native CalB, after photoirradiation at increasing equivalents of PEG-tz (0.5 – 10.0 eqs). Bands indicated by **i** represent the conjugated product, while **ii** represents native CalB.

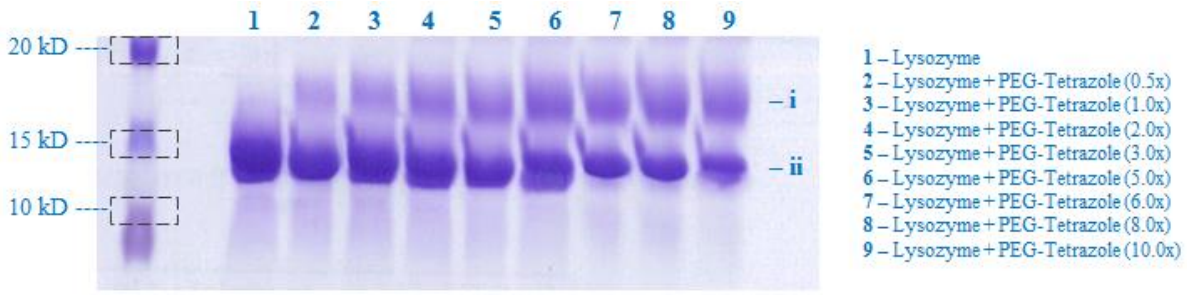

Figure I4. SDS-PAGE of the product of PEG-tz and native lysozyme, after photoirradiation at increasing equivslents of PEG-tz (0.5 – 10.0 eqs). Bands indicated by **i** represent the conjugated product, while **ii** represents native lysozyme.

APPENDIX J:

Protein Database Structures

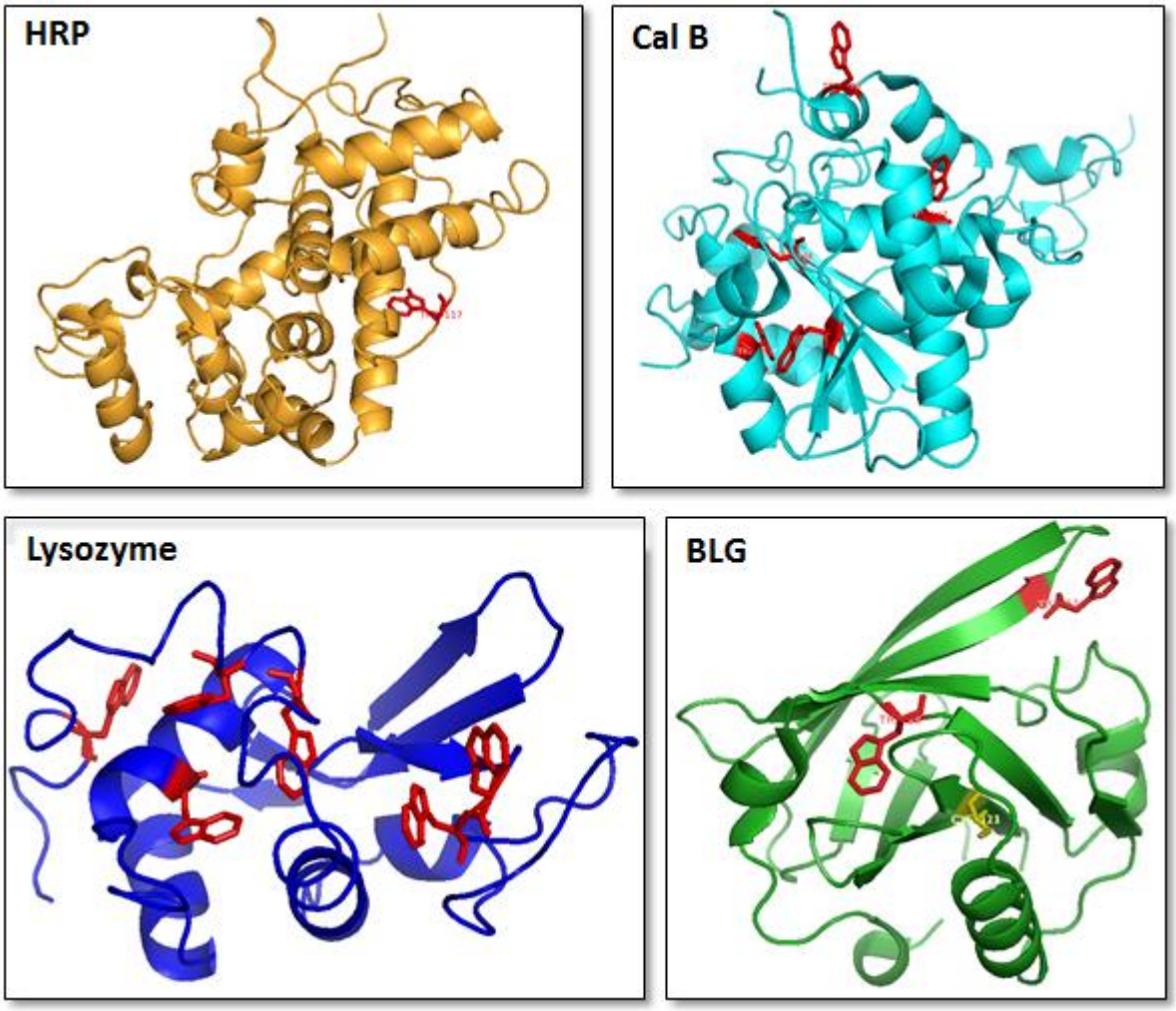

Figure J1. Graphic representations of HRP, CalB, Lysozyme and BLG, with tryptophan residues shown in red. The picture was rendered using PyMOL (PDB ID for HRP, CalB, lysozyme, and BLG: 1ATJ, 3ICV, 6LYZ and 1QG5, respectively). HRP, CalB, BLG and lysozyme contain one (Trp-117), five (Trp-86, Trp-99, Trp-138, Trp-147, and Trp-189), two (Trp-19 and Trp-61), and six tryptophan residues (Trp-28, Trp-62, Trp-63, Trp-108, Trp-111, and Trp-123), respectively.